Study on Bond and Peeling Characteristics between CFRP Plates and Concrete under Fatigue Loading

March 2014

Wei Zhang

Study on Bond and Peeling Characteristics between CFRP Plates and Concrete under Fatigue Loading

Graduate School of Systems and Information Engineering

University of Tsukuba

March 2014

Wei Zhang

CONTENTS

LIST OF TABLES

LIST OF FIGURES

DISSERTATION ABSTRACT

Fiber-reinforced polymer (FRP) systems have emerged as an alternative to traditional techniques for strengthening concrete, such as steel plate bonding, section enlargement, and external post-tensioning. FRP strengthening systems use FRP composite materials as supplemental externally bonded reinforcement. FRP systems offer several advantages over traditional strengthening techniques, including their light weight, ease of installation, and noncorrosive nature.

Strengthening of reinforced concrete (RC) structures using carbon FRP (CFRP) has emerged as a potential solution to the problems associated with civil infrastructure. Many researchers have reported significant increases in the strength and stiffness of CFRP-retrofitted concrete structures. Nevertheless, brittle failures of such retrofitted systems could prevent the full utilization of CFRP. One possible brittle failure mode is premature debonding of the CFRP, which could occur at load levels significantly lower than the strength of the CFRP material used in the retrofitted system. Therefore, the various failure mechanisms possible in CFRP-strengthened concrete structures must be better understood to achieve a reliable retrofit design. Innovative structural detailing is also necessary to utilize CFRP systems more effectively.

When considering the rehabilitation of an RC structure, such as a bridge that has been subjected to repetitive cyclic loading, the detrimental effects of fatigue over the life of the structure must be assessed. When such an assessment indicates that the structure or structural component is approaching its fatigue endurance limit, a strategy is needed to extend its fatigue life. One potential solution is the bonding of FRP composites. However, FRP debonding through the concrete substrate has been identified as an important failure mode because it occurs at lighter load levels and the failure is very brittle. Indeed, the durability of the FRP-to-concrete bond is recognized as being critical to the performance of an externally bonded FRP repair system. Therefore, clearly identifying the degrading effect of fatigue loading on the performance of externally bonded FRP systems is important.

The technique of bonding steel plates to the external surfaces of RC structures to enhance flexural strength or stiffness has been employed worldwide since the late 1960s. Recent increases in bridge design loading requirements worldwide have highlighted the need for fast, efficient, and durable strengthening methods. Although external steel plate bonding can provide a satisfactory solution in many cases, it does have disadvantages, including the need to maneuver heavy plates on site, potential steel corrosion, and the need for on-going maintenance.

CFRP plates offer several advantages over steel, including their resistance to corrosion, light weight, and excellent mechanical strength. CFRP is an ideal material for use in the structural repair and strengthening of concrete structures. The main

attributes of CFRP plates are their high strength, light weight, better resistance to chemicals compared with steel, good fatigue strength, and noncorrosive nature. The bond behavior between CFRP plates and concrete plays an important role in the effectiveness of CFRP strengthening. The evaluation of fatigue performance is also considered an important issue in the strengthening of concrete structures. The work reported in this thesis considers the development of a comprehensive approach to understanding the bond and peeling characteristics of CFRP plate-strengthened concrete under fatigue loading.

The following is a brief description of the contents of each chapter in the thesis.

Chapter one introduces the research background on structural strengthening and rehabilitation using FRP composites in place of other materials and reviews the literature on the use of FRP composite materials to strengthen concrete structures. The research objectives are enumerated, and the research approach is described. Finally, the aims and outline of this doctoral thesis are introduced.

Chapter two introduces experimental investigations of CFRP plate debonding behavior using beam specimens flexurally strengthened by CFRP plates and relative vertical displacement imposed on the two sides of a shear crack in each beam. The test results confirm the effectiveness of mixed-mode (shear-peeling) debonding in CFRP plates and local debonding with peeling off as an important factor affecting the fatigue life of concrete structures strengthened by CFRP plates.

Chapter three describes fatigue loading tests of double-faced bond specimens, carried out to investigate the influence of bond behavior for different concrete strengths, different types of CFRP plates and different levels of the upper limit fatigue load. The test results show that the fatigue behavior of the bonding surface between a CFRP plate and concrete can be characterized by an *S*-*N* diagram representing the relationship between the upper limit of the bond stress and the number of load cycles at debonding. To clarify the fatigue bond damage and predict the fatigue life of the bond, a bond-slip model based on fatigue cycles (N) and the unloading branch stiffness (k_i) in slip was developed. In addition, the transverse displacement in the CFRP plates and the concrete substrate was measured. The variation in transverse displacement exhibited an obvious discernible peeling phenomenon with debonding propagation. The experiment results indicate that the CFRP plate, upon peeling off, moved from the specimen center to the loading end as the number of fatigue cycles increased. The peeling off of the CFRP plate is an important failure mode affecting the debonding progress in the fatigue test.

Chapter four presents the experimental results and the calculation method for analyzing the bond strength between CFRP plates and concrete interfaces debonded by both shear and peeling. Twenty-two special double-faced rectangular shear specimens with CFRP plates bonded on two sides were tested in uniaxial tensile

loading. The specimens were designed for various initial angles at the middle to ensure that the interface acts in both shear and peeling. Three concrete compressive strengths were used in this investigation. The results revealed that the bond strength decreases considerably due to the peeling effect. In addition, the initial attachment angle plays an important role in the bond strength, combined with the angle effect. Based on the test results, a calculation method is proposed based on modifying one of the existing bond strength models for the FRP sheet-to-concrete bonding system. The proposed modification can accurately predict the bond strength between CFRP plates and concrete.

Chapter five summarizes the thesis with a retrospective view of the research objectives and presents the conclusions drawn from the work. Recommendations for future research are also highlighted in this chapter.

CHAPTER 1
Introduction

1.1 Research Background

A substantial amount of society's resources worldwide are invested in existing concrete structures, such as bridges, tunnels, and various types of buildings. Each of these structures has an expected function and expected life span. However, both the function and life span can be influenced by external factors, such as degradation and altered load situations. Mistakes made in the design or during the construction phase can also influence the functioning and life span of a structure. Repairing and/or strengthening these structures can maintain or improve both their functioning and life spans.

The strengthening or retrofitting of existing concrete structures to resist higher design loads, correct deterioration-related damage, or increase ductility has traditionally been accomplished using conventional materials and construction techniques. Externally bonded steel plates, steel or concrete jackets and external post-tensioning are some of the many traditional techniques available. In the context of the strengthening problem, advanced composites have the potential to provide another promising solution.

In recent years, the use of fiber-reinforced polymer (FRP) materials has emerged as an alternative to traditional strengthening techniques due to the superior properties of these materials, such as their formability, ease of fabrication and bonding, resistance to corrosion, and light weight. Indeed, FRP reinforcement is one of the most promising new developments for concrete structures. FRP reinforcing elements provide lighter, easier-to-assemble and more durable structures that are free of the deterioration caused by the corrosion of steel. FRPs consist of synthetic or organic high-strength fibers, most of which are impregnated with a resin matrix. FRPs are available in the form of grids, rods, and ropes for reinforcing and prestressing concrete members. Various types of FRP reinforcement are currently available in Japan, including rods (round and rectangular), strands, braids, and grids. These types FRP reinforcement are available with fibers of carbon and aramid (rods), carbon (strands), aramid (braids) and carbon, and aramid and glass (grids). FRP reinforcement in sheet form (FRP sheets) is typically applied to strengthen or repair existing structures. Sheets with fiber in one direction are used for strengthening, whereas sheets with fiber in two directions are used for repairs, to improve or restore durability and to avoid concrete pieces from falling from the structure surface.

In the last decade, the development of strong epoxy glue has led to a technique that has great potential in the field of upgrading structures. The technique involves gluing steel or FRP plates to the concrete surface. The plates then act compositely with the concrete and help to carry the loads. FRP can be more convenient than steel for a

number of reasons. FRP materials have higher ultimate strength and lower density than steel. Their installation is easier, and due to their low weight, temporary support until the adhesive gains sufficient strength is not required. FRP reinforcement can also be formed on site into complicated shapes and can easily be cut to length on site.

Debonding in FRP-strengthened members occurs in regions with high stress concentrations, which are often associated with material discontinuities and the presence of cracks. The propagation path of debonding initiated from stress concentrations is dependent on the elastic and strength properties of the repair and substrate materials, as well as their interfacial fracture properties.

The term "debonding failure" is often associated with a significant decrease in member capacity due to the initiation or propagation of debonding. Theoretically, debonding in FRP-strengthened members can occur within or at the interfaces of materials that form the strengthening system, favoring the propagation path that requires the least amount of energy. Crack propagation in one of the constituent materials is generally preferred over interface debonding in the design of structural joints; however, the latter is often encountered, particularly in cases of poor surface preparation or application. The majority of the debonding failures reported in the literature have occurred in the concrete substrate. However, other debonding mechanisms can also be observed, depending on the geometric and material properties.

Repeated loading alters the fundamental properties of the constituent materials in reinforced-concrete (RC) structures, which may lead to progressive damage propagation. The application of FRP to strengthen or retrofit existing structures should consider the fatigue characteristics of the FRP-concrete bond. Although many tests have been conducted to investigate the strengthening of RC members with FRP plates, many aspects of the use of FRP plates remain unclear. To date, little is known about fatigue damage to FRP plate-concrete bonding systems that experience mixed-mode fracturing, and in-depth research of the long-term performance of such systems is necessary before FRP plates gain full acceptance as materials that can be used in civil engineering.

Compared to the fairly extensive experimental and analytical studies on the monotonic behavior of FRP-strengthened RC members, relatively few studies have been reported on the fatigue behavior of FRP-strengthened RC beams.

Past research into the fatigue performance of FRP-strengthened RC beams has mainly focused on demonstrating the overall effectiveness of this strengthening technique. In most investigations to date, the load or deflection ranges applied to the beams have been such that the resulting strain amplitudes in the reinforcing steel have been small. Under these conditions, the bond performance of the FRP reinforcement is not a primary concern because the fatigue response is largely governed by the performance

of the steel reinforcement and concrete. Furthermore, given the brittle characteristics of the adhesive or concrete in tension, as well as the varying environmental and loading conditions to which a structure can be subjected during its lifetime, the possibility of other failure modes, such as debonding of the FRP reinforcement, should be considered. A clear understanding of the behavior at the interface between the concrete and the bonded FRP reinforcement is thus required.

The bond between concrete and FRP plates plays an important role in the strengthening of concrete structures. This bond is brittle and therefore exhibits little ductility at failure. Thus, failure of FRP plate-strengthened concrete structures may occur suddenly. In other words, adhesively bonded plates are highly prone to premature debonding or peeling. The most common forms of peeling, identified from tests on simply supported RC beams adhesively bonded with tension face plates, can be categorized as shear peeling, flexural peeling, combined flexural and shear peeling. To ensure the properties of the bond between concrete members and externally bonded FRP plates, the bond properties should be better understood.

1.2 Literature Review

With FRP composite materials being used increasingly in civil engineering applications, numerous experimental investigations and analytical studies have been carried out since the 1990s. This section presents a review of the state of the art and the related research work conducted to date.

1.2.1 Bond between Strengthening Materials and Concrete

With the development of technology to upgrade existing concrete structures using externally bonded FRP composites, a number of issues related to the conventional structural behaviors of concrete structures after being upgraded have been studied over the past decade. Among these issues has been a keen interest in clarifying the mechanisms of the interface bond between FRP composites and concrete substrates, because the bonding interface is relatively weak in comparison with the neighboring materials in the whole upgraded system. In most strengthening cases, the interface bond is critical for transferring stresses from the existing concrete structures to the externally bonded FRP composites. When a structural element is encircled in FRP composites, the mechanical role of the interface bond becomes less important, but it retains the function of maintaining the integrity and durability of the composite FRP-concrete systems. Therefore, strong understanding of the interface bond is a prerequisite for achieving a more reliable but rational design for concrete structures externally bonded with FRP composites.

Good bond properties are essential to the success of the external reinforcement technique for repairing or strengthening RC members. Swamy et al. [1.1], Van Gemert [1.2], and Kobatake et al. [1.3] conducted detailed investigations of the

properties of the bond between concrete and steel plates. These researchers used double-lap shear tests to determine the maximum and average shear stress values, the force distribution, and the mode of force transfer. Bizindavyi et al. [1.4], Chajes et al. [1.5], [1.6], and Neubauer and Rostasy [1.7] performed identical pull-out tests on composite-to-concrete joints. The aims of these investigations were to study the shear stress distributions of the bonded interface, to quantify anchorage lengths and to investigate the influence of the concrete strength and glue line thickness on the bond strength. The pull-out test results indicated that there is a measurable bond length beyond which no further increase in the transferred load can be achieved. This length has been shown to be a function of the properties and geometry of the specimens and to depend on the surface preparation.

1.2.2 Bond between FRP Sheets and Concrete

It can be said the macro-mechanical behavior of RC members upgraded with FRP sheets, including their fundamental failure modes and their effects on strength, capacity, and ductility, have been well established to date, based on a large number of experimental and analytical studies over the past decade. However, to achieve a refined design for concrete structures to be upgraded with FRP sheets, further study is needed into the fundamental issues, such as interfacial bond fracture mechanisms, selection of bonding or strengthening material, and design detailing. For reliable but rational and cost-effective use of FRP materials, refined upgrading designs should follow performance-based design concepts, for which the accuracy of predicting the performances of FRP-upgraded concrete members relies on accurate material laws, as well as advanced analytical methods.

The Japan Concrete Institute (JCI) established a technical committee on retrofitting technology (2001 to 2003), which focused on the interface bond properties between existing concrete structures and retrofitting materials for both adhesive bonding and overlaying retrofitting technologies. The objective of the committee was to gain insight into the micro- and macro-interfacial bonding mechanisms, the selection of the optimal interface materials and upgrading methods, the improved prediction of the performances of upgraded concrete structures, and, finally, the improvement of current upgrading techniques from both a construction and materials point of view. In general, the research topics on FRP sheet-concrete interfaces can be addressed by the following:

1. Parametric studies on interface bond, including the effects of all interface components: concrete, bonding layer, and FRP sheets;
2. Test methods for evaluating the interface bond properties;
3. Bond strength and anchorage design;
4. Failure mechanisms of interface bond and bond modeling;
5. Effects of interface bond on the member behavior of concrete structures after retrofitting;

6. Optimized design of interface bond;
7. Durability of interface bond.

For the past few years, external bonding of FRP sheets has emerged as a popular method for strengthening RC structures. In this strengthening method, the performance of the FRP-to-concrete interface in providing effective stress transfer is of crucial importance. Indeed, a number of failure modes in FRP-strengthened RC members are directly caused by the debonding of the FRP from the concrete. Therefore, for the safe and economical design of externally bonded FRP systems, a sound understanding of the behavior of the FRP-to-concrete interface needs to be developed.

The various debonding failure modes can be categorized as shear (mode II failure), tension (mode I failure), and a combination of shear and tension (mixed-mode failure).

① Failure of the FRP sheet-concrete bond under shear (mode II failure)

Various test methods, including the single-lap, double-lap, bending, and inserted shear bond tests (see Figs. 1.1-1.4), have been developed to characterize local interfacial shear bond behavior by studying the strain distribution in the FRP sheets or to evaluate the average interfacial bond strength. The interface parameters evaluated include the average shear bond strength, the effective bond length, the maximum shear bond stress, the interfacial fracture energy, and the local bond stress-slip relationship.

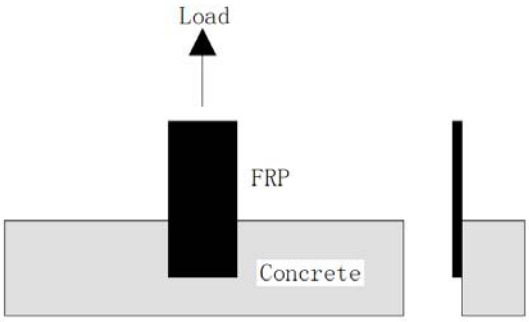

Fig. 1.1 Single-lap shear bond test

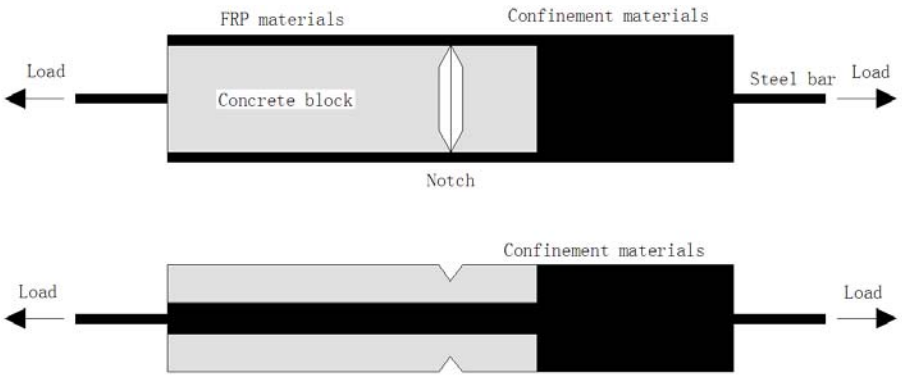

Fig. 1.2 Double-lap shear bond test

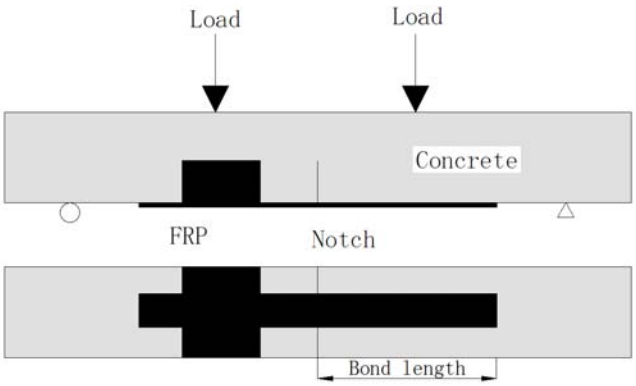

Fig. 1.3 Bending-type shear test

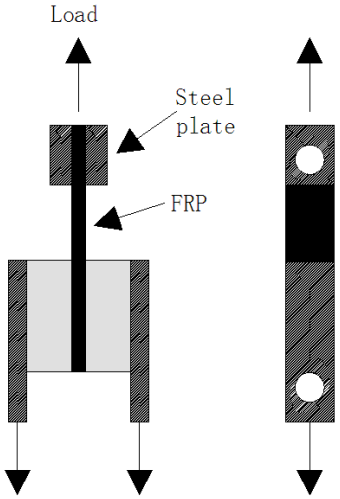

Fig. 1.4 Inserted-type shear bond test

② Failure of the bond between FRP sheets and concrete under tension (mode I failure)

Tensile tests for the interface between FRP sheets and concrete to verify the interface bond quality are easier to perform than shear bond tests. Three types of tensile test methods have been reported (Figs 1.5-1.7). Fig. 1.5 illustrates the direct tensile test method adopted by the "Design and Construction Guidelines for Continuous Fiber-Reinforced Concrete Structures'' of the Architectural Institute of Japan (AIJ). This method is convenient because it evaluates the interface bond qualitatively by observation. Figs 1.6 and 1.7 illustrate the three-point bending and wedge splitting tests, respectively [1.8]-[1.10]. These tests can be used to evaluate the Mode I fracture energy and the tension-softening diagram of FRP sheet-concrete interfaces. The bond properties of FRP sheet-concrete interfaces under tension can be examined parametrically and quantitatively using these two methods. Three-point bending tests have also been used to evaluate the bond degradation of FRP sheet-concrete interfaces after exposure to severe environmental and fatigue loading [1.11].

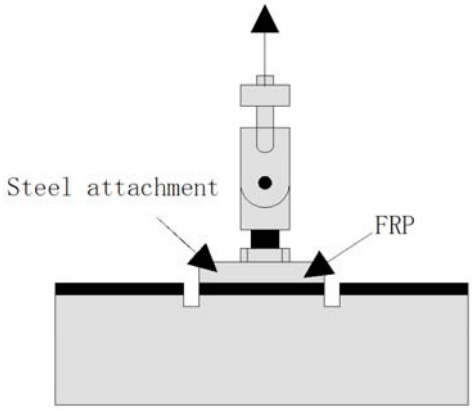

Fig. 1.5 Direct tension test

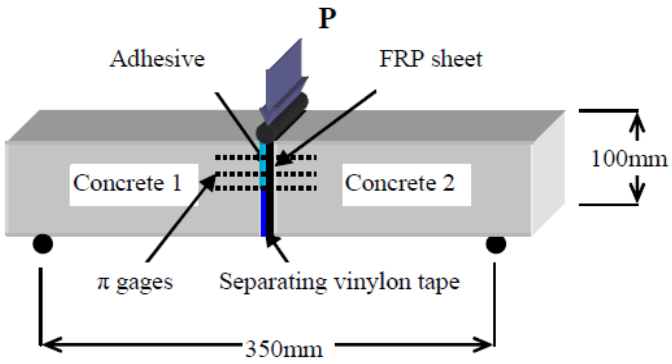

Fig. 1.6 Three-point bending test

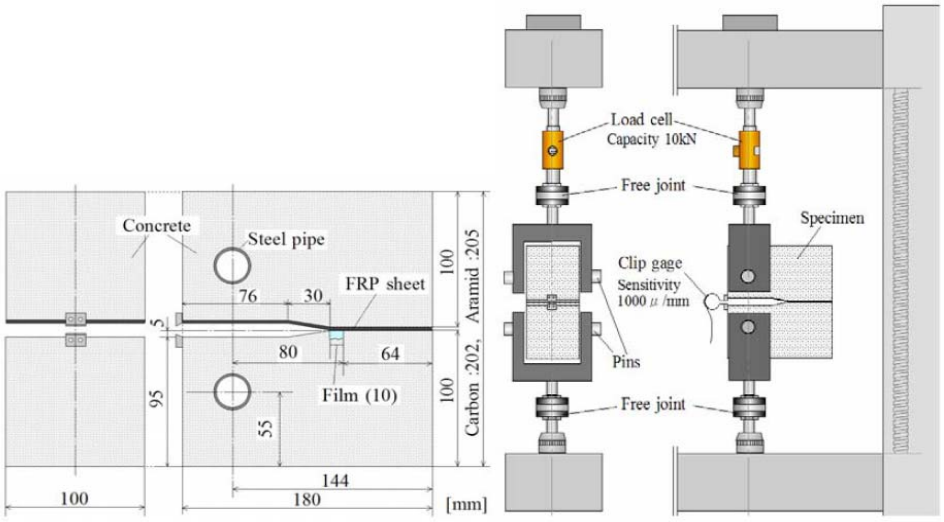

Fig. 1.7 Wedging splitting test

③ Failure of the bond between FRP sheets and concrete under a combination of shear and tension (mixed-mode failure)

A more representative interface bond failure for concrete structures retrofitted with FRP is a combined mode, given that FRP sheet-concrete interfaces are subjected to shear and tension simultaneously. Karbhari and Engineer developed a bond test

method to evaluate the bond between FRP composites and concrete under mixed-mode loading conditions by producing different interface peeling angles [1.12]. Another widely reported mixed-mode failure of the FRP sheet-concrete interface occurs in FRP-strengthened RC beams loaded in flexure [1.6 and 1.9]. The interface debonding may initiate at the tip of a shear-flexural crack, with peeling caused simultaneously by a crack opening in the longitudinal direction and crack sliding in the vertical direction.

A new application of FRP strengthening technology in Japan involves bonding FRP sheets to the bottom surfaces of tunnel linings or elevated bridges to prevent pieces of deteriorated concrete from falling. In these strengthening cases, the FRP sheet-concrete interfaces are subjected mixed-mode loading, as shown in Fig. 1.8. Two types of test methods have been used to determine the bond properties of interfaces under static loading conditions [1.13]-[1.15]. One is a beam-type dowel test for FRP sheet-concrete interfaces in which a one-directional FRP sheet is bonded to the bottom of a notched concrete beam (see Fig. 1.9). The other is a slab-type shear punching test in which a bidirectional rather than a unidirectional FRP sheet is attached to the bottom of a concrete slab. Two fundamental bond characteristics of FRP sheet-concrete interfaces under the dowel action are obtained from both types of tests: (1) the peeling angle is constant during the interface debonding process, and (2) the vertical force per unit width that an FRP sheet-concrete interface can bear is a constant value during the interface debonding process.

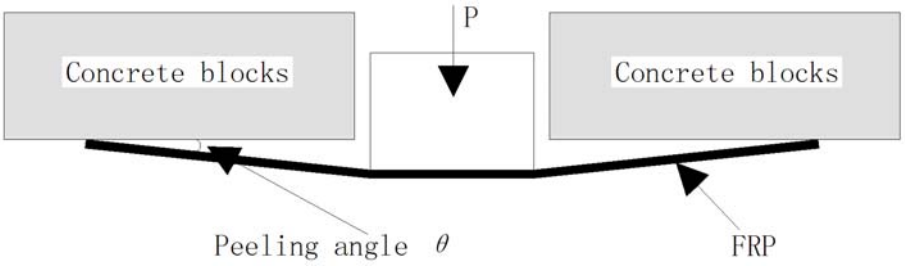

Fig. 1.8 Dowel test for the FRP sheet-concrete interface

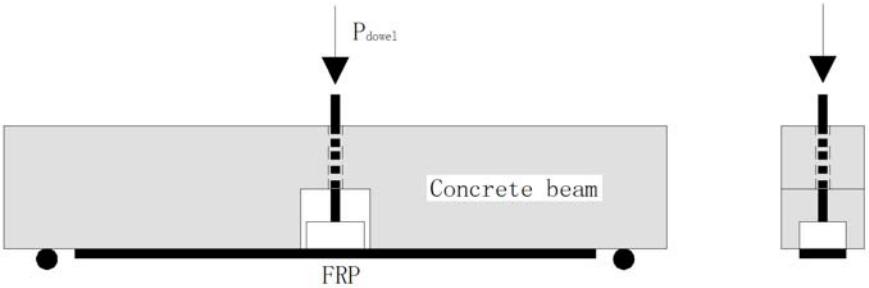

Fig. 1.9 Beam-type (one-directional sheet) dowel force test

Furthermore, a study of the shear-peeling bond strength between FRP sheets and concrete was performed by Md. Shah Alam et al. [1.16]. The specimens were designed for different step angles in the middle, to ensure that the interface acted under both shear and peeling conditions (see Fig. 1.10). Their study presented the experimental results of bond strength between FRP sheets and concrete interfaces

under both shear bond and peeling conditions. The results revealed that the bond strength decreased considerably due to the peeling effect. In addition, the step angle and fiber stiffness played important roles in bond strength for a combined effect. The highest bond strength was observed for the lowest axial stiffness of the laminate. Based on these test results, a modification was proposed to one of the existing bond strength models. The proposed modification improved the prediction of the bond strength between FRP laminate and concrete.

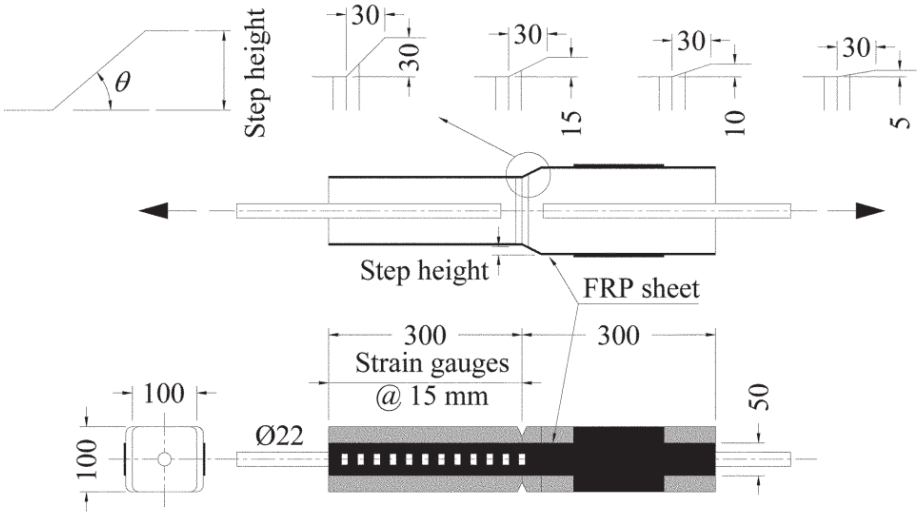

Fig. 1.10 Shear-peeling bond test

1.2.3. Bond between FRP Plates and Concrete

It has been several decades since traditional strengthening techniques, such as steel plate bonding, were used in renovation engineering to strengthen and retrofit reinforced concrete members. In recent years, FRP plates have been used as supplemental externally bonded reinforcement. The development of the carbon fiber-reinforced polymer (CFRP) plate bonding repair technique has shown to be applicable to many existing strengthening problems in the building industry, not only for strengthening but also for cases of rebuilding, as well as when mistakes have been made during the design or construction phase. This technique can be defined as one in which CFRP plates of relatively small thicknesses are bonded with an epoxy adhesive to, in most cases, a concrete structure, to improve its structural behavior and strength. The CFRP plates do not require much space, and they contribute to composite action between the adherents. The adhesive that is used to bond the plate to the concrete surface is a hardy two-component epoxy adhesive. Before FRP plates are bonded to the surface of the concrete, the surface should first be cleaned or sandblasted down to the aggregate to ensure a good bond between the concrete and FRP plates. The old structure and the new bonded material create a structural relationship that has greater strength than the original structure.

As they are increasingly used with FRP materials, CFRP plates not only have been used to strengthen reinforced concrete beams or girders with deficient flexural/shear

strength, but they also have been introduced to strengthen deteriorated slabs, masonry wall, bridge girders, and piers. Using FRP wraps around concrete columns, the load capacity can be improved by lateral confinement [1.17]-[1.18]. For the flexural strengthening of concrete beams, FRP plates are bonded to the tension face using epoxy-based adhesive, which increases both the strength and stiffness of the beams [1.19]-[1.21]. For shear strengthening, FRP plates are bonded to both sides of the RC beam to provide an additional contribution to its shear capacity [1.22].

Since the 1990s, many experimental studies of RC beams strengthened with FRP plates have been conducted all over the world [1.23]-[1.29]. These experimental investigations have focused on the following three aspects, according to their research objectives:

1. Investigations focusing on the shear strengthening of RC beams;
2. Investigations related to the flexural strengthening of RC beams;
3. Investigations emphasizing the interfacial properties between concrete and FRP plates.

In all, the bonding of FRP plates on tensile surfaces has been proved to be an effective method for increasing both the strength and stiffness of concrete members. For a flexurally strengthened RC beam under external loading, the beam can fail by FRP debonding from the bottom of a major flexural crack in the span. This failure mode can also be found in FRP-strengthened, one-way slabs. Debonding failure is induced by the presence of high shear stress concentrations at the interface around the bottom of the flexural cracks. With an increasing external load, the interfacial crack propagates toward the plate end until final failure is reached. It is usually observed that the failure occurs in the concrete, and a thin layer of concrete is attached to the surface of the debonded FRP plate. Hence, for concrete members strengthened with externally bonded FRP, the concrete/FRP interfacial behavior should be an important focus of investigation.

1.2.4. Fatigue Characteristics of FRP-Strengthened Concrete Elements

Recently, many structures, such as bridges, have failed to meet structural and functional requirements as a result of corrosion, the expansion of fatigue cracks, and improper maintenance. In most cases, these types of damage only occur within certain areas of the structure, and the cost of strengthening the structure is much less than the cost of replacing the whole structure. Traditional retrofitting methods typically involve welding, bolting, or riveting steel plates to the damaged location. These methods have several drawbacks, such as the weight that the steel adds to the structure, the fatigue sensitivity of weld defects, stress concentrations, and stress redistribution. FRP possesses notable advantages as a structural material, including high strength, good corrosion resistance, and better fatigue performance than steel.

Therefore, FRP has been widely applied in strengthening and repairing concrete structures.

Wight and Erki (2001) [1.30] studied the fatigue of prestressed CFRP sheets used to strengthen concrete slabs. Six one-way, reinforced concrete slabs were constructed and tested to investigate the effectiveness of using prestressed CFRP sheets for strengthening concrete slabs subjected to fatigue loading. The test results confirmed that strengthening reinforced concrete slabs with bonded CFRP sheets, especially prestressed CFRP sheets, increased fatigue life. Strains in the steel reinforcement, plastic creep strains in the concrete, and deflections all decreased. Crack widths were greatly reduced when the CFRP sheets were prestressed.

Additionally, some key investigations [1.31]-[1.33] have clearly shown that FRP-strengthened reinforced concrete beams have performed better in terms of fatigue than their non-strengthened companions. In most cases, it has been observed that the failure of FRP-strengthened beams is initiated by successive yielding of the reinforcing steel under tension in one or several locations, culminating in the fatigue rupture of the bars [1.31]. Whenever debonding of the FRP laminate occurred, it was considered to be a secondary failure mode, resulting from the yielding and rupture of the reinforcing steel, as well as excessive widening of the cracks. Based on the results reported by Heffernan (1997) [1.31], it appears that the fatigue life of a concrete beam depends mainly on the fatigue of the tension steel-reinforcing bars, provided that the serviceability of the beam (cracking in the tension region) is negligible. Barnes and Mays (1999) [1.33] suggested that a reasonable criterion for design would be to expect that, for a plated beam, the fatigue life would be the same as that of a comparable non-strengthened beam, as long as the resulting stress amplitudes in the tension steel reinforcing bars remained identical. However, they cautioned that, as far as the fatigue performance is concerned, there could be a shift in failure mode from reinforcing-steel-dominated failure (for under-reinforced members) to bending or shear-dominated failure modes for over-reinforced members.

To evaluate the effectiveness of epoxy-bonded FRP in prolonging the fatigue lives of concrete structures, some researchers have conducted studies on the fatigue behavior of concrete structures strengthened with FRP and have found that FRP can significantly extend the fatigue lives of concrete structures while effectively reducing the crack growth rate. [1.34]-[1.36]

The fatigue durability of FRP-concrete interfaces is another important issue. Fatigue failures of reinforced concrete members are usually governed by the fatigue fracture of the reinforcement rather than debonding of the FRP from the concrete substrate. However, cyclic loading tests on FRP-concrete bonded interface have shown that interface debonding propagates progressively as the number of fatigue cycles increases. [1.37] An FRP-concrete interface with sufficient anchorage length may retain its interface bonding capacity after the number of cycles expected to cause

fatigue failure. Nevertheless, progressive local interface delamination adversely affects the serviceability of FRP-strengthened members and may trigger a deterioration with a combination of failure modes. This possibility underscores the necessity of studying the fatigue performance of FRP-concrete bonded interface in which the concrete substrate has debonded as a result of a combination of fracture modes.

Studies of the fatigue behaviors of FRP-to-concrete joints were undertaken by Bizindavyi et al. (2003) [1.36]. In that research, the method used to bond the FRP laminates to the concrete blocks consisted of in-place bonding and curing of the GFRP fabric and CFRP sheets directly on the concrete. The concrete surface was first sandblasted and then cleaned by air blasting. During the preparation of the specimens, a relatively uniform thickness of 1-1.2 mm of adhesive layer was assured using aluminum guides. The bonded joints were allowed to cure for a minimum of 14 days before the cyclic bond tests were performed. Bizindavyi et al. presented results from an experimental investigation of a bonded FRP-to-concrete interface under fatigue loading. The results for the effects of fatigue loading on slip at the FRP-concrete interface, crack opening, and strain profiles along the bonded FRP joint were presented and discussed. A power-law expression for the so-called "*S*-*N*" curves (cyclic stress ranges versus numbers of cycles to failure) was proposed, and the parameters in this expression were determined from the experimental data. The influences of various parameters, such as bond length, bond width, and cyclic bond stress levels, on fatigue behavior were discussed.

To date, no appropriate studies have been published that have described mixed-mode fractures of the FRP plate-concrete interface under fatigue-loading conditions. In general, mixed-mode fracture failure can be suppressed by limiting the opening of shear cracks. Therefore, it is important to investigate mixed-mode failure debonding due to shear crack opening, based on the action of FRP plates in experimental tests of FRP-reinforced RC beams. Thus, it is important to conduct fatigue tests in which shear cracking affects the flexural strengthening efficiency of FRP plates.

1.3. Objective and Scope

Although research on the bond behavior of FRP-strengthened concrete elements under static and fatigue loading has been extensively studied, as described earlier, the substantial existing research on the bond behavior of FRP-strengthened concrete elements has not focused much attention on the characteristics of debonding in fatigue. Therefore, the principal objective and scope of this thesis research are as follows:

First, the characteristics of mixed-mode (shear and peeling) debonding due to shear crack formation in beams flexurally strengthened by CFRP plates and subjected to static and fatigue loading were investigated.

Next, fatigue testing of double-faced shear bond specimens was carried out to examine the fatigue bond behavior of CFRP plate-concrete systems. The fatigue failure of the bond surface between CFRP plates and concrete can be characterized by an *S-N* diagram representing the relationship between the ratio of the upper limit of fatigue loading to calculated bond strength and the number of cycles to failure, based on the results of experiments conducted to investigate the influence of different concrete strengths and the levels of the upper limit of fatigue loading. The different debonding modes that occur at the fracture interface were also observed. Furthermore, the effect of peeling behavior on fatigue damage was examined.

Finally, an experiment was conducted to examine the bond behavior of CFRP plates and concrete systems in combined fracture mode (peeling and shear) using initial-angle double-lap shear bond specimens. The specimens were designed for different initial angles at the middle of the specimen to ensure that the interface acts in both shear and peeling. A calculation method is proposed for prediction of the bond strength between a CFRP plate and concrete under combined shear-peeling fracture conditions.

1.4 Outline of the Thesis

The work reported in this thesis addresses the development of a comprehensive approach to understanding the bond and peeling behavior of CFRP plate-strengthened concrete structures under fatigue loading.

The following is a brief description of the contents of each chapter in the thesis:

Chapter one introduces the research background on structural strengthening and rehabilitation using FRP composites in place of other materials and reviews the literature on the use of FRP composite materials to strengthen concrete structures. The research objectives are enumerated, and the research approach is described. Finally, the aims and outline of this doctoral thesis are introduced.

Chapter two introduces experimental investigations of CFRP plate debonding behavior using beam specimens flexurally strengthened by CFRP plates and relative vertical displacement imposed on the two sides of a shear crack in each beam. The test results confirm the effectiveness of mixed-mode (shear-peeling) debonding in CFRP plates and local debonding with peeling off as an important factor affecting the fatigue life of concrete structures strengthened by CFRP plates.

Chapter three describes fatigue loading tests of double-faced bond specimens, carried out to investigate the influence of bond behavior for different concrete strengths, different types of CFRP plates and different levels of the upper limit fatigue load. The test results show that the fatigue behavior of the bonding surface between a CFRP plate and concrete can be characterized by an *S-N* diagram representing the

relationship between the upper limit of the bond stress and the number of load cycles at debonding. To clarify the fatigue bond damage and predict the fatigue life of the bond, a bond-slip model based on fatigue cycles (N) and the unloading branch stiffness (k_i) in slip was developed. In addition, the transverse displacement in the CFRP plates and the concrete substrate was measured. The variation in transverse displacement exhibited an obvious discernible peeling phenomenon with debonding propagation. The experiment results indicate that the CFRP plate, upon peeling off, moved from the specimen center to the loading end as the number of fatigue cycles increased. The peeling off of the CFRP plate is an important failure mode affecting the debonding progress in the fatigue test.

Chapter four presents the experimental results and the calculation method for analyzing the bond strength between CFRP plates and concrete interfaces debonded by both shear and peeling. Twenty-two special double-faced rectangular shear specimens with CFRP plates bonded on two sides were tested in uniaxial tensile loading. The specimens were designed for various initial angles at the middle to ensure that the interface acts in both shear and peeling. Three concrete compressive strengths were used in this investigation. The results revealed that the bond strength decreases considerably due to the peeling effect. In addition, the initial attachment angle plays an important role in the bond strength, combined with the angle effect. Based on the test results, a calculation method is proposed based on modifying one of the existing bond strength models for the FRP sheet-to-concrete bonding system. The proposed modification can accurately predict the bond strength between CFRP plates and concrete.

Chapter five summarizes the thesis with a retrospective view of the research objectives and presents the conclusions drawn from the work. Recommendations for future research are also highlighted in this chapter.

CHAPTER 2

CFRP Plate Debonding Behavior in Flexurally Strengthened RC Beams

2.1 Introduction

The plate bonding technique is now established as a simple and convenient repair method for enhancing the flexural performance of concrete structures and bridge beams and slabs in particular. The advantages of this technique are that the work can be carried out while the structure is still in use and that it is economical compared to other methods. Traditionally, steel plates have been used, but there are problems associated with using steel plates as external reinforcement for existing concrete structures, including the need for careful surface preparation of the steel prior to bonding, uncertainty regarding adhesive bond durability and potential corrosion at the steel-adhesive interface, the awkwardness of maneuvering heavy steel plates, the resulting need for restrictions on plate length and the need for many lapped joints, the need for anchor bolts, and maintenance painting. FRP plates do not suffer from corrosion problems, and most of their mechanical and physical properties are better than those of steel.

However, in external reinforcement of a reinforced concrete beam, debonding may be induced by a major flexurally or shear-induced crack in the span. Under such conditions, there is a relative vertical displacement on the two sides of the major crack. The FRP plate is then subject to both tensile and peeling forces, resulting in a combination of shear sliding and opening displacement along the FRP-concrete interface. In this investigation, the combined effects of tensile and peeling on CFRP plate debonding are studied.

Bonding of FRP plates to the tensile side has been demonstrated to be an effective strengthening method for flexurally strengthened RC beams. Different failure modes for RC beams strengthened with FRP plates have been reported in several experimental investigations (Ritchie et al. 1991[2.1]; Saadatmanesh and Ehsani 1991[2.2]). The failure modes are summarized as follows and illustrated in Fig. 2.1:

(1) Rupture of the FRP plate at the mid-span,
(2) Concrete crushing in the compression zone,
(3) Shear failure,
(4) Concrete cover separation,
(5) Plate end interfacial debonding, and
(6) Intermediate crack-induced debonding failure.

FRP rupture and concrete crushing can be considered flexural failures, whereas concrete cover separation, plate end debonding, and intermediate crack-induced debonding can be considered local failures.

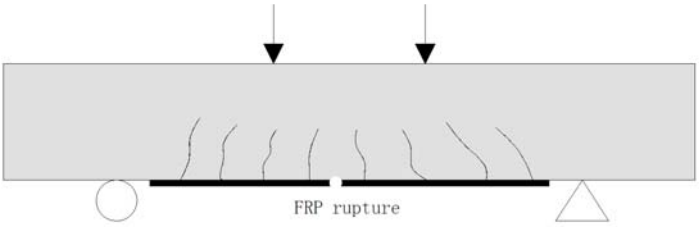

(a) FRP rupture

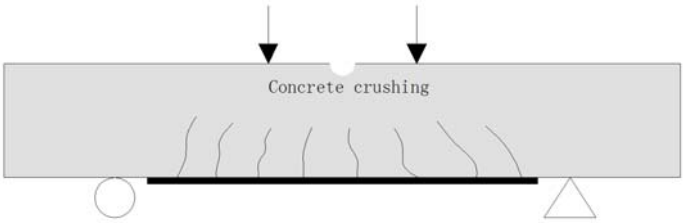

(b) Crushing of compression concrete

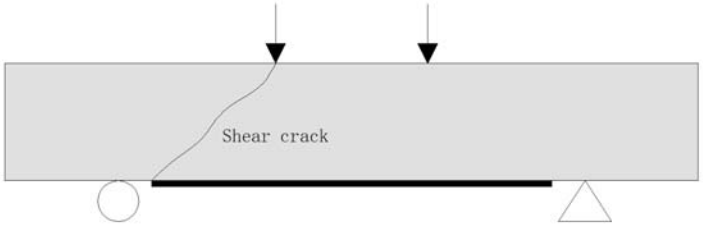

(c) Shear failure

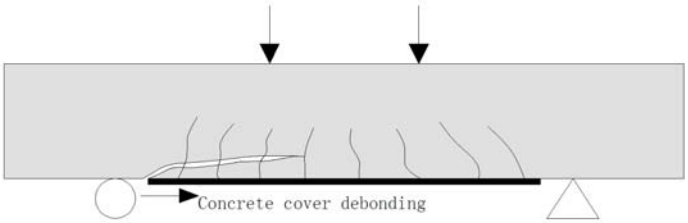

(d) Concrete cover separation

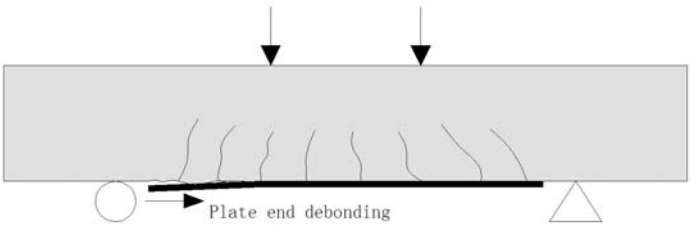

(e) Plate end interfacial debonding

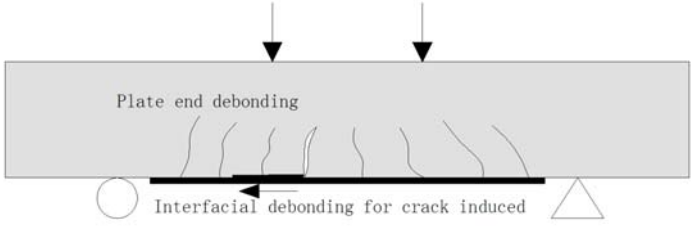

(f) Crack-induced debonding

Fig. 2.1 Possible failure modes for FRP-strengthened RC beams

Early studies in this area focused on analyzing failure modes due to concrete crushing or FRP plate rupturing. When the ultimate failure of the strengthened beam results from flexural failure (concrete crushing or rupture of the FRP plate), the ultimate load-carrying capacity can be calculated from conventional section analysis for the concrete members (Wei et al. 1991 [2.3], Triantafillou and Plevris 1992 [2.4]). However, the failure mechanisms of local failures are more complicated than those of flexural failures.

Concrete cover separation is often observed in experimental investigations of concrete beams strengthened by externally bonded FRP plates. It is accepted that this failure mode is induced by the formation of a crack at or near the plate end due to the high interfacial shear and normal stress concentrations caused by the abrupt termination of the FRP plate. Once a crack occurs in the concrete near the plate end, the crack will propagate to the level of the tension reinforcement and extend horizontally along the bottom of the tension steel reinforcement. As the external load increases, the horizontal crack may propagate to cause the concrete cover to "peel off" with the FRP plate.

In addition, in plate-end debonding failure, FRP debonding initiates from the plate end and propagates toward the mid-span of a concrete beam. Plate-end debonding failure is considered to be induced by high interfacial shear and normal stresses at the concrete-adhesive interface near the plate end. Upon debonding, a thin layer of concrete generally remains attached to the FRP plate, indicating that the failure occurs on the concrete side of the concrete-adhesive interface. This debonding failure is considered to be governed mostly by the material properties of concrete.

The plate end is not the only possible location at which debonding failure can be initiated. Debonding can also occur in the vicinity of flexural or shear cracks in concrete beams, as shown in Fig. 2.2. When FRP-strengthened RC beams are loaded in flexure, flexural/shear cracks tend to open and induce high interfacial shear stress, which leads to the initiation of FRP debonding from the concrete substrate. The propagation of the crack from the bottom to the plate end will lead to the ultimate failure of the strengthened beam.

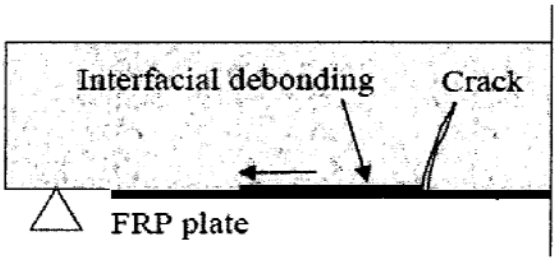

Fig. 2.2 Major crack-induced debonding

Many studies have been performed to understand the bond characteristics between concrete and FRP sheets under different test conditions (for example, the single shear

test, the double shear test, the direct tensile test, the modified beam test, and the test with curvature in beam). However, the laminate-concrete interface is susceptible to the relative vertical displacement of the shear cracks in the beam. This displacement can lead to the delamination or peeling of the FRP sheet from the concrete. Some authors have reported that retrofitted beams could fail due to the failure of the concrete layer between the FRP sheet and steel or due to the delamination or peeling of the FRP sheet from the concrete. Karbhari et al. [2.5] conducted a pure peeling test to determine the bond strength between concrete and FRP sheets. Triantafillou and Plevris [2.6] proposed a model for the peeling of debonding mechanisms. However, CFRP plate-concrete bonding systems subjected to combination of fracture have not been studied often.

Furthermore, the fatigue durability of FRP/concrete interfaces is another important issue. It was reported that the fatigue life of RC members increased after FRP strengthening. The fatigue failures of strengthened members are usually governed by the fatigue fracture of steel reinforcement, rather than the overall debonding of FRP from the concrete substrate. However, cyclic loading tests of the FRP/concrete bonded interface showed that interface debonding propagates progressively with increases in fatigue cycles. An FRP/concrete interface with sufficient anchorage length could keep its interface bonding capacity after expected fatigue cycles. Nevertheless, progressive local interface peeling adversely affects the serviceability of FRP-strengthened members and could trigger brittle failure combined with fracture (shear and peeling). This observation implies the necessity of studying the fatigue performance of FRP/concrete bonded interfaces subjected to shear and peeling. Therefore, the objective of this research was to study the interfacial bond behavior between FRP plates and concrete for combined shear and peeling conditions under fatigue loading.

As stated previously, local debonding results from the delamination induced by the opening (Mode I) of a flexural shear crack and the existence of a relative vertical displacement between the two sides of the crack. Furthermore, as the number of loadings increases, the crack will tend to propagate due to crack opening. Therefore, the load condition is another important factor that affects local delamination under the combination of flexure and shear.

In chapter 2, the CFRP plate–concrete bonding system has been applied for flexurally strengthening the RC beam to investigate fatigue local debonding characteristics based on deflections changing responded to peeling off in CFRP plate between concrete surface and CFRP plate surface during shear span.

2.2 Outline of Experiment

2.2.1 Test Specimens

Three RC beams, named RC-S, CS-S, and CS-F, were fabricated in the laboratory. The RC-S and CS-S beams were tested to confirm shear failure according to the initial design and to serve as control beams to evaluate the maximum load level in the fatigue testing of beam CS-F.

The beams were 150 mm wide, 235 mm high and 2,200 mm long. The tension and compression bars consisted of three 19-mm-diameter and two 10-mm-diameter steel reinforcing bars. All beams were provided with shear reinforcement consisting of 6-mm-diameter bars spaced 125 mm apart for two shear spans. The stirrup ratio was 0.34%. The dimensions and cross-sectional details of the test beams are shown in Fig. 2.3. The beams were designed for major failure in shear. Two of the beams were strengthened with CFRP plates at the bottom, and all of the beams were strengthened with CFRP sheets on the sides of the beams, as shear failure only occurred on the opposite side. All of the beams were tested in four-point bending. Beams RC-S and CS-S were tested under static loading, and beam CS-F was tested under fatigue loading.

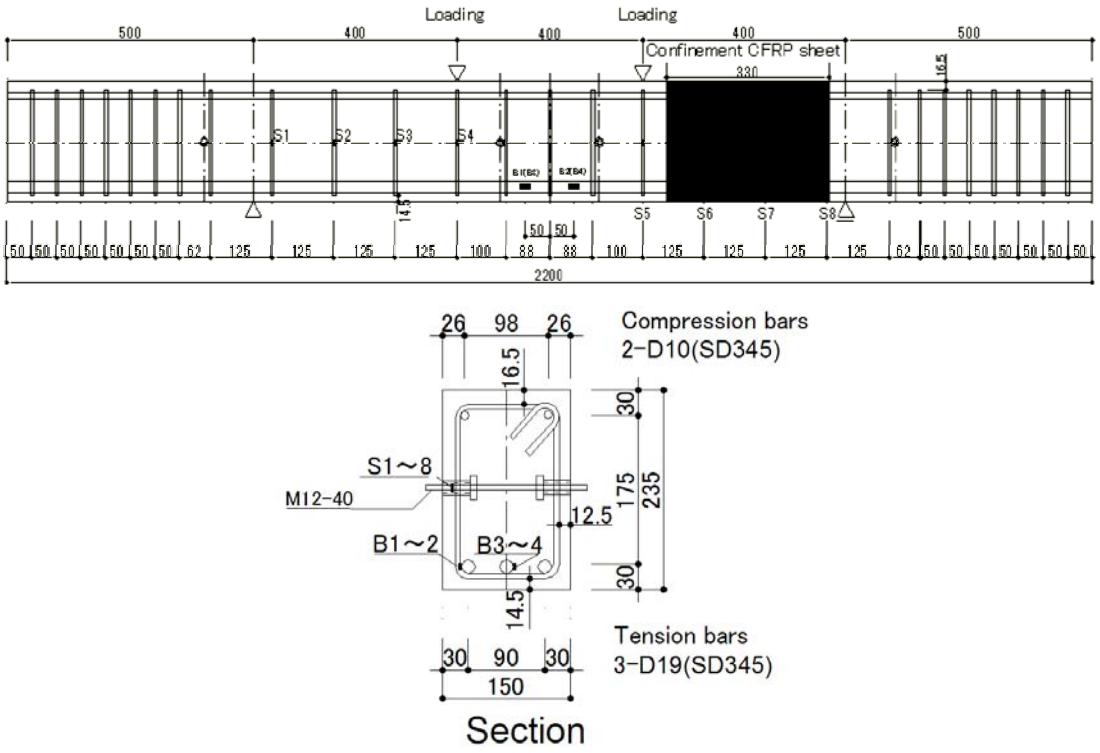

Fig. 2.3 Specimen details

2.2.2. Material Properties

The concrete was determined, by testing of 100 × 200 mm cylinder test specimens. The compressive strength was 22.8 MPa. The mechanical properties of the concrete are summarized in Table 2.1. The tensile test results for the main bars and the stirrups are listed in Table 2.2, and the stress-strain relationship is shown in Fig. 2.4. The CFRP plates had a thickness of 1 mm and a width of 50 mm. The area of the cross section was 50 mm^2. The ultimate strength and elastic modulus of the CFRP plate were 2,400 MPa and 156 GPa, respectively. The ultimate tensile strain was 1.54%. The CFRP plate properties are those reported by the manufacturer.

Table 2.1 Mechanical properties of concrete

Concrete	Compressive strength σ_B (MPa)	Splitting strength σ_t (MPa)	1/3 Secant modulus E_c (GPa)
Fc 21	22.8	2.19	22.9

Table 2.2 Mechanical properties of reinforcing bar

Type	Note	Tensile strength (MPa)	Yield strength (MPa)	Elastic modulus (GPa)	Elongation (%)
D6(SD295)	Stirrup	517	367*[1]	176	-*[2]
D10(SD345)	Compression bar	553	390	190	22.9
D19(SD345)	Tension bar	588	397	185	22.0

*[1]:0.2% offset strength; *[2] rupture outside marks

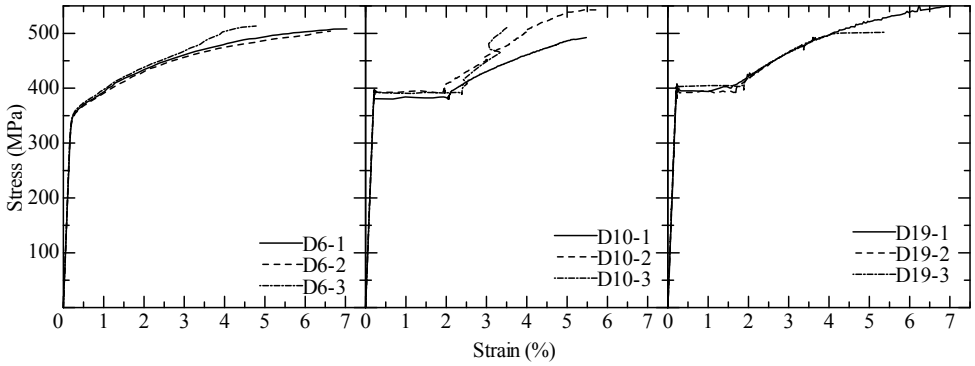

Fig. 2.4 Stress-strain relationship of the reinforced steel

2.2.3 Loading and Measurement

Beams RC-S and CS-S were tested under static loading, and beam CS-F was tested under fatigue loading. Previous research has clearly demonstrated that FRP-strengthened structures present better fatigue performance than unstrengthened

structures. In most cases, it has been observed that the failure of the structure is initiated by successive yielding of the reinforcing steel in tension, in one or more locations. When debonding of the FRP laminate occurred, it was considered to be a secondary failure mode resulting from the yielding and failure of steel rebar. The objective of this research is to investigate the bond and peeling characteristics between concrete and CFRP plates under fatigue loading. An upper limit fatigue load greater than those that would be observed in the field was selected to ensure fatigue-dominated responses. The target upper limit of fatigue load was selected — a "high upper limit fatigue load," the fatigue life of which should be shorter. Additionally, the shear crack opening increased obviously due to the high upper limit fatigue load, and the mixed-mode debonding induced by the shear crack phenomenon can be observed clearly.

Therefore, in this test, the upper and lower load limits were chosen to correspond to 90% and 6%, respectively, of the experimental maximum load of the static-load specimen CS-S. The fatigue load was applied as a 1-Hz sine wave of constant amplitude. This frequency was selected because conventional infrastructure elements such as bridges typically face loading at varying frequencies between 1 and 5 Hz.

High upper limit fatigue load typically implies that the maximum load exceeds the service load levels of the beams [2.7]-[2.10] and occasionally exceeds the yield capacity of the unstrengthened beams [2.11]-[2.13]. The benefit of these high upper limit fatigue load applications is that relatively rapid fatigue failure of FRP plate-strengthened beams (i.e., low cycle fatigue) can be observed. Therefore, in our experimental investigation, high upper limit fatigue load was applied.

Displacements were measured at the mid-span, the loading points, and positions D4 to D11 to compare the deflection differences of the concrete substrate and the CFRP plate to confirm debonding. A load cell integrated into the actuator system was used to record the loads and control the test. A schematic of the instrumentation used is shown in Fig. 2.5. Strains were measured on tensile bars at the mid-span (strain gauges B1, B2, B3, and B4 in Fig. 2.3) and at the stirrup strains (S1, S2, S3, and S4). Strains were also measured on the CFRP plate surface, using 2-mm-long strain gauges.

In fatigue testing, full-cycle recordings were obtained for the following cycles: at the 1st cycle and every 20th cycle up to 200 cycles, at every 200th cycle up to 1,000 cycles, at every 1,000th cycle up to 10,000 cycles, at every 10,000th cycle up to 100,000 cycles, and at every 80,000th cycle up to 1,000,000 cycles.

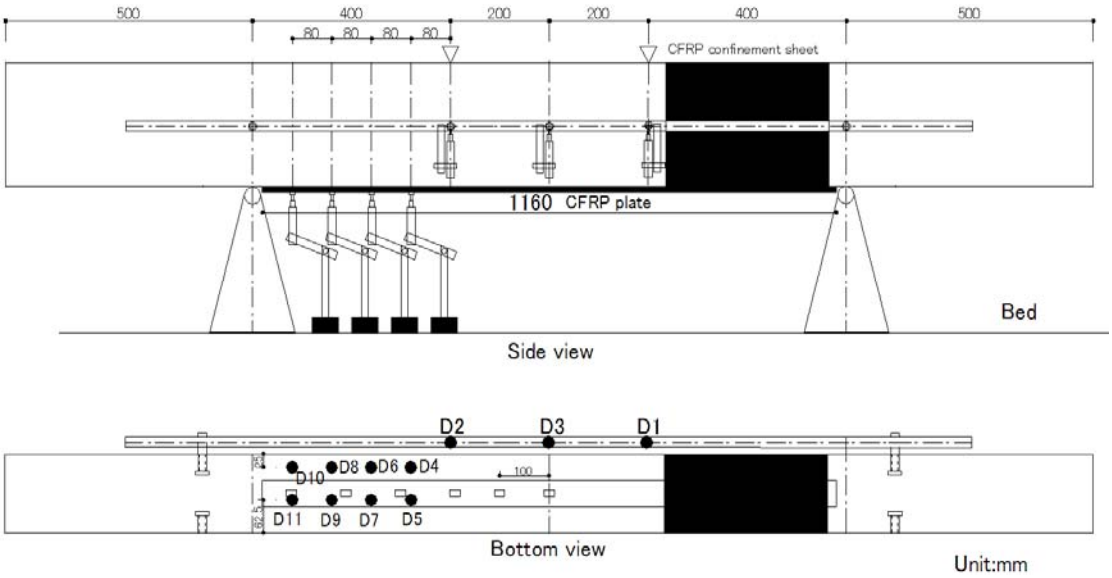

Fig. 2.5 Test setup

2.3 Experimental Results and Discussions

2.3.1 Static Test Results for Specimen RC-S

Specimen RC-S failed in shear, as shown in Fig. 2.6. Fig. 2.7 shows the load-deflection relations. The deflection increased from D1 to D2 due to the shear deformation of the left-side span.

Table 2.3 lists the shear capacities calculated using the procedures given in the AIJ, JSCE, and ACI codes. [2.14]-[2.16] The JSCE and ACI codes yield conservative estimates for the shear capacity of the specimen, compared to the AIJ code. The estimate from the AIJ code agreed well with the test result.

Fig. 2.6 Failure mode of specimen RC-S

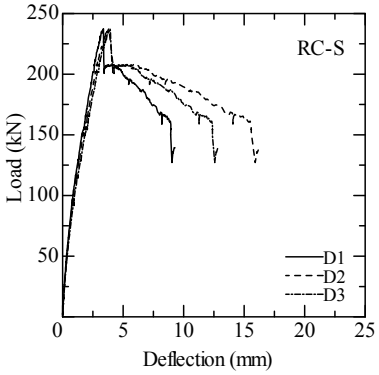

Fig. 2.7 Load-versus-deflection relation at the given cycle

Table 2.3 Comparisons of the values calculated with standard codes

Specimen	AIJ code V_{cal} (kN)	JSCE code V_{cal} (kN)	ACI code V_{cal} (kN)	Experimental result V_{exp} (kN)
RC-S	201.8 (1.18)*	157.7 (1.50)*	143.0 (1.66)*	237.3

* V_{exp}/V_{cal}.

Fig. 2.8 presents the load-strain relationship for the stirrups at positions S1 to S4. As shown in the figure, the stirrup strains at positions S2 and S3 reached the yield strain of 2,085 μ.

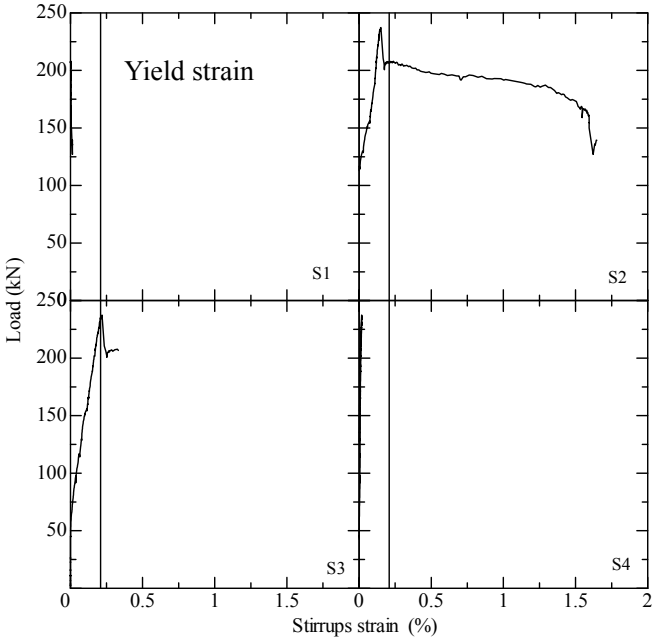

Fig. 2.8 Load-versus-stirrup strain relationship

2.3.2 Static Test Results for Specimen CS-S

Fig. 2.9 presents the failure mode of specimen CS-S. This specimen failed in shear, and peeling off of the CFRP plate from the concrete substrate at the region of the shear crack was observed. In other words, the delamination of the CFRP plate was induced by the opening up (Mode I) of a shear crack, and a relative vertical displacement occurred between the two sides of the crack, thus confirming the mixed-mode (peeling and shear) debonding induced by a shear crack.

Fig. 2.9 (a) Failure mode of specimen CS-S

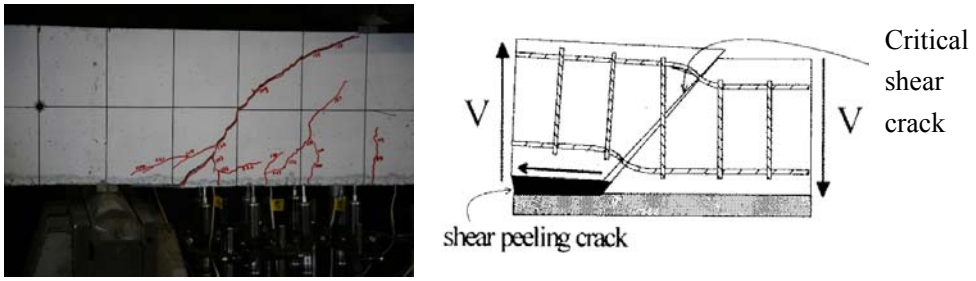

Fig. 2.9 (b) Shear peeling mechanism due to shear crack

The load-deflection relationship is shown in Fig. 2.10. The deflection increased from D1 to D2 due to the shear deformation of the left-side span as in the case of specimen RC-S. Furthermore, it can be seen that the differences in the comparison of D8 and D9 and the comparison of D10 and D11 in response to the peeling off of the CFRP plate were confirmed.

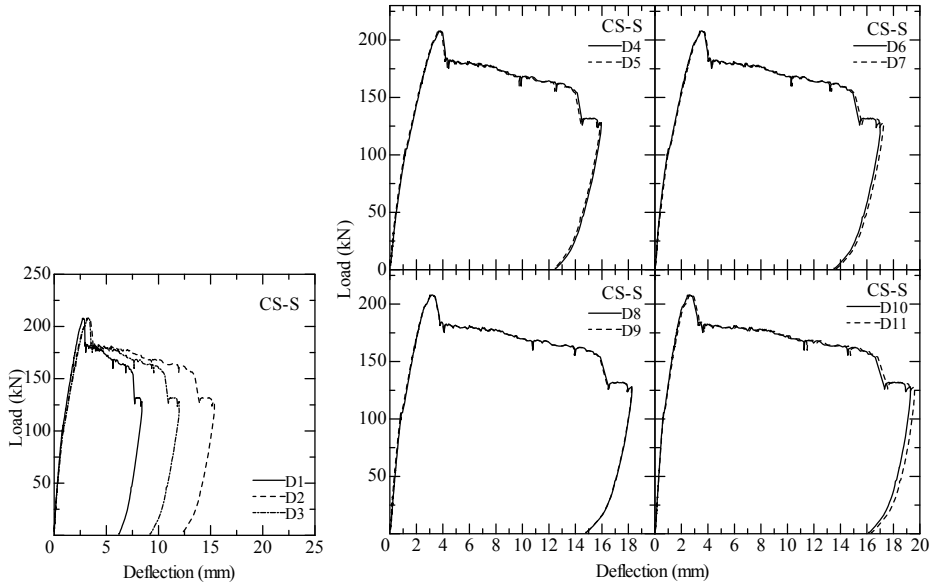

Fig. 2.10 Load-versus-deflection relationship at the given positions

Table 2.4 shows a comparison of the shear capacities calculated from the AIJ code, JSCE code, and ACI code procedures and the test results. In comparison to the experimental results for Specimen RC-S, a lower peak load was observed for Specimen CS-S.

Table 2.4 Comparison of experimental results with values calculated from procedures in standard codes

Specimen	AIJ code V_{cal} (kN)	JSCE code V_{cal} (kN)	ACI code V_{cal} (kN)	Experimental result V_{exp} (kN)
CS-S	201.8 (1.03)*	157.7 (1.32)*	143.0 (1.45)*	207.9

* V_{exp}/V_{cal}.

The load-tension bar strain and load-stirrup strain relations are shown in Fig. 2.11. All of the measured strains increased with increasing load in the tension bars. However, none of the measured tension bar strains reached the yield strain of 2,146 μ at the maximum load. For the load-stirrup strain relation, the S2 strain reached a yield strain of 2,085 μ.

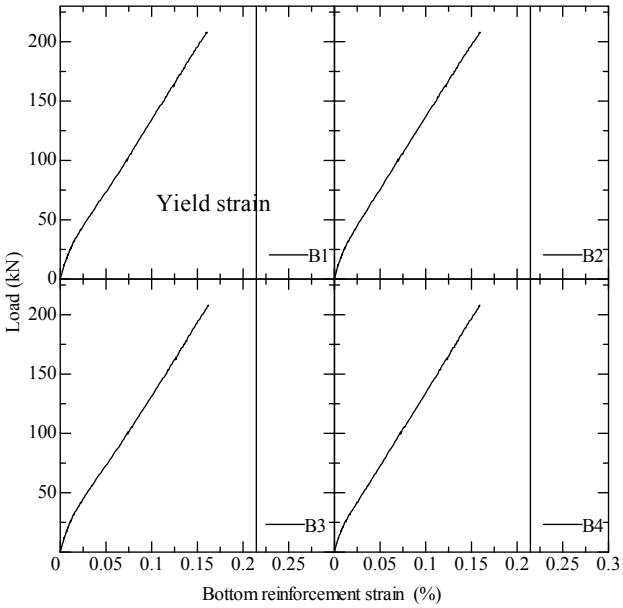

(a) Bottom reinforcement

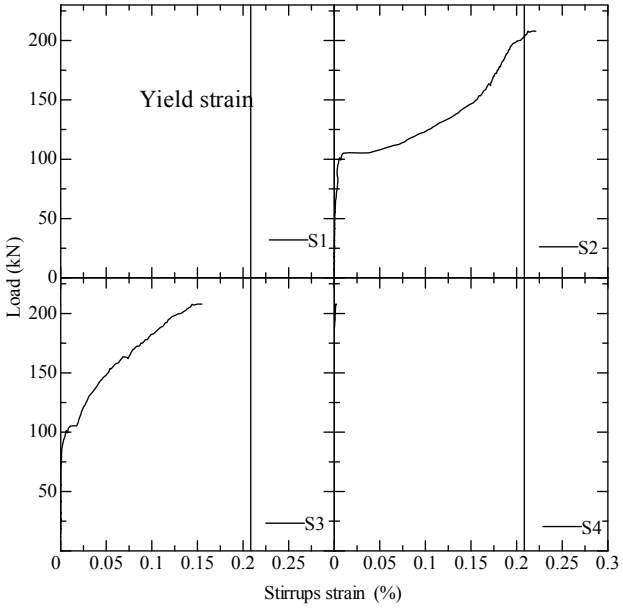

(b) Stirrup

Fig. 2.11 Load-versus-strain relationship

The strain distribution of the CFRP plate is shown in Fig. 2.12. As this figure shows, strains increase as the load increases. In addition, within the flexural span (0-200 mm), the same trend of a small decrease in strain along the plate with increasing load is evident. However, within the shear span (200-500 mm), a sudden decrease in strain is observed with increasing load near the edge of beam, due to peeling of the CFRP plate.

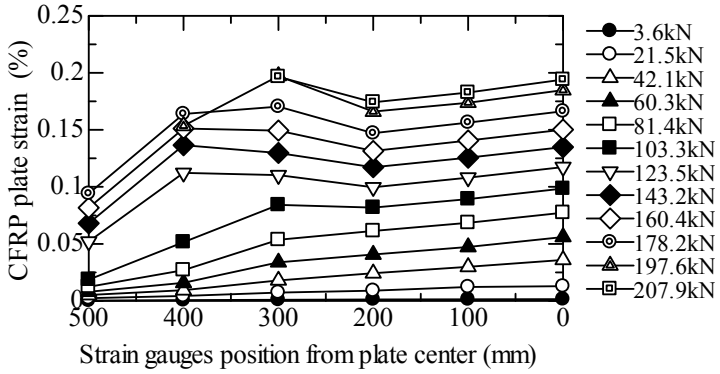

Fig. 2.12 CFRP plate strain distribution

2.3.3 Fatigue Test Results for Specimen CS-F

Fig. 2.13 shows photos of the specimen at the 1st, 100th, 1,000th, and 2,800th load cycles. The results of the fatigue test indicate that the specimen failed in shear at 2,800 fatigue cycles. The mixed-mode debonding phenomenon was observed around the position of the shear crack produced at the bottom of the beam.

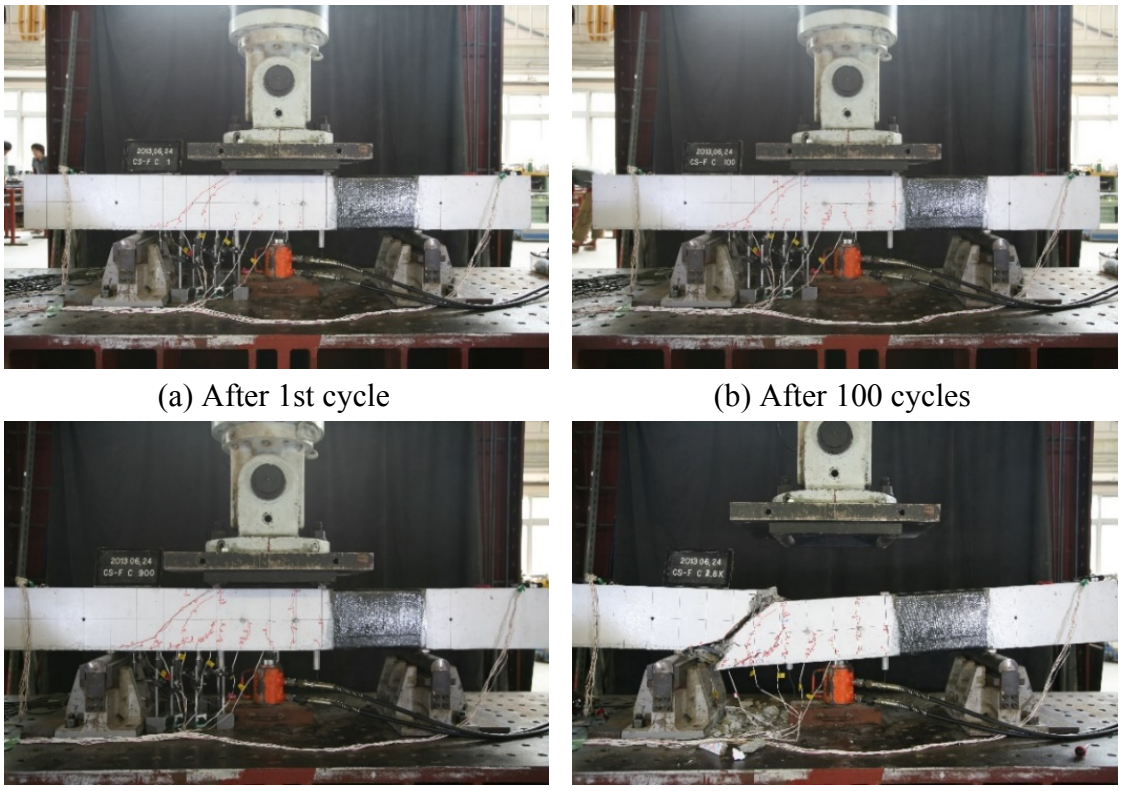

(a) After 1st cycle (b) After 100 cycles

(c) After 1,000 cycles (d) After 2,800 cycles

Fig. 2.13 Photos of the specimen

Fig. 2.14 presents the displacement transitions for positions D1 to D11 at the upper limit of the fatigue load level versus the number of cycles. The displacements increased almost linearly with the number of cycles until near failure, when plotted on

a log scale. The displacements increased rapidly for all measured positions near failure. The displacement was larger in D9 than D8 because the CFRP plate peeled off at the shear crack region after 1,000 fatigue cycles. This phenomenon is more evident close to the shear crack opening with increasing fatigue cycles, as shown in the comparison of D10 and D11.

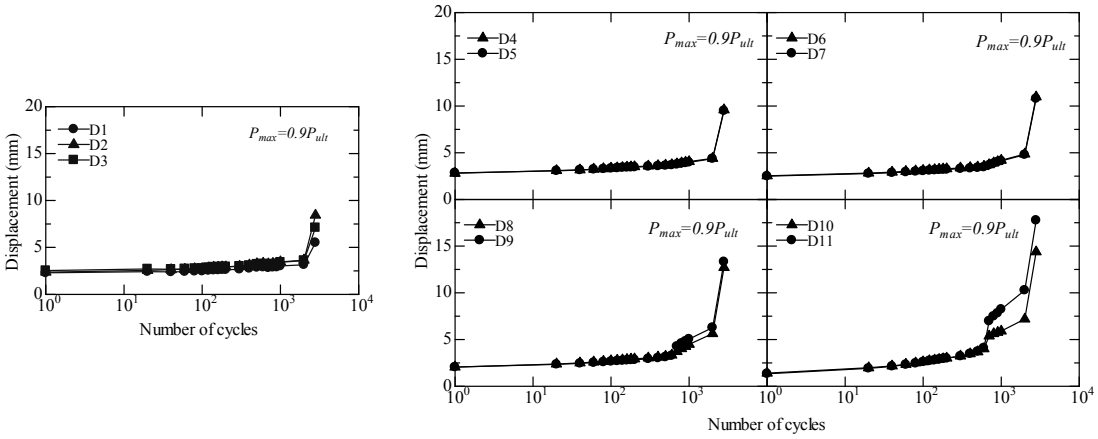

Fig. 2.14 Displacement-versus-fatigue cycle relationships at the given positions

The applied load-versus-deflection relationships for all fatigue cycles at the mid-span (D2) and the loading points (D1 and D3) are shown in Fig. 2.15. The deflection response was D3>D2>D1 at all fatigue cycles, due to the CFRP sheet being confined opposite the shear span of the test part. Intervening cycles are also shown to provide an indication of the damage accumulation and the stiffness degradation. In this test, failure occurred after only 2,800 cycles at the upper-limit load.

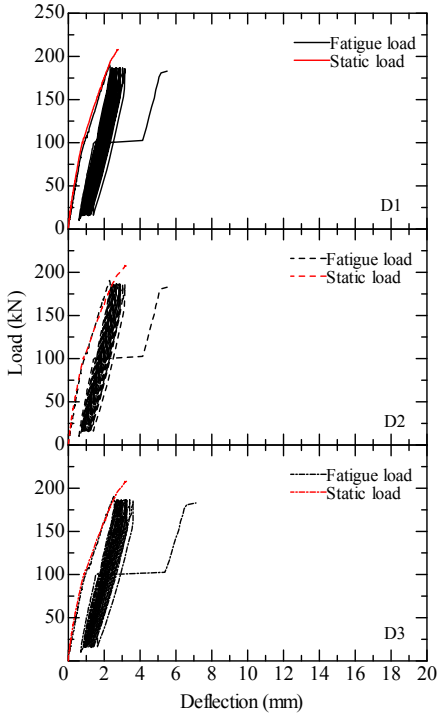

Fig. 2.15 Applied load-versus-deflection relations

Fig. 2.16 presents the applied load-versus-displacement relationships for points D4 to D11. As previously stated, the aim is to investigate CFRP plate debonding in mixed mode induced by a shear crack. Although the stiffness did not change remarkably, the residual and maximum displacements seemed to increase as the number of cycles increased. A sudden increase in the displacement occurred at some points due to shear crack opening, which is known to lead to increased residual deformations. Fig. 2.17 presents the transitions of displacements at positions D10 and D11 of specimen CS-F. The difference in displacement between D10 and D11, which was first observed at 838 steps (after 700 cycles) in response to the beginning of the peeling off of the CFRP plate, was confirmed.

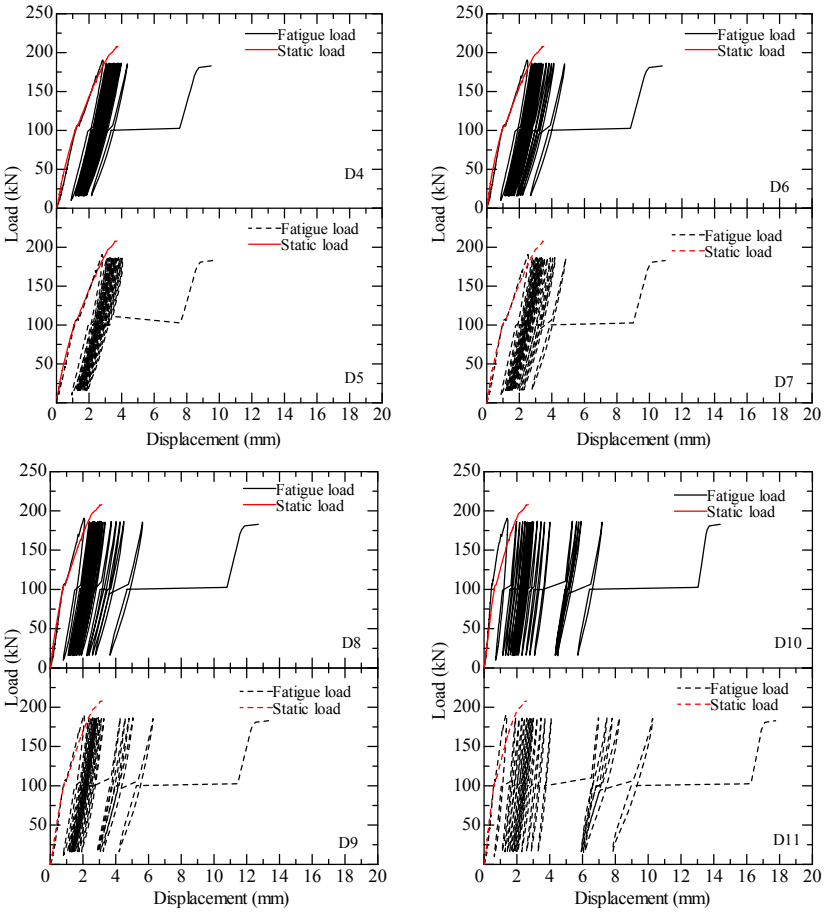

Fig. 2.16 Applied load-versus-displacement relations

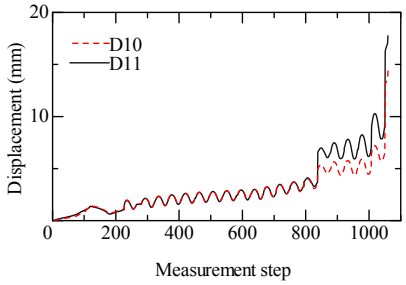

Fig. 2.17 Transitions of displacements D10 and D11

Fig. 2.18 presents the strain in the tension bars, stirrups, and CFRP plate as a relation of the number of cycles at the upper limit of the fatigue loading. The strain in the tension bars and stirrups was observed to remain almost constant as the number of fatigue cycles increased. The stirrups strain magnitudes were in the order of S3>S2>S4>S1 due to the path of the shear crack. The plate strains at locations C4, C5, and C6 indicate slow degradation by peeling of the CFRP plate due to shear cracking that occurred during the first load cycle. As the number of load cycles increased, the shear crack opening caused the CFRP plate peeling off, resulting in sudden drops at positions C1, C2, and C3 due to relative vertical displacement through the shear crack after 700 cycles.

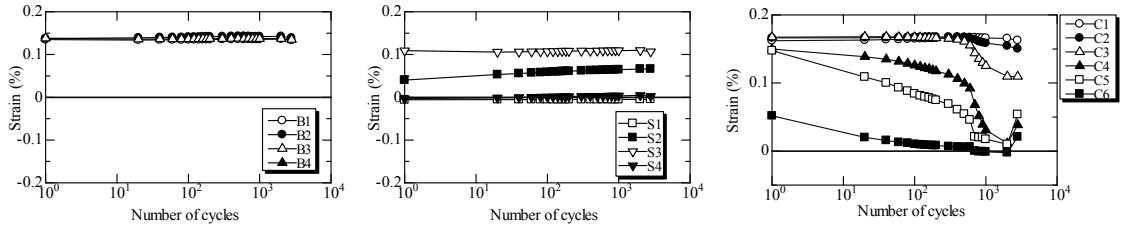

(a) Bottom reinforcement (b) Stirrups (c) CFRP plate

Fig. 2.18 Strain-versus-fatigue cycle relationships

The CFRP plate strain distributions at the 1st, 100th, 1,000th, and 2,000th cycles are shown in Fig. 2.19. The CFRP plate strain increased as the applied load increased, as shown by all gauges along the plate. The longitudinal strain distributions in the CFRP plate tended to become closer after the shear crack occurred (at 119 kN) with a uniform decrease in the strains. In addition, as illustrated in the figure, the peeling off of the CFRP plate moved from the plate end to the specimen center, corresponding to the shear crack opening, as the number of fatigue cycles increased.

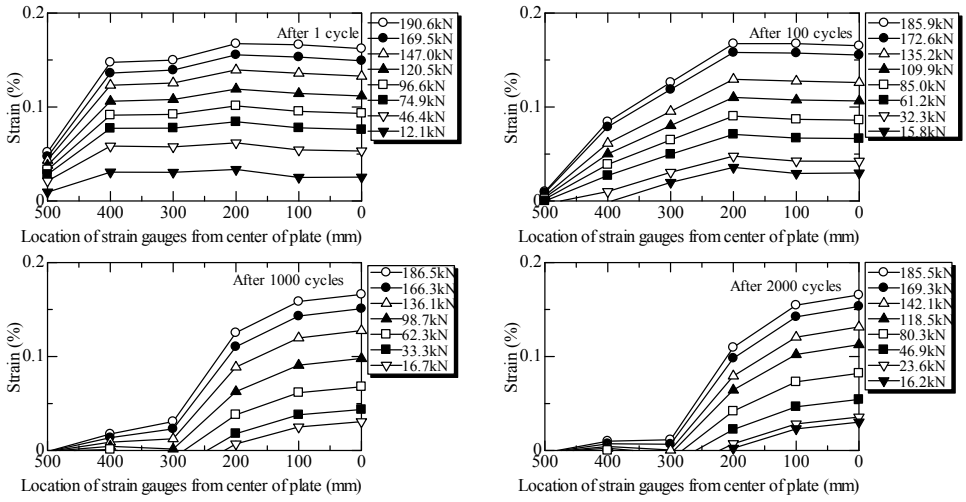

Fig. 2.19 CFRP plate strain distributions versus fatigue cycles

2.4 Conclusions

All specimens failed in shear. CFRP plate debonding as a result of mixed-mode fracture induced by a shear crack was verified. In flexurally strengthened concrete beams, when delamination is induced by the opening of a shear crack, a relative vertical displacement occurs between the two sides of the crack. The failure involves both interfacial shear and peeling (a combination of Modes I and II), which in turn increases the probability of premature local collapse. Hence, the bond performance of this type of structure when strengthened by a CFRP plate depends not only on the shear bond strength of the interface but also on the combined effect of the shear bond and peeling. In evaluating the performance of the externally bonded CFRP plate strengthening technique, the interfacial bond strength between the CFRP plate and the concrete under different failure modes is the crucial importance.

CHAPTER 3

Bond Behavior between CFRP Plates and Concrete under Fatigue Loading

3.1. Introduction

Debonding failure is often studied in direct shear testing, which involves a CFRP plate bonded to a concrete prism. By pulling the CFRP plate in the direction of its length, the bond capacity can be determined. The maximum bond capacity for a given CFRP plate width and thickness can be determined by performing direct shear testing of members with different CFRP plate bond lengths. Many studies have examined the bond behavior of FRP-concrete systems. The Japan Concrete Institute (JCI) established a technical committee on retrofitting technology (2001 to 2003) that focused on the interface bond properties between existing concrete structures and retrofitting materials for both adhesive bonding and overlaying retrofitting technologies. The "Guide for the Design and Construction of Externally Bonded FRP Systems for Strengthening Concrete Structures" (ACI 440.2R-2) provides guidance on the selection, design, and installation of FRP systems for externally strengthening concrete structures. Information on the material properties, design, installation, quality control, and maintenance of FRP systems used as external reinforcement is presented.

The behavior of bonded FRP systems under fatigue loading is, however, expected to degrade relative to their statically loaded counterparts. Thus, designs for FRP-reinforced concrete structures should account for bond failure associated with deterioration due to fatigue loads. Fatigue loading is recognized as having a deleterious effect on the performance of externally bonded FRP retrofit systems. Although many studies have reported on the fatigue behavior of FRP sheet-concrete systems, few of them have focused on the fatigue behavior of FRP plate-concrete systems.

The tests described in this chapter are the first in which the bond behavior of CFRP plates bonded to concrete has been investigated under fatigue loading. Fatigue testing of double-faced bond specimens was carried out. The fatigue behavior of the bond surface between the CFRP plates and the concrete can be characterized by an *S-N* diagram, which represents the relationship between the bond stress and the number of cycles at debonding, on a semi-logarithmic scale, based on the experimental results of the influence of the bond behavior for different concrete strengths, types of CFRP plates, and upper fatigue loads. The different debonding modes for the various fracturing modes are also discussed.

In strengthening RC beams by external bonding of FRP plates, the performance of the

FRP-to-concrete interface in mixed-mode fracture is the crucial importance. Indeed, a number of debonding failures of FRP-strengthened concrete members have been caused by shear and peeling of the FRP from the concrete. To clarify the details of peeling phenomenon, transverse displacements were measured.

Finally, this chapter proposes a new methodology for assessing fatigue bond damage based on local bond stress-slip relationships for the purpose of studying the interfacial behavior of CFRP plate-to-concrete interface under fatigue loading, the relationship of the bond behavior to the number of fatigue cycles (N), and the effect of the unloading stiffness k_i.

3.2. Experimental Program for Static Loading

3.2.1. Specimens

Specimen details are shown in Fig. 3.1. In this experimental program, prism specimens with cross-sectional sizes of 150 mm ×150 mm and lengths of 800 mm were used. The two steel bars had no connection at the center of the specimen. A crack was introduced at the notch after attaching the CFRP plate. Thus, the two prisms were connected only through the CFRP plates. The CFRP plates were bonded at the opposite sides of the specimens. An epoxy adhesive was used to bond the CFRP plates. One of the sides of each specimen was wrapped by a CFRP sheet, which permitted the delamination of the CFRP plate on the opposite side only. The CFRP plate bond length used for this experiment was set to 400 mm. The CFRP plate width was 50 mm. Nine specimens were tested, as shown in Table 3.1. The test variables were the concrete compressive strength and the CFRP plate type.

Table 3.1 Specimen list

Specimens	Concrete strength (MPa)	CFRP plate	Remarks
C13HS-M	13.5	High-strength GM510	-
C13HE-M		High-stiffness HM520	-
C13HE-M-C			With confinement jig
C21HS-M	21	High-strength GM510	-
C21HS-M-1			-
C21HS-M-2			-
C21HE-M		High-stiffness HM520	-
C36HS-M	36	High-strength GM510	-
C36HE-M			-

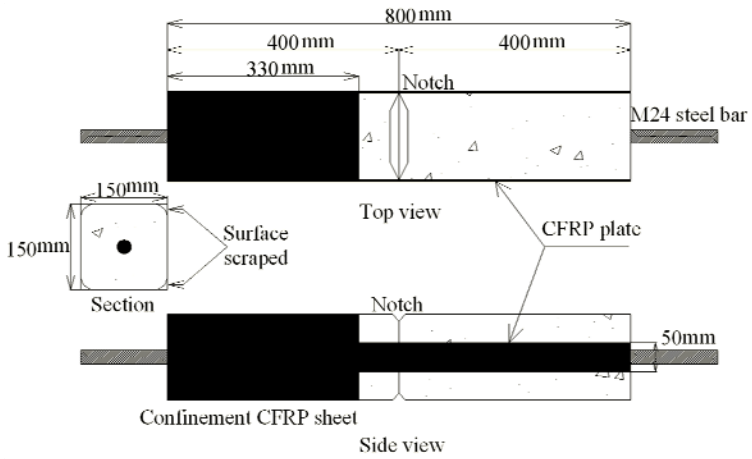

Fig. 3.1 Specimen details

3.2.2. Material Properties

Table 3.2 presents the properties of the CFRP plates used in this experiment. The values were obtained from the manufacturer. High-strength and high-stiffness CFRP plates were used. The concrete strengths are provided in Table 3.3.

Table 3.2 CFRP plate properties

CFRP plate type	Name	Thickness (mm)	Elastic modulus (GPa)	Tensile strength (MPa)
High strength	GM510	1.0	156	2,400
High stiffness	HM520	2.0	450	1,200

Table 3.3 Concrete properties

Concrete Type	Compressive strength (MPa)	1/3 Secant modulus (GPa)	Splitting strength (MPa)
Target 13.5 MPa	21.2	21.4	1.96
Target 21 MPa	25.0	22.3	2.40
	25.6	22.8	2.36
Target 36 MPa	39.5	24.9	3.01

3.2.3. Loading and Measurement

In this experiment, a 1-MN actuator was used to produce static loading. Each specimen was set on Teflon sheets to reduce friction with the table. The total displacement and crack width at the center were measured using linear variable displacement transducers (LVDTs), as shown in Fig. 3.2. The strain distribution was obtained from nine strain gauges set on the CFRP plates on one face (the gauge face) at intervals of 50 mm, one gauge on the opposite side (the no-gauge face) at the center of the specimen, and two pi gauges set on the notch. To investigate peeling of the CFRP plate, the transverse displacements were measured. The instrumentation details are presented in section 3.3.5.

Because specimen C36HE-F75 (see Section 3.3.3) failed by concrete splitting and pulling out of the steel bar at an early stage in the loading cycles, a concrete confinement jig, shown in Fig. 3.3, was used for specimen C13HE-M-C and C21HE-F75-C to prevent splitting failure. Specimen C13HE-M-C was used to investigate the influence of the confinement jig under static loading with specimen C13HE-M.

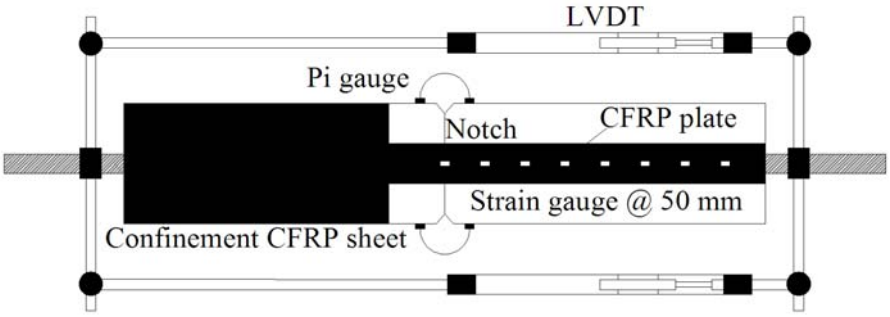

Fig. 3.2 Data acquisition schematic

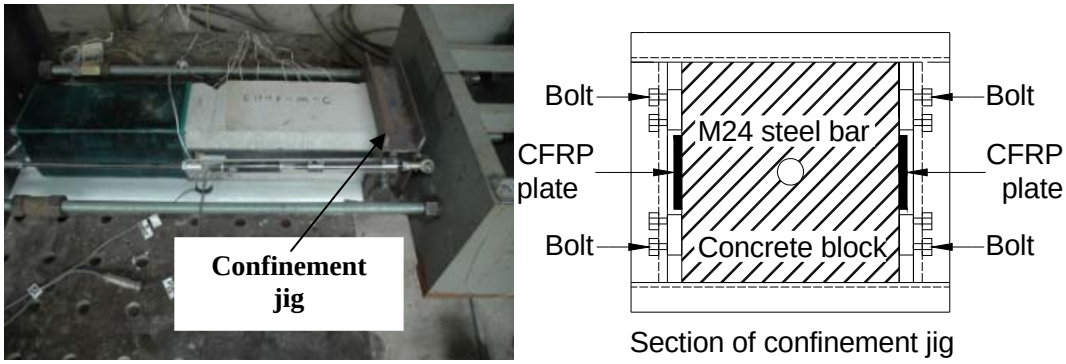

Fig. 3.3 Confinement jig to prevent concrete splitting

3.2.4. Experimental Results

3.2.4.1. Failure Progress

All nine specimens were submitted to tensile force until total failure of the bond system occurred. The typical specimen failures are presented in Fig. 3.4. The HE specimen interface layers were thicker than those of the HS specimens. All of the static load specimen initial failures were on the concrete face. Specimen C36HS-M was debonded from the concrete face near the notch, and the left part was debonded from the adhesive face.

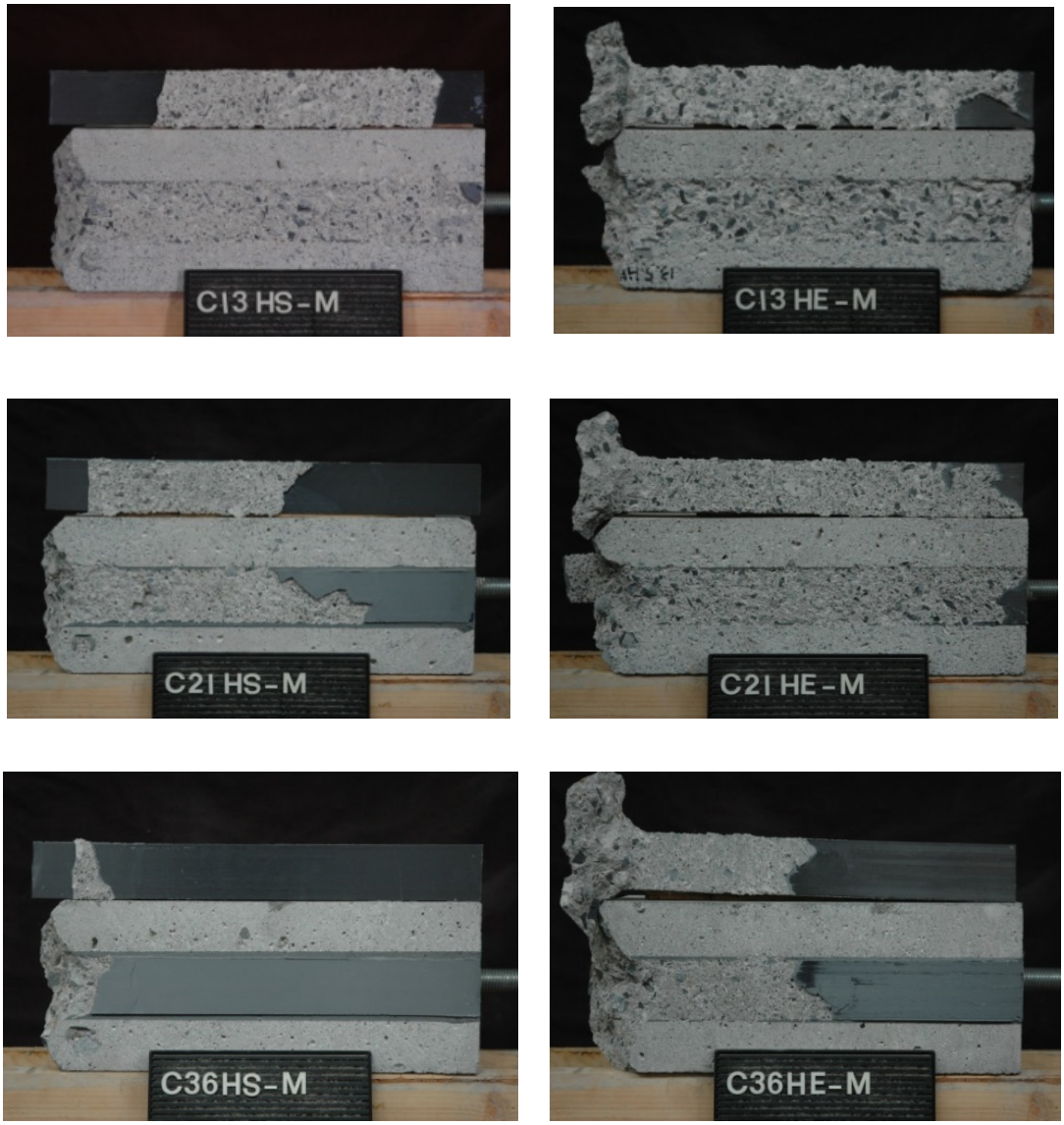

Fig. 3.4 Typical failure under static loading

3.2.4.2. Load-Displacement Relationships

The load-displacement graph was plotted using the total displacement (δ_{total}) and crack width (δ_{cr}) data obtained. The total displacement is the average of the displacements at two opposite edges, and the crack width is the average of the widths from the two pi gauges. These graphs are presented in Fig. 3.5, in which the behavior of the specimens during the test is shown in greater detail. The crack width in the HS specimen at the maximum load was approximately 0.2 mm greater than in the HE specimen. However, the maximum load at failure was significantly lower than that of the HE specimen.

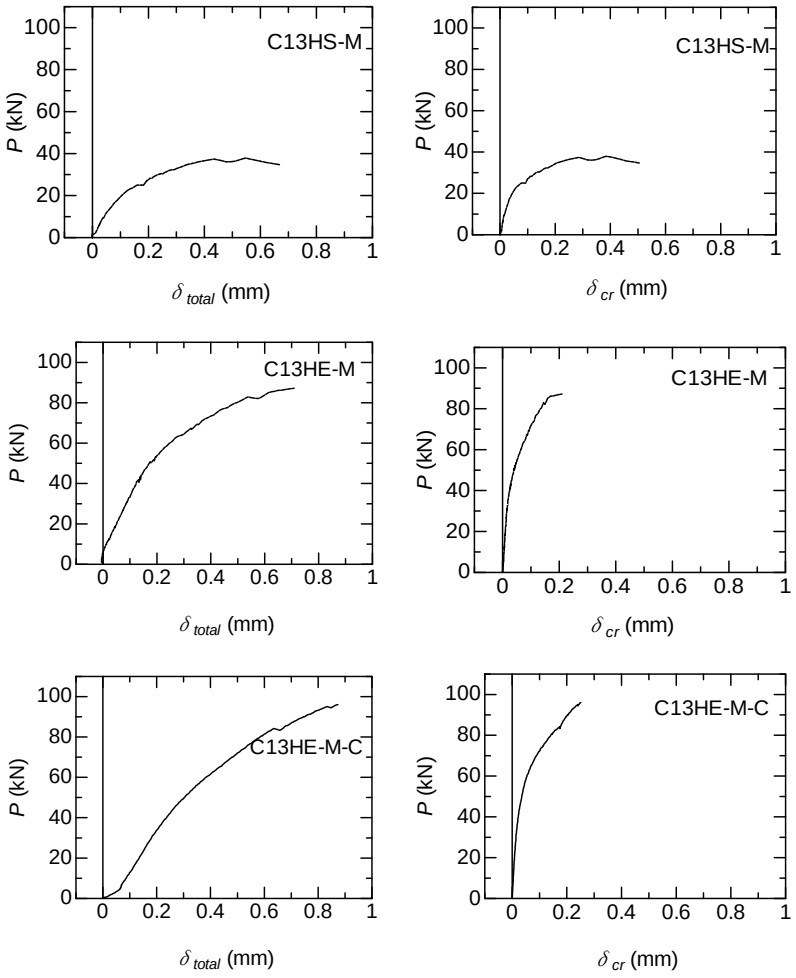

Fig. 3.5. (a) Load-displacement relationships

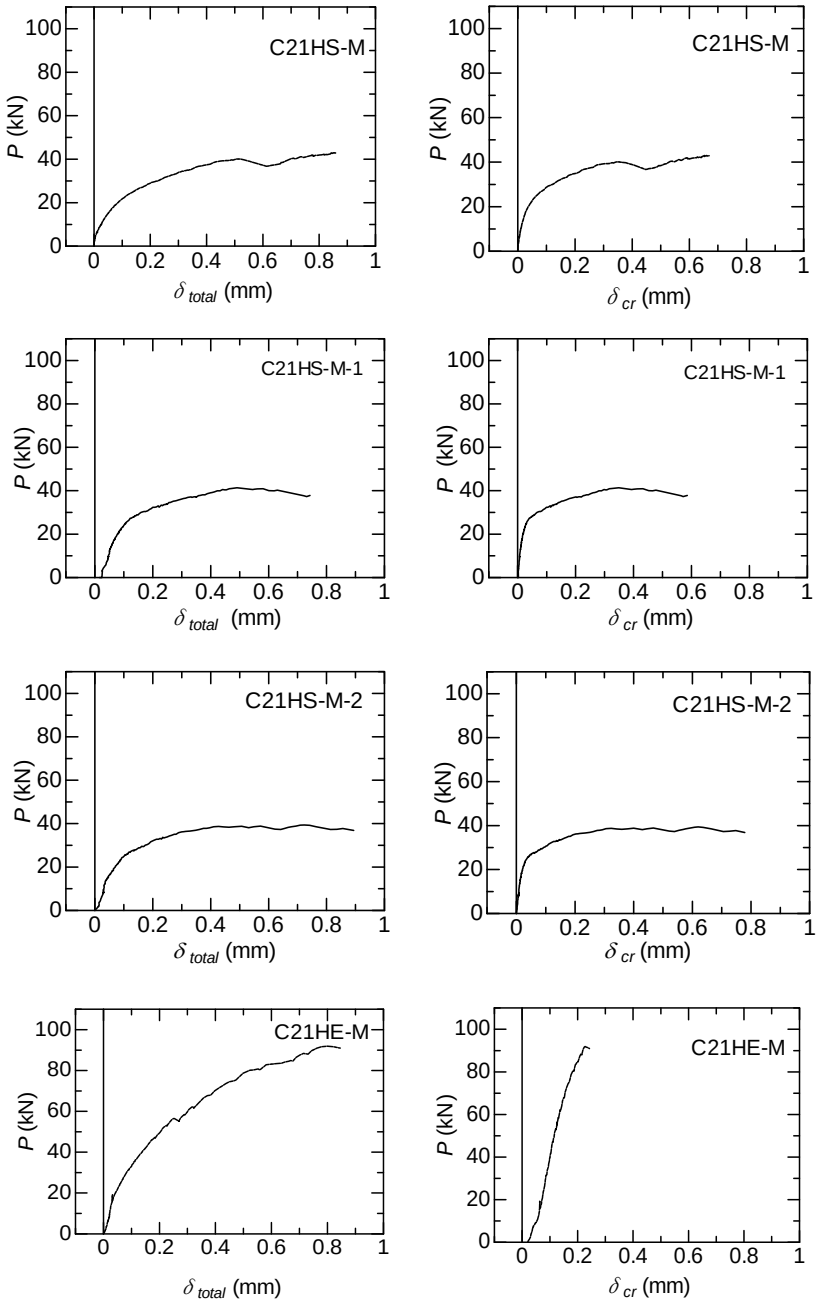

Fig. 3.5 (b) Load-displacement relationships

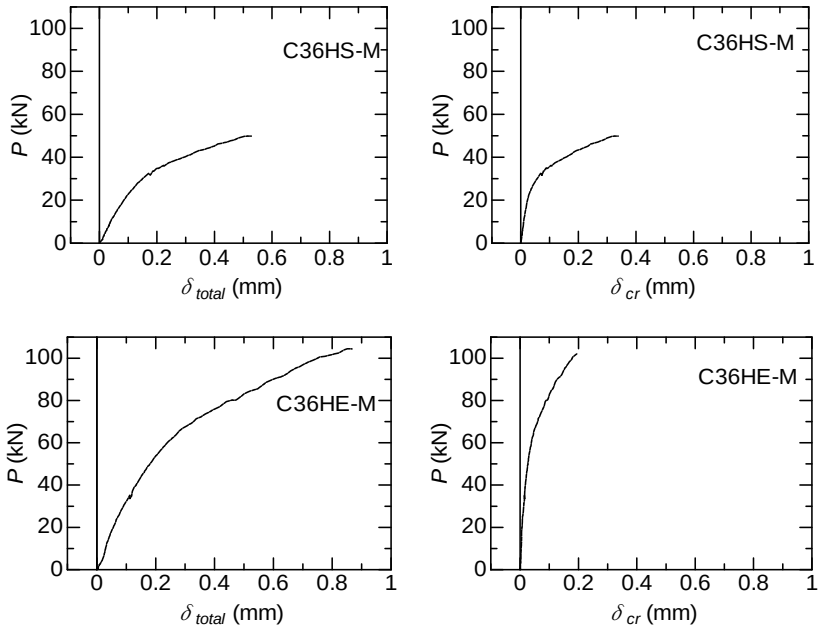

Fig. 3.5 (c) Load-displacement relationships

3.2.4.3. Bond Strength

Many methods for evaluating the bond strength between CFRP sheets and concrete have been proposed. Some of these methods are based on empirical relations calibrated with experimental data (Maeda et al. 1997 [3.1]; Tanaka 1996 [3.2]). Other methods are based on fracture mechanics theories, with numerous parameters calibrated with experimental data (Yuan and Wu 1999 [3.3]; Kanakubo 2003[3.4]).

The bond strength between a CFRP plate and concrete can be calculated using the prediction formula proposed by Matsunaga (2008) [3.5], shown below (Table 3.4).

$$\tau_{b,\max} = 2.5 \times \sigma_B^{0.23} \tag{3.1}$$

$$l_e = \sqrt{\frac{2 \times t_f \times E_f \times S_e}{k_e \times \tau_{b,\max}}} \tag{3.2}$$

$$P_b = k_e \times \tau_{b,\max} \times b_f \times l_e (l_b > l_e) \tag{3.3}$$

$$P_b = k \times \tau_{b,\max} \times b_f \times l_b (l_b < l_e) \tag{3.4}$$

$$k = \frac{1-k_e}{2} \times \cos\left(\frac{l_b}{l_e}\pi\right) + \frac{1+k_e}{2} \tag{3.5}$$

where the maximum local bond stress is $\tau_{b,max}$, the concrete compressive strength is σ_B, the effective bond length is l_e, the width is b_f, the thickness is t_f, the elastic modulus of the CFRP plate is E_f, the local slip of the effective bond area is s_e (0.234 mm), the

stress coefficient of the equivalent bond stress block (EBSB) in the case of an effective bond length is k_e (0.428), the bond length is l_b, the bond strength is P_b, and the stress coefficient of the EBSB is k.

Table 3.4 Bond strength with calculated values

Specimen	Calculated value						
	k_e	k	s_e (mm)	$\tau_{b,max}$ (MPa)	λ_f (mm)	l_e (mm)	P_{max} (kN)
C13HS-M	0.428	-	0.234	5.06	30,812	184	39.85
C13HE-M	0.428	0.440	0.234	5.06	177,763	441	89.06
C13HE-M-C	0.428	0.440	0.234	5.06	177,763	441	89.06
C21HS-M	0.428	-	0.234	5.24	29,734	180	40.37
C21HS-M-1	0.428	-	0.234	5.27	29,734	180	40.60
C21HS-M-2	0.428	-	0.234	5.27	29,600	180	40.60
C21HE-M	0.428	0.436	0.234	5.24	171,544	433	91.39
C36HS-M	0.428	-	0.234	5.82	26,804	171	42.60
C36HE-M	0.428	0.429	0.234	5.82	154,639	411	99.87

The calculated and experimental results are compared in Table 3.5. The ratios of the experimental to calculated values are close to one, which indicates that the experimental values are nearly the same as the calculated values.

Table 3.5 Comparison of the calculated and experimental values

Specimen	Calculated value P_{max} (kN)	Experimental value P_{max} (kN)	Experimental/Calculated
C13HS-M	39.85	37.90	0.951
C13HE-M	89.06	87.24	0.980
C13HE-M-C	89.06	96.01	1.078
C21HS-M	40.37	42.97	1.064
C21HS-M-1	40.60	41.94	1.033
C21HS-M-2	40.60	39.99	0.985
C21HE-M	91.39	91.92	1.006
C36HS-M	42.60	49.84	1.170
C36HE-M	99.87	104.46	1.046

3.2.4.4. Influence of the Confinement Jig

Because specimen C36HE-F75 (see Section 3.3.3) failed due to concrete splitting and pulling out of the steel bar at the early loading cycle, a concrete confinement jig, shown in Fig. 3.3, was installed for specimen C13HE-M-C and C21HE-F75-C to prevent splitting failure. Specimen C13HE-M-C was tested to investigate the influence of the confinement jig under static loading with specimen C13HE-M. The results indicated that the bond strength of C13HE-M-C was 10% higher than that of C13HE-M. Fig. 3.6 presents the P-δ curves for this specimen.

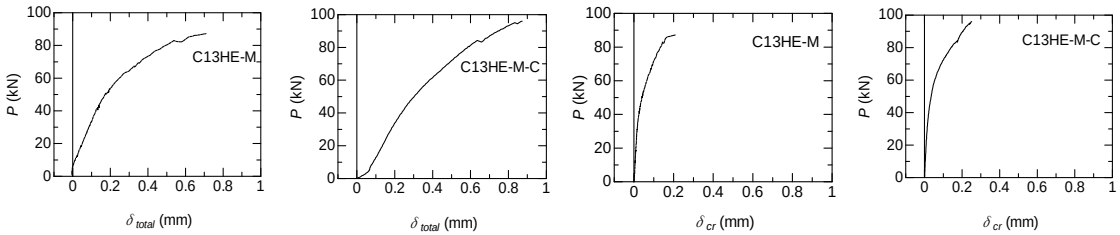

Fig. 3.6. *P*-*δ* curves

3.2.4.5. Strain Distribution of the CFRP Plate

The data obtained from the strain gauges on the CFRP plate were used to examine strain distributions. Fig. 3.7 presents the strain distributions of all specimens under static loading. Certain portions of the strain distributions had larger slopes where the active bonding stress exists. The local strain of the HS specimen was greater than that of the HE specimen, and the strain was nearly zero at the load end.

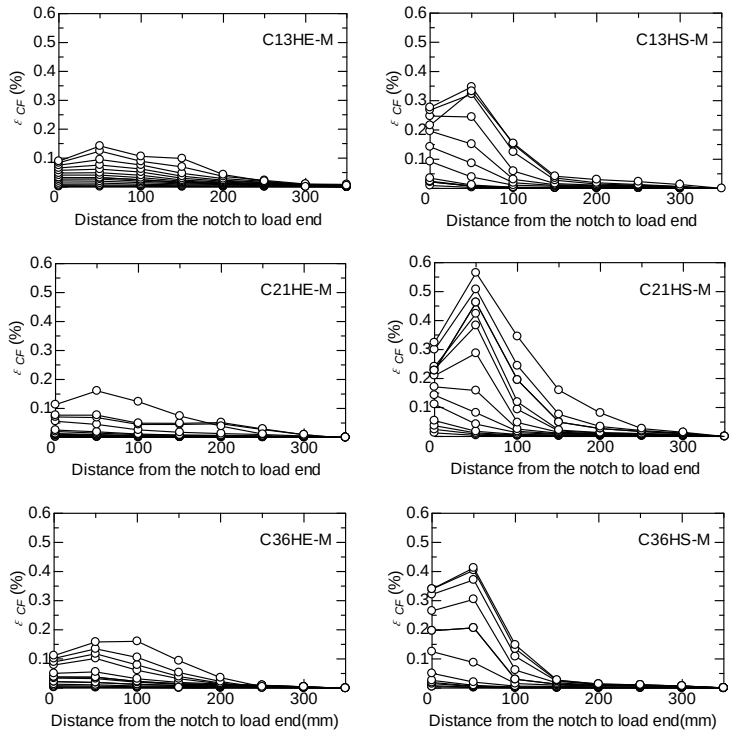

Fig. 3.7 Strain distribution

3.2.4.6. Local Bond Stress and Slip

The difference in the tensile force was obtained from the strain at section *i* and the relative strain in the preceding section *i*-1. The average bond stress at section *i*, $\tau_{b,i}$, was calculated by dividing the difference in the tensile force by the surface area of the plate, as shown in Equation (3.6).

$$\tau_{b,i} = \frac{(\varepsilon_{f,i} - \varepsilon_{f,i-1}) \cdot t_f \cdot E_f}{\Delta l_b} \quad (\tau_{bi} = 6-13) \tag{3.6}$$

where

$\varepsilon_{f,i}$ = strain in the CFRP plate at section *i*

t_f = thickness of the CFRP plate

E_f = elastic modulus of the CFRP plate

Δl_b = interval between gauges (= 50 mm)

The slip of section *i*, s_i, is the sum of the differences between the elongation of the CFRP and that of the equivalent section composed of concrete, an epoxy layer, and a steel bar, measured from the free end of the plate (the loaded end of the specimen) to section *i*. The relative displacement between the concrete and the plate at the local end of the plate was assumed to be zero. The slip was calculated using the following equations:

$$s_i = s_{i-1} + (\delta_{f,i} - \delta_{m,i}) \quad (\tau_{b,i} = 6-13, s_1 = 0) \tag{3.7}$$

$$\delta_{f,i} = \frac{\varepsilon_{f,i} - \varepsilon_{f,i-1}}{2} \cdot \Delta l_b + \varepsilon_{f,i-1} \cdot \Delta l_b \tag{3.8}$$

$$\delta_{m,i} = \frac{\varepsilon_{m,i-1} - \varepsilon_{m,i}}{2} \cdot \Delta l_b + \varepsilon_{m,i} \cdot \Delta l_b \tag{3.9}$$

$$\varepsilon_{m,i} = \frac{P_{m,i-1} - 2 \cdot \tau_{b,i} \cdot b_f \cdot \Delta l_b}{A_m \cdot E_m} \tag{3.10}$$

$(\varepsilon_{m,1} = P_{m,1} / A_m \cdot E_m,\ P_{m,1} = P_{load})$

where

$\delta_{f,i}$ = elongation of the CFRP plate at section *i*

$\delta_{m,i}$ = elongation of the equivalent section *i*

$\varepsilon_{m,i}$ = strain of the equivalent section *i*

$P_{m,i}$ = force acting on the equivalent section *i*

b_f = width of the plate

P_{load} = tensile load applied by the loading machine

$A_m \cdot E_m$ = stiffness of the equivalent concrete section

$= A_c \cdot E_c + A_s \cdot E_s + A_{ad} \cdot E_{ad}$

A_c, A_s, A_{ad} =cross-sectional areas of concrete, steel, and adhesive, respectively

E_c, E_s, E_{ad} =elastic modulus of concrete, steel, and adhesive, respectively

Local bond stresses versus slip (τ_b *vs. s*) graphs for each gauge interval were plotted after calculating all of the data. Fig. 3.8 and Fig. 3.9 show the positions of the strain gauges and the local bond stress-slip curves, respectively. The CFRP plate strains changed only slightly at strain gauge positions 10 and 13. Therefore, the curves are not visible in these position graphs.

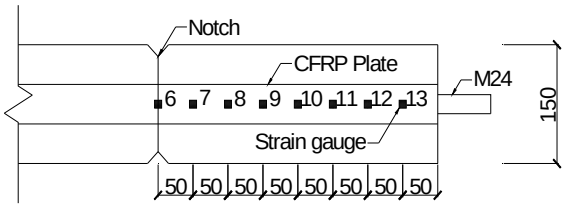

Fig. 3.8 Positions of strain gauges

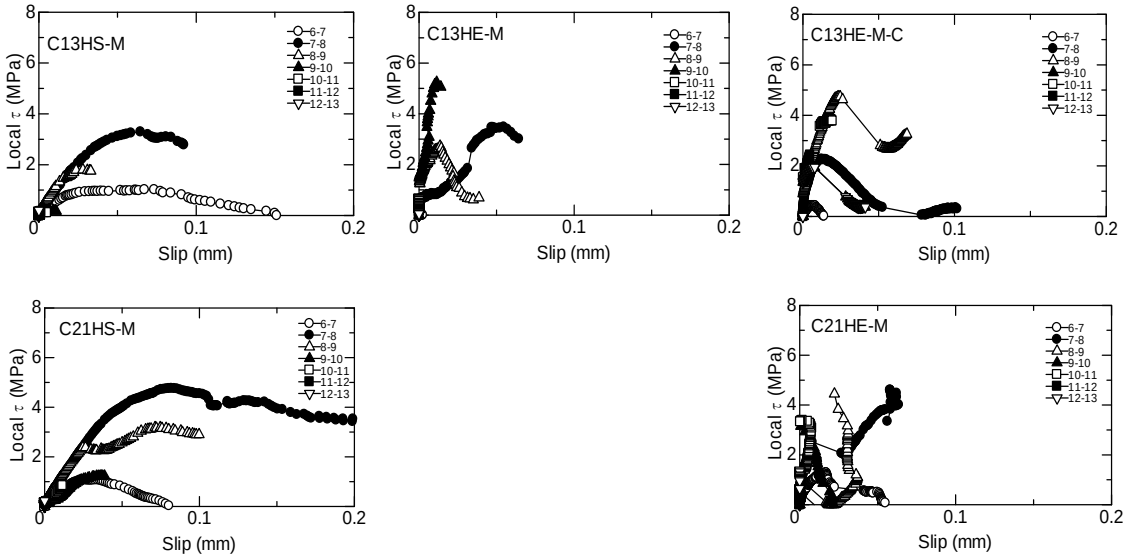

Fig. 3.9 (a) Local bond stress and slip curves

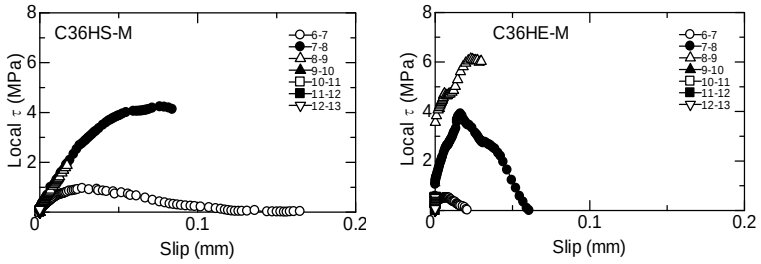

Fig. 3.9 (b) Local bond stress and slip curves

Fig. 3.10 presents comparisons of the local bond stress-slip relationships obtained for static loading. The formula used is the Popovics model, as shown below. [3.6]

The experimental result fits the Popovics model closely, confirming that the Popovics model represents the local bond stress-slip relationship well.

$$\frac{\tau_b}{\tau_{b,\max}} = \frac{s}{s_{\max}} \times \frac{n}{(n-1)+(s/s_{\max})^n} \tag{3.11}$$

$$\tau_{b,\max} = 2.5\sigma_B^{0.23} \tag{3.12}$$

$$s_{max} = 0.0429 \text{ mm} \tag{3.13}$$

$$n = 3 \tag{3.14}$$

where $\tau_{b,max}$ = maximum local bond stress, s_{max} = slip at $\tau_{b,max}$, and n = 3.

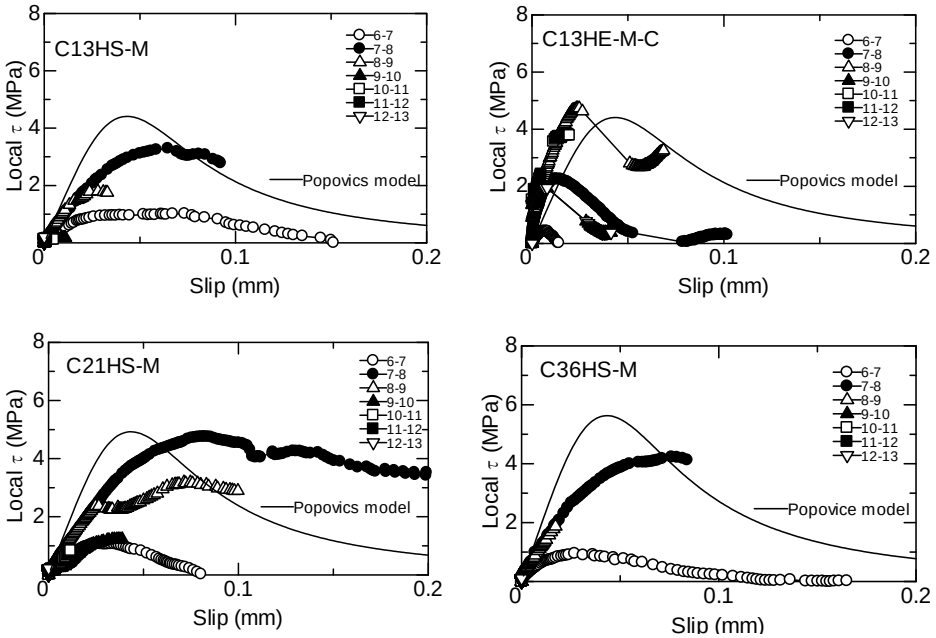

Fig. 3.10 Popovics model comparisons

3.3. Experimental Program for Fatigue Loading

3.3.1. Specimens

The specimens used for the fatigue load testing were the same size as those used for the static load testing. A total of 15 specimens were tested. The specimens are listed in Table 3.6. The test variables were the concrete compressive strength, the CFRP plate type, and the upper limit of the fatigue loading, which had values of 50%, 60%, 70%, 75%, 80%, 85%, and 90%.

Table 3.6 Specimen list

Specimens	Concrete strength (MPa)	CFRP plate	Fatigue load*	
			Upper limit	Lower limit
C13HS-F70	13.5	High-strength GM510	70%	10%
C13HS-F80			80%	10%
C13HS-F90			90%	10%
C21HS-F60	21	High-strength GM510	60%	10%
C21HS-F70			70%	10%
C21HS-F70-T			70%	10%
C21HS-F75-T			75%	10%
C21HS-F80			80%	10%
C21HS-F80-T			80%	10%
C21HS-F85-T			85%	10%
C21HE-F75-C		High-stiffness HM520	75%	10%
C36HS-F50	36	High-strength GM510	50%	10%
C36HS-F60			60%	10%
C36HS-F70			70%	10%
C36HE-F75		High-stiffness HM520	75%	10%

* Percentage of the bond strength under static load

3.3.2. Material Properties

All of the materials used in the fatigue tests were the same as those used in the static tests. Table 3.7 and Table 3.8 listed the properties of the CFRP plates and the concrete, respectively.

Table 3.7 CFRP plate properties

CFRP plate type	Name	Thickness (mm)	Elastic modulus (GPa)	Tensile strength (MPa)
High strength	GM510	1.0	156	2,400
High stiffness	HM520	2.0	450	1,200

Table 3.8 Concrete properties

Concrete Type	Compressive strength (MPa)	1/3 Secant modulus (GPa)	Splitting strength (MPa)
Target 13.5 MPa	21.2	21.4	1.96
Target 21 MPa	25.0	22.3	2.40
	25.6	22.8	2.36
Target 36 MPa	39.5	24.9	3.01

3.3.3. Loading and Measurement

A 1-MN actuator was used for loading in the tests. Each specimen was set on a Teflon sheet to reduce friction with the table. The total displacement and crack width at the center of the specimen were measured using LVDTs, as same in the static tests. The details of the testing setup were also the same as in the static tests. The strain distribution was obtained from nine strain gauges with length of 2 mm, placed on the CFRP plates on one face at intervals of 50 mm. One gauge was placed on the opposite side at the specimen center. Two pi gauges were set at the position of the notch.

The repetition frequency of the fatigue loading was set to 1 Hz. This frequency was chosen because conventional infrastructure elements, such as bridges, typically experience loading at varying frequencies of 1-5 Hz. Sinusoidal loading was used. The upper-limit fatigue loadings were set to 50%, 60%, 70%, 75%, 80%, and 90% of the bond strength under static loading (P_{max}), which was among the load-carrying capacity parameters investigated in the static tests. The lower limit of the fatigue loading was set to 10% in all experiments. Up to one million fatigue cycles were applied if debonding did not occur.

Recordings of full cycles were taken for the following cycles: at the first cycle and every 20th cycle up to 200 cycles, at every 200th cycle up to 1,000 cycles, at every 1,000th cycle up to 10,000 cycles, at every 10,000th cycle up to 100,000 cycles, and at every 80,000th cycle up to 1,000,000 cycles, as shown in Table 3.9. Static post-fatigue loading to failure was carried out for those specimens that did not fail under fatigue loading.

Table 3.9 Measurement intervals

Cycles	Measurement interval
1	first cycle
to 200	per 20 cycles
to 1,000	per 200 cycles
to 10,000	per 1,000 cycles
to 100,000	per 10,000 cycles
to 1,000,000	per 80,000 cycles

Because specimen C36HE-F75 failed due to concrete splitting and pulling out of the steel bar early in the testing process, as shown in Fig. 3.11, the concrete confinement jig was set for specimen C21HE-F75-C to prevent splitting failure, as shown in Fig. 3.12.

Fig. 3.11 Splitting failure of specimen C36HE-F75

Fig. 3.12 Specimen C21HE-F75-C with a confinement jig and the failure surface

3.3.4. Experimental Results

3.3.4.1. Fatigue Progress

The different debonding modes that occurred at different upper limits of fatigue loading and for different CFRP plate types and concrete strengths were observed. All of the fatigue specimens' experimental results are summarized in Table 3.10, and representative photographs are shown in Fig. 3.13. The upper-limit bond stress τ_{up} in Table 3.10 is calculated from Eq. (3.15):

$$\tau_{up} = P_{up} / 2b_f l_b \tag{3.15-1}$$

$$\tau_{low} = P_{low} / 2b_f l_b \tag{3.15-2}$$

where P_{up} = the upper-limit load, P_{low} = the lower-limit load, b_f = the width of the CFRP plate, and l_b = the bond length of the CFRP plate.

Table 3.10 Fatigue test results

Specimen	Upper-limit load P_{up} (kN)	Lower-limit load P_{low} (kN)	Upper-limit bond stress τ_{up} (MPa)	Lower-limit bond stress τ_{low} (MPa)	Failure cycles	Failure mode
C13HS-F70	26.53	3.97	0.663	0.0993	127,445	Debonding at adhesive layer followed by peeling off of the concrete
C13HS-F80	30.32	3.97	0.758	0.0993	256,819	
C13HS-F90	34.11	3.97	0.853	0.0993	164,012	
C21HS-F60	25.78	4.30	0.645	0.1075	No failure*	-
C21HS-F70	30.08	4.30	0.752	0.1075	28,191	Debonding at the adhesive layer followed by peeling off of the concrete
C21HS-F70-T	28.68	4.10	0.717	0.1025	61,313	
C21HS-F75-T	30.72	4.10	0.768	0.1025	5,573	Debonding at the concrete layer
C21HS-F80	34.38	4.30	0.860	0.1075	1,779	
C21HS-F80-T	32.77	4.10	0.819	0.1025	400	
C21HS-F85-T	34.82	4.10	0.871	0.1025	600	
C21HE-F75-C	68.94	9.19	1.724	0.2298	No failure*	-
C36HS-F50	24.92	4.98	0.623	0.1245	No failure*	-
C36HS-F60	29.90	4.98	0.748	0.1245	205,175	Debonding at the adhesive layer
C36HS-F70	34.89	4.98	0.872	0.1245	4,145	
C36HE-F75	78.35	10.45	1.959	0.2613	-	Concrete splitting

* Up to one million cycles

Basically, the bond force-transferring capacity of the CFRP/concrete interface tended to decrease with the concrete's compressive strength. In contrast, the failure cycles of specimen C13HS-F70, C13HS-F80, and C13HS-F90 were 127,445 cycles, 256,819 cycles, and 164,012 cycles, respectively. It was found that the rule that a shorter fatigue life would result from applying high-level fatigue load to these specimens was not followed.

As we know, for static failures of CFRP/concrete bonded interface, local interface debonding is initiated with an increase in the tensile force in CFRP plates. Once the pullout force in CFRP plates reaches a critical value, macro-debonding occurs, leading to overall failure of the entire interface. However, for the fatigue failures of CFRP/concrete bonded interfaces, local interface debonding can be caused by a gradual increase of the local slip; even the tensile stress in CFRP plates is kept at a certain value that is smaller than the maximum pullout force. The local interface debonding can propagate with the increase in fatigue cycles. Once the maximum bond force that the left bonded length can bear becomes less than the tensile force applied to the CFRP plates, a fatigue failure of the entire bonded interface will occur.

The failure face of specimen C13HS-F90 was divided into two parts. First, debonding started at the notch at the concrete surface and propagated to the load end. Second, as the number of fatigue cycles increased, the failure face changed to the adhesive face until the CFRP plate was completely debonded. The failure face of specimen C21HS-F80 was entirely on the concrete surface. The failure face mechanism of specimen C36HS-F70 was nearly the same as that of specimen C13HS-F90, except that the failure face on the concrete surface was less than that of C13HS-F90. Specimen C36HS-F50 remained unchanged through one million cycles, after which it was subject to static loading until failure. Up to the application of one million cycles, the debonding was mainly from the adhesive face. Thus, after complete debonding, two parts of the failure face were observed.

Failure cycle: 127,445 | Failure cycle: 256,819 | Failure cycle: 164,012

Post-fatigue failure | Failure cycle: 28,191 | Failure cycle: 1,779

Post-fatigue failure | Failure cycle: 205,175 | Failure cycle: 4,145

Fig. 3.13 Typical failure surfaces after fatigue loading

3.3.4.2. Load and Displacement Relationships

Fig. 3.14 presents the load-crack width curves obtained at major measurement intervals for all specimens. The hysteresis curves of all specimens are similar throughout the one-million-cycle tests. For any given cycle, the load-crack width curves exhibit an ascending branch and a descending branch that are close to each other. The area enclosed by the loops from B (200 cycles) to D (1,000 cycles) does not change significantly. For the specimens subjected to low-level (≤50%) fatigue loading and the HE specimens, the slopes of the early loops decrease slightly in the early cycles and then remain unchanged thereafter, indicating a slight reduction in the bond stiffness at the beginning that does not deteriorate further during subsequent cycles. However, for the specimens subjected to high-level (>50%) fatigue loading, the slopes of the loops decrease gradually until the end of the tests, indicating a continuous degradation in the bond stiffness.

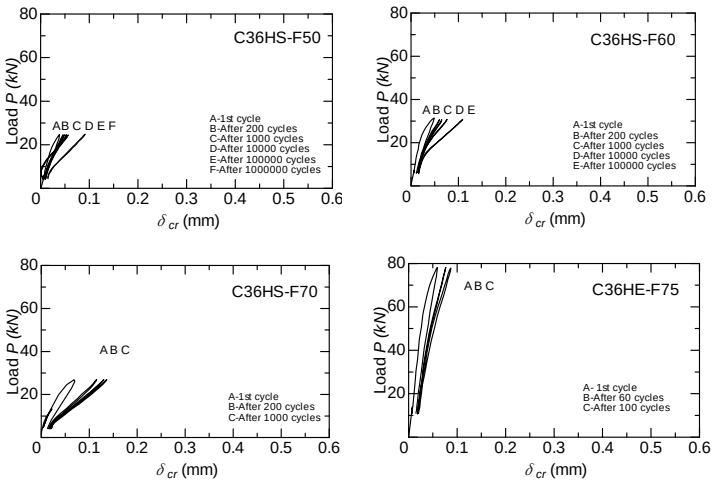

Fig. 3.14 (a) Load-crack width curves

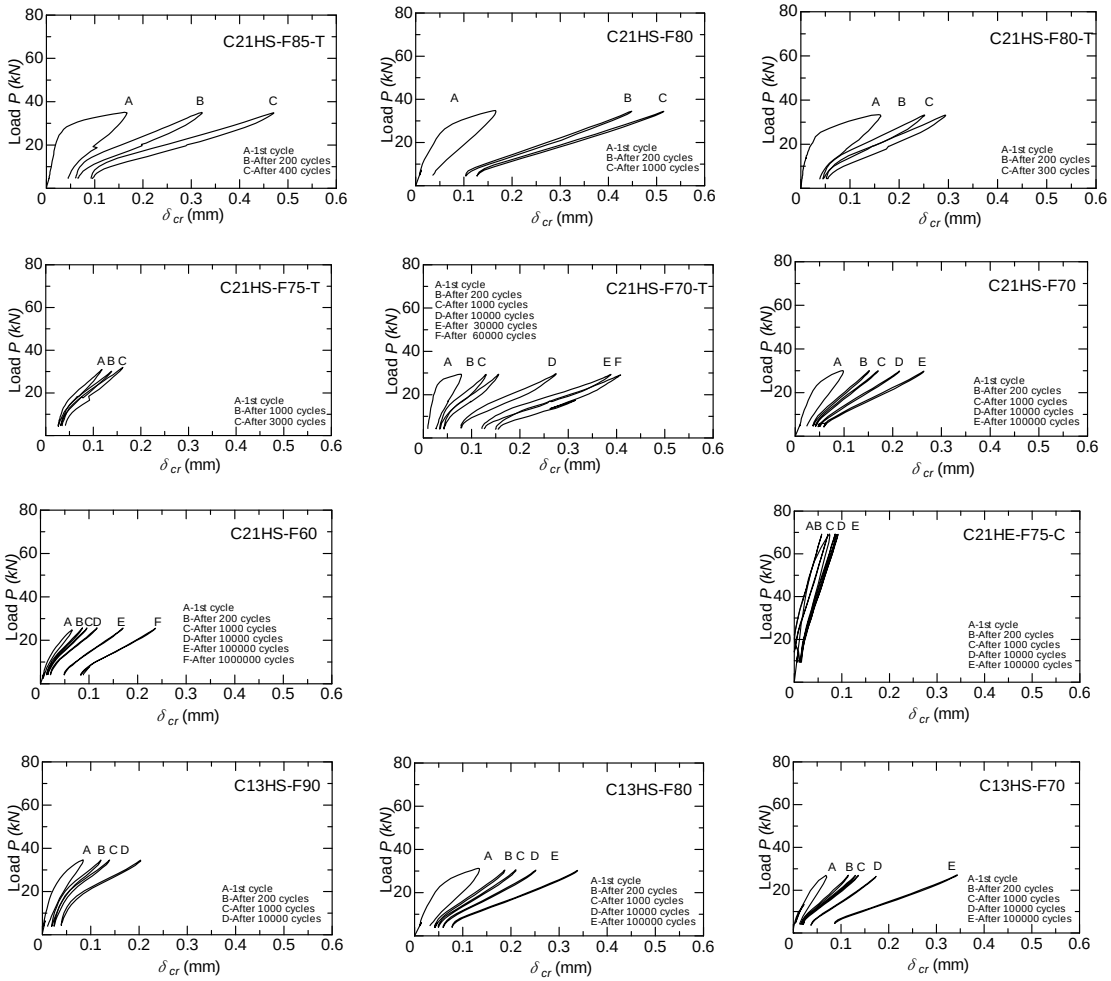

Fig. 3.14 (b) Load-crack width curves

3.3.4.3. Strain Distribution

Fig. 3.15 to Fig. 3.29 present the strain distributions for particular numbers of fatigue cycles. The largest strain is observed at 50 mm from the notch in some specimens, due to a small concrete piece remaining on the CFRP plate. The strain in the HE specimens is lower than that in the HS specimens. In addition, the active bond stress moves from the notch to the load end. The strain distribution curves illustrate that as the number of fatigue cycles increased, the maximum local bond stress moved from the notch to the load end. The HS specimens exhibited higher local bond stress than the HE specimens.

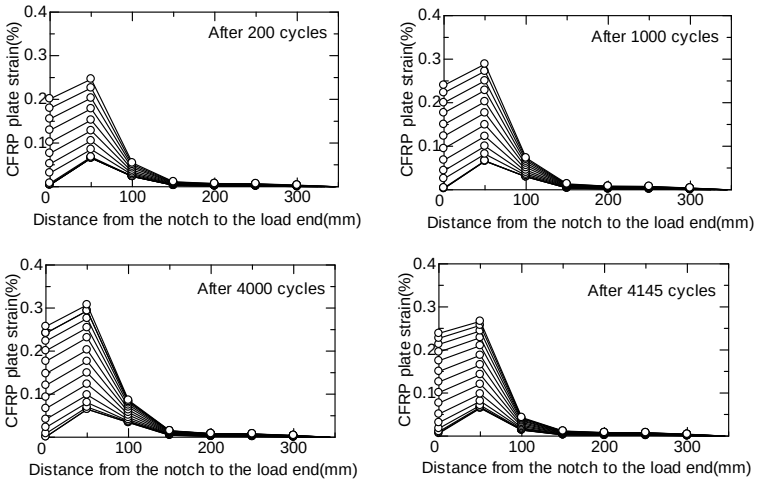

Fig. 3.15 Strain distribution of Specimen C36HS-F70

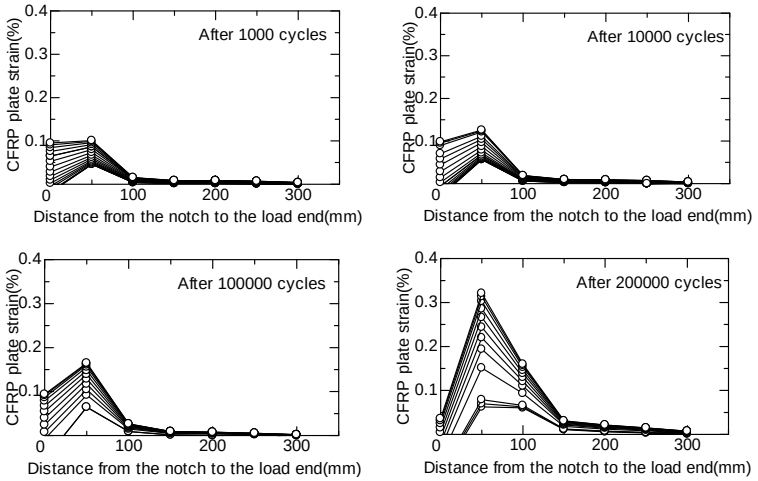

Fig. 3.16 Strain distribution of Specimen C36HS-F60

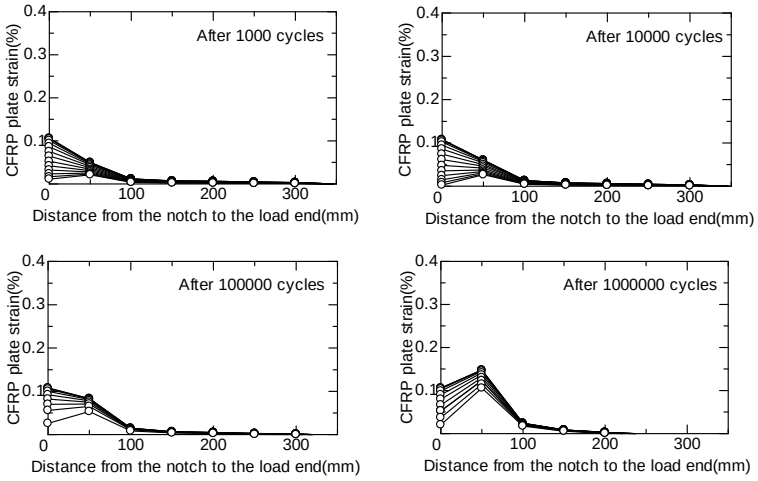

Fig. 3.17 Strain distribution of Specimen C36HS-F50

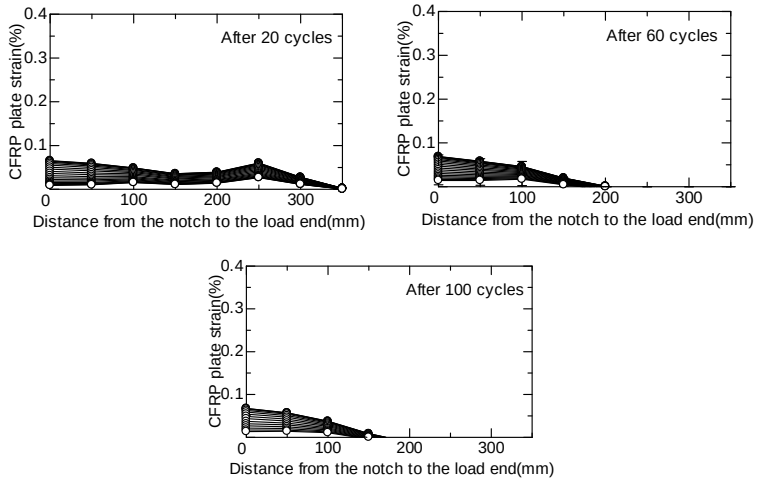

Fig. 3.18 Strain distribution of Specimen C36HE-F75

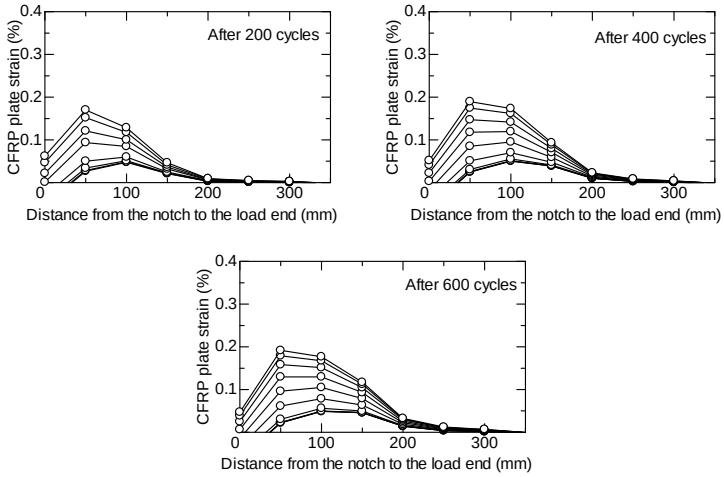

Fig. 3.19 Strain distribution of Specimen C21HS-F85-T

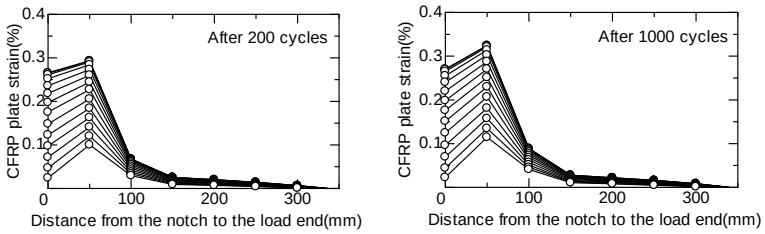

Fig. 3.20 Strain distribution of Specimen C21HS-F80

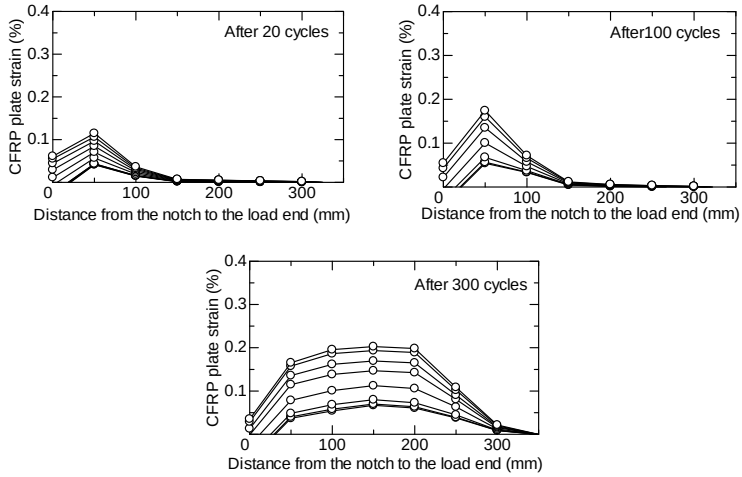

Fig. 3.21 Strain distribution of Specimen C21HS-F80-T

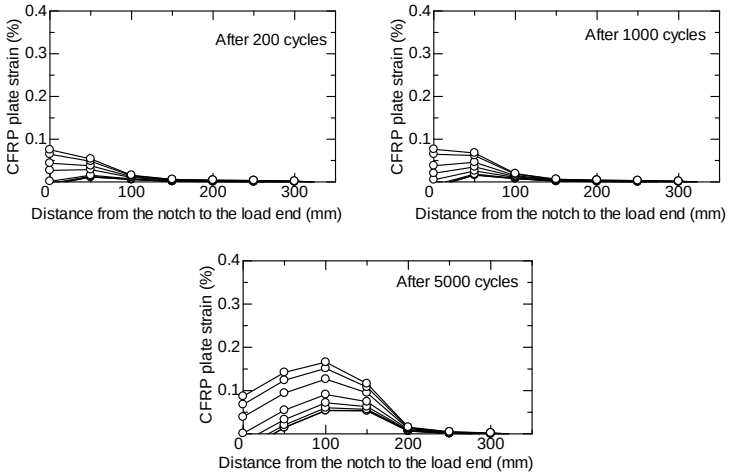

Fig. 3.22 Strain distribution of Specimen C21HS-F75-T

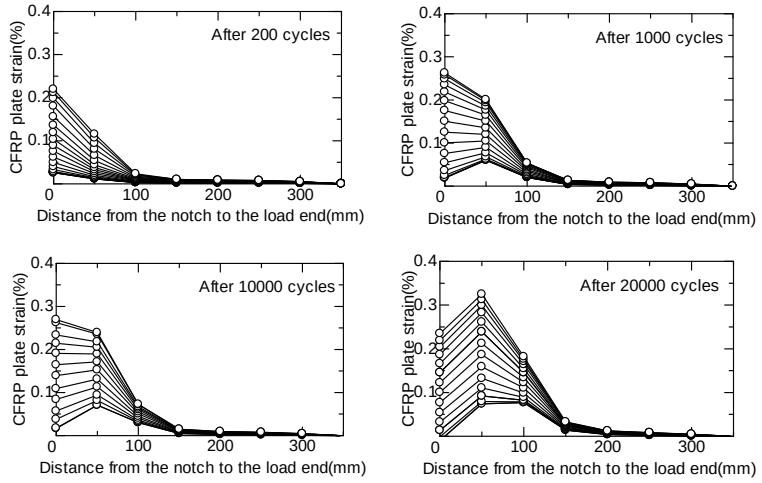

Fig. 3.23 Strain distribution of Specimen C21HS-F70

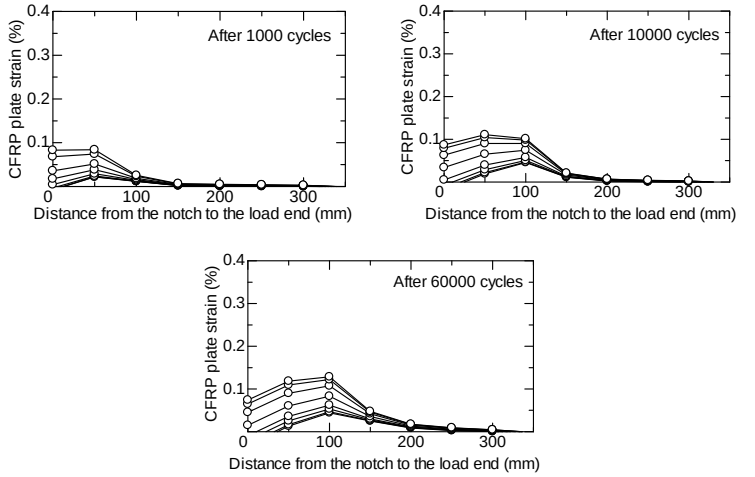

Fig. 3.24 Strain distribution of Specimen C21HS-F70-T

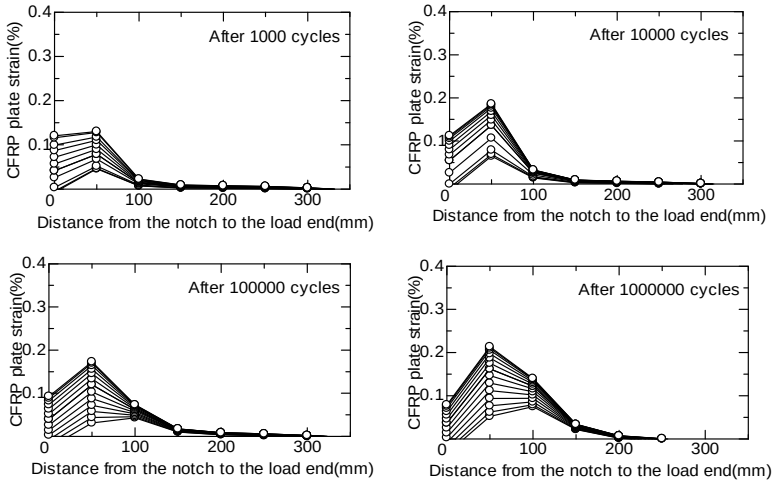

Fig. 3.25 Strain distribution of Specimen C21HS-F60

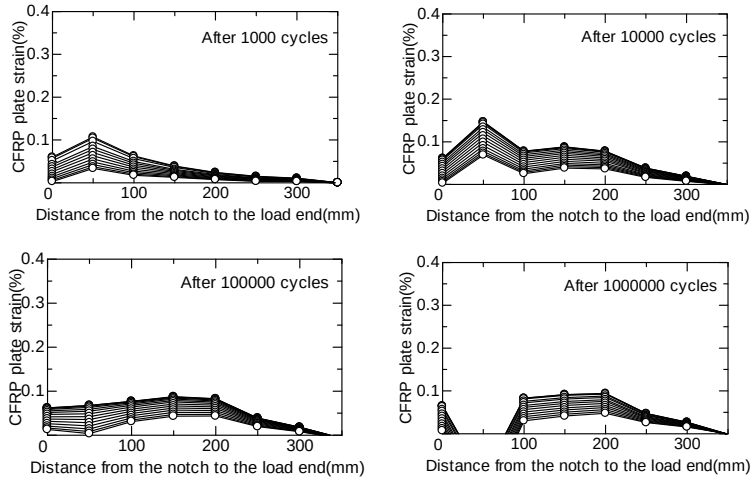

Fig. 3.26 Strain distribution of Specimen C21HE-F75-C

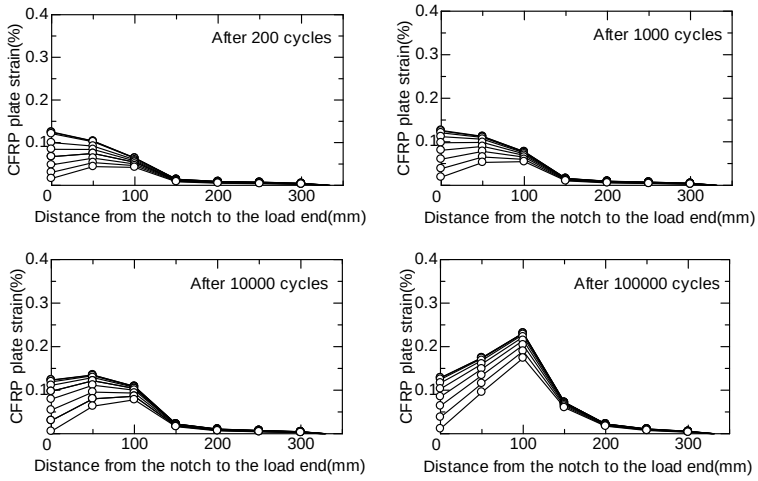

Fig. 3.27 Strain distribution of Specimen C13HS-F90

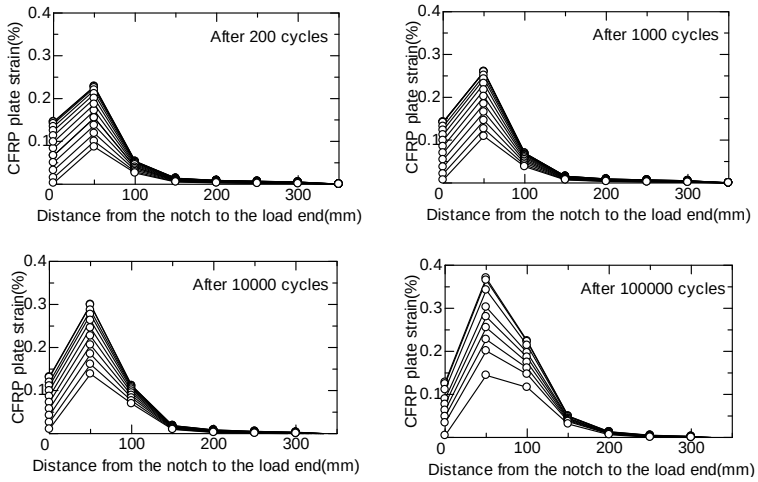

Fig. 3.28 Strain distribution of Specimen C13HS-F80

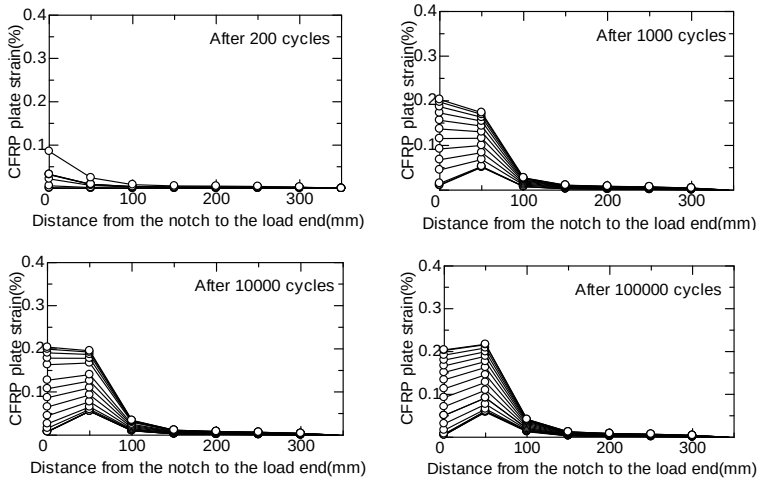

Fig. 3.29 Strain distribution of Specimen C13HS-F70

3.3.4.4. Post-Fatigue Monotonic Behavior

The specimens that endured one million load cycles without failing—C21HS-F60, C36HS-F50, and C21HE-F75-C—were loaded monotonically to failure. Fig. 3.30 compares the load-crack width and total displacement curves of these specimens with those of the static specimens.

The post-fatigue bond strengths of specimens C21HS-F60 and C36HS-f50 were similar to the strengths under static loading. However, the post-fatigue bond strength of specimen C21HE-F75-C was higher than that under static loading of specimen C21HE because the specimen with the confinement jig had a 10% higher bond strength.

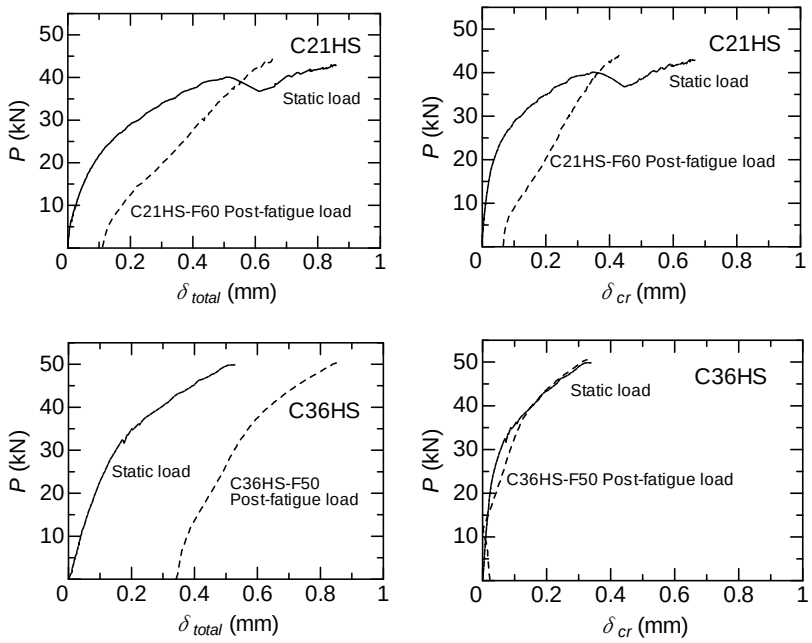

Fig. 3.30 (a) Post-fatigue load-displacement curve

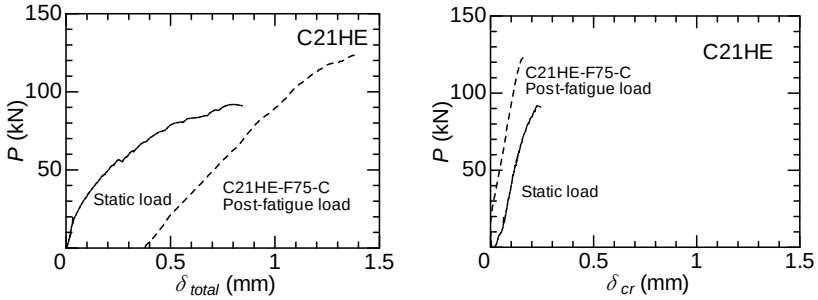

Fig. 3.30 (b) Post-fatigue load-displacement curve

3.3.4.5. Fatigue Life Prediction for Debonding

A useful way to visualize the time to failure for a specific material is with an *S-N* curve. "*S-N*" indicates the alternating stress versus fatigue cycles to failure, which is plotted as the alternating bond stress σ_a on the vertical axis and the logarithm of the number of cycles to failure on the horizontal axis. The alternating bond stress, σ_a, is calculated via Equation (3.16). The *S-N* curve is shown in Fig. 3.31.

$$\sigma_a = \frac{\tau_{up} - \tau_{low}}{2} \tag{3.16}$$

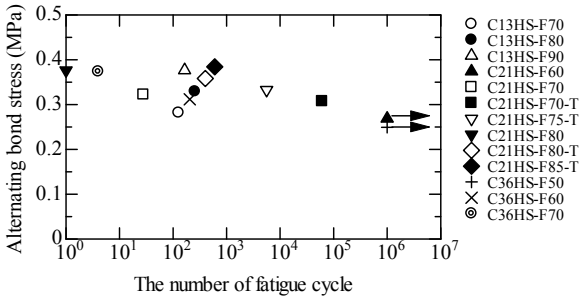

Fig. 3.31 *S-N* curve

To evaluate better the fatigue characteristics of each piece of concrete's compressive strength, a regression method was adopted for this study. The fatigue life prediction method assumes a linear relation between the ratio of the upper-limit fatigue load to the static load strength and the logarithm of the number of load cycles to failure *N*, as expressed in Equation (3.17).

$$\frac{P_{up}}{P_{\max}} = a \cdot \log N + 1 \tag{3.17}$$

where P_{up} = the upper limit fatigue load on the CFRP plate, P_{max} = the bond strength under a static load, N = the number of fatigue cycles, and a = a coefficient for the concrete compressive strength.

The change of the slope in Eq. 3.17 might indicate a change in the fatigue resistance based on concrete compressive strength; in other words, the reduced slope of Eq. 3.17 indicates that the current FRP plate-concrete bonding system might lose its fatigue resistance at a fast rate. A summary of the concrete compressive strength constants is given as follows. These constants indicate that, as with all similar applications, the bond, and thus the capacity, is controlled by the concrete compressive strength. Above all, coefficients with relationships with concrete compressive strength were generated by linear regression.

a = -0.038 (in case of C13HS specimens)
a = -0.065 (in case of C21HS specimens)
a = -0.080 (in case of C36HS specimens)

Fig. 3.32 (a) presents the normalized maximum applied load in the upper-limit load (P_{up}/P_{max}) versus the number of cycles to failure (N). A linear regression analysis of the results for specimens C13HS, C21HS, and C36HS yielded the relation between the coefficient and compressive strength shown in Fig. 3.32 (b). The following best-fit curve was obtained:

$$\frac{P_{up}}{P_{\max}} = -0.0021\sigma_B \cdot \log N + 1 \quad (\sigma_B \text{ in MPa}) \tag{3.18}$$

For a given type of CFRP plate, a higher concrete compressive strength corresponds to a shorter fatigue life.

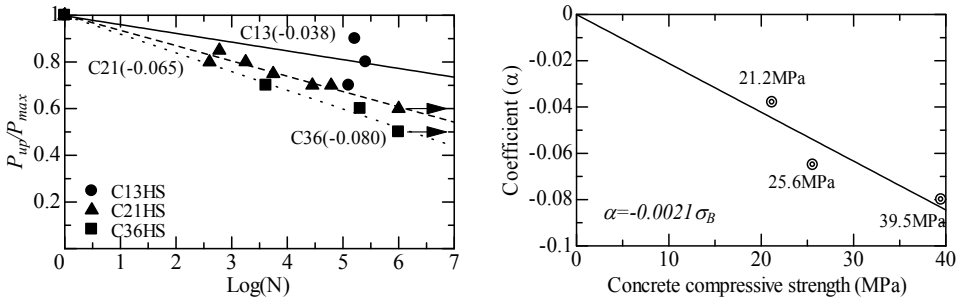

(a) (b)

Fig. 3.32 Fatigue life prediction method

In the present research, as shown in Fig. 3.32(a), little difference was observed in the slopes of the regression lines for the three types of concrete compressive strength, suggesting that the same mechanism of failure might be operating in all three concrete strengths. In other words, the concrete strength was treated as the dominant factor in fatigue performance. In all of the above, the coefficient could be linked to changes in concrete strength, based on linear regression.

3.3.4.6. Local Bond Stress-Slip Relationship

The method for calculating the local bond stress and slip for specimens subjected to

fatigue loading is the same as the method used for specimens subjected to static loading. The local bond stress-versus-slip (τ *vs.* s) graphs for the 0-50-, 50-100-, and 100-150-mm gauge intervals for the C21HS-F70 specimen are plotted in Fig. 3.33, which illustrates that the local bond stress-slip relationship of the selected specimens under fatigue loading is nearly elastic. However, the stiffnesses of the curves decrease as the number of fatigue loading cycles increases. The maximum bond stress also decreases for the 0-50- and 50-100-mm intervals.

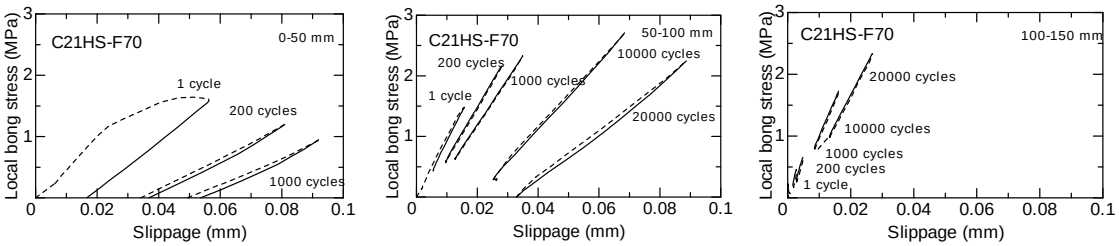

Fig. 3.33 Local bond stress-slip curve of specimen C21HS-F70

3.3.5 Proposed Local Bond Stress-Slip Relation under Fatigue Load Conditions

3.3.5.1 Envelope Curve According to the Popovics Model

The objective of this section is to propose a model that can represent the local bond stress-slip relationship under fatigue load conditions. First, the Popovics model is chosen to express the envelope curve. This model, which was originally proposed to describe the stress-strain curve for concrete compressive behavior, is shown below.

$$\frac{\tau_i}{\tau_{\max}} = \frac{s_i}{s_{\max}} \cdot \frac{n}{(n-1)+(s_i / s_{\max})^n} \tag{3.19}$$

$$\tau_{\max} = 2.5\sigma_B^{0.23} \tag{3.20}$$

where τ_i = local bond stress

s_i = slip (mm)

$\tau_{\max}$ = maximum local bond stress

$s_{\max}$ = slip at $\tau_{\max}$ (= 0.0429 mm)

n= constant (= 3)

σ_B = concrete compressive strength

The adaptability of the Popovics model to local bond stress-slip curves was previously investigated for FRP sheet-to-concrete bonding systems [3.6]. This model has also

been adapted to the development of local bond stress-slip curves for CFRP plate-to-concrete bonding systems for the case of monotonic loading [3.5], and the values of τ_{max}, s_{max}, and n used were those obtained in that study.

Fig. 3.34 provides examples of the envelope curve from the Popovics model for the C21HS-F series and their experimental curves. The local bond stress and slip are normalized by Eq. (3.20) and s_{max}, respectively. The experimental curves correspond to the fatigue load condition just inside the envelope curves.

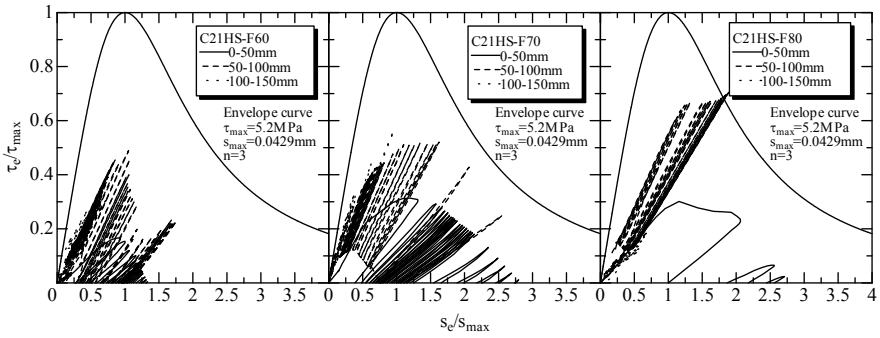

Fig. 3.34 Normalized local bond stress-slip relations for the C21HS-F series

3.3.5.2 Model of the Local Bond Stress-slip Relationship for Fatigue Loading

As described in the previous section, the local bond stress-slip relations in fatigue loading are nearly linear. The stiffness of the curve gradually decreases as the number of fatigue cycles increases. If this part of the curve is included in the unloading and reloading branches of the curves, the local bond stress-slip relation under fatigue loading can be characterized by a certain point on the envelope curve and by the stiffness, as shown in Fig. 3.35. The stiffness of the local bond stress-slip relation under fatigue loading can be evaluated using the unloading branch of the experimental curve, and thus, the unloading branches based on the experimental values have a linear relation for all fatigue cycles. Therefore, the stiffness of the unloading branch (k_i) at all fatigue cycles can be obtained. This model uses a linear approximation of the unloading-reloading path for simplicity.

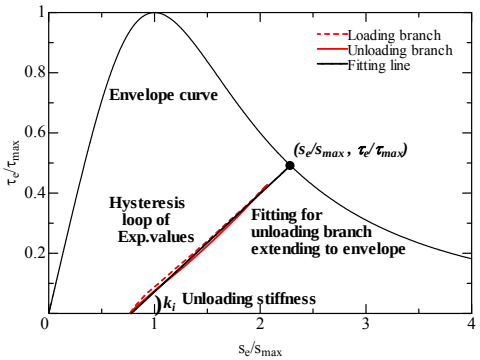

Fig. 3.35 Unloading branch stiffness

Fig. 3.36 illustrates the relationship between the stiffness of the unloading branch k_i and s_e/s_{max} for specimen C21HS-F70 at the gauge intervals of 0-50, 50-100, and 100-150 mm. s_e is defined as the slip at the cross point on the envelope curve and the extended line from the experimental unloading branch, as shown in Fig. 3.35. The solid line indicates the values estimated from the least-squares regression equation shown as Eq. (3.21).

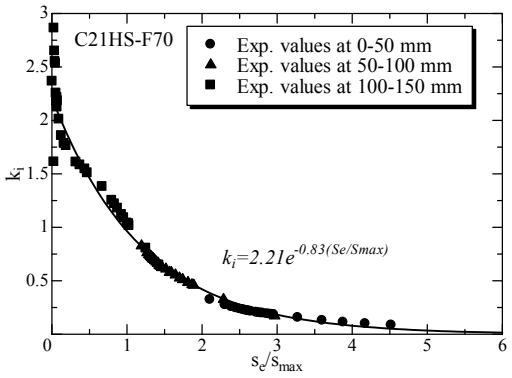

Fig. 3.36 Unloading branch stiffness and slip relationship

$$k_i = 2.21 \cdot e^{-0.83 \cdot (\frac{s_e}{s_{\max}})} \tag{3.21}$$

where

k_i= stiffness of the local bond stress-slip relation in fatigue

s_e= slip on the envelope curve

The decrement of the stiffness is evaluated by the decrement ratio, which is defined as the stiffness at any arbitrary loading cycle divided by the stiffness of the unloading branch at the first loading cycle, k_i/k_1.

As we know, modeling of fatigue damage has two major aspects: establishing a fatigue failure criterion; and a damage accumulation rule. In the traditional approach to fatigue, the failure criterion relates to fatigue failure (i.e., fatigue life) regarding the number of applied loading cycles to cause that failure (usually having fixed or constant amplitude). An analytical expression of the fatigue failure criterion is the *S*-*N* curve, which plots the stress level, *S*, of the constant-amplitude cycles against the characteristic number of cycles to failure, *N*, at this stress level. In modeling fatigue damage with an *S*-*N* curve, the shape of the curve is usually fixed by an empirical parametric expression; these parameters are used to match the shape to a particular set of experimental data. Because of the large scatter of experimental fatigue lives, particularly at lower stress levels, practical measurement of these shape parameters requires statistical methods, such as linear and nonlinear regression analysis.

Likely a more sound approach, from a physical point of view, is to treat damage accumulation as the process of evolution of a damage parameter under the loading history. This evolution is most naturally specified in terms of a differential equation with regard to the loading cycles, although other mathematical expressions might also

prove appropriate. Examples for the damage parameter include residual stiffness and residual strength.

In association with such an approach, the failure criterion is postulated in terms of a critical (failure) value for the chosen damage parameter. Integration of the evolutionary damage equation can be undertaken for either constant or variable-amplitude loadings. For the constant amplitude case, analytical integration is often possible, which also allows for a relationship between the critical damage parameter and the fatigue life, *N*, to be established. From this relationship, an *S*-*N* curve model can also be derived, which places the *S*-*N* curve approach on a sound basis.

Fig. 3.37 illustrates the relationship between the stiffness decrement ratio k_i/k_1 and the number of fatigue loading cycles *N* on a logarithmic scale. Regression analysis yielded Eq. (3.22):

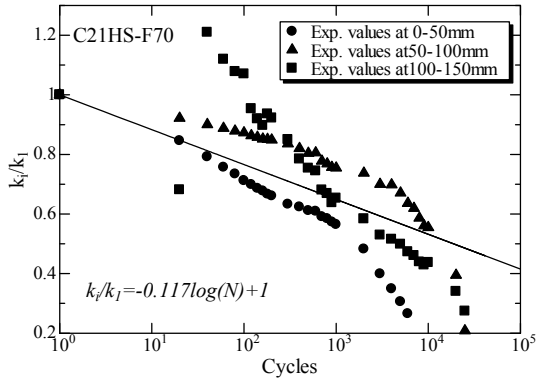

Fig. 3.37 Unloading branch stiffness and fatigue cycle relationship

$$\frac{k_i}{k_1} = 1 - 0.117 \cdot \log(N) \tag{3.22}$$

where

k_i= stiffness of the local bond stress-slip relation in the fatigue cycle
k_1= unloading stiffness at the first cycle
N= number of fatigue cycles

Fig. 3.37 shows the relationship between fatigue life (number of loading cycles until failure) and the stiffness decrement ratio k_i/k_1. It can be seen that the *S*-*N* curve can be approximately described as linear if *N* is expressed on a logarithmic scale, and the fatigue life decreases with increases in the stiffness decrement ratio.

In science and engineering, a semi-log graph or semi-log plot is a method of visualizing data that are related according to an exponential relationship. One axis is plotted on a logarithmic scale. This type of plot is useful when one of the variables being plotted covers a large range of values, and the other has only a restricted range — the advantage being that it can bring out features in the data that would not easily

be seen if both variables had been plotted linearly.

Many researchers have developed fracture models to predict the theoretical load response for the debonding failure mode of FRP attached to concrete for static loading conditions (Taljsten 1996[3.7]; Yuan et al. 2001[3.8]; Wu and Niu 2000[3.9]). In the present research, linear regression analysis of the fatigue test results was conducted to develop a relation for the ratio of the unloading branch stiffness (k_i) to the unloading stiffness at the first cycle as a function of the number of fatigue cycles (N). According to this model, the bond shear stress increases linearly with the interfacial slip until it reaches the stress (τ_e) at the Popovics envelope, representing the hysteresis path at any arbitrary number of fatigue cycles. Therefore, as the number of fatigue cycles increases, the bond stiffness decreases along the envelope of the Popovics curve because interfacial softening is assumed. In summary, the failure mode under fatigue loading, based on the proposed model, should be identical to that for a specimen of the same concrete compressive strength under static loading.

Furthermore, it is indicated that the S-N relationships for all of the CFRP plate/concrete bonded interfaces can become unique if the stiffness k_i is expressed by the stiffness decrement ratio. In other words, the fatigue life is independent of the stiffness decrement by local position changing for the CFRP plate/concrete interface if the same stiffness decrement ratio is maintained.

3.3.5.3 Adaptability of the Proposed Model

3.3.5.3.1 Method of Analysis

An analysis was performed to confirm the proposed local bond stress-slip relationship for fatigue loading. This analysis was performed by calculating the equilibrium with the acting force and the compatibility of deformation of an infinitesimal element, as shown in Fig. 3.38. This analytical method can be summarized in the following steps:

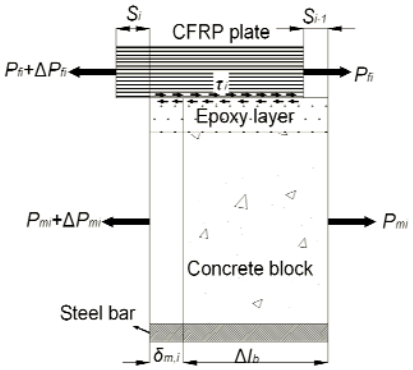

Fig. 3.38 Infinitesimal element

1. The values of k_1 at the intervals 0-50, 50-100, and 100-150 mm are obtained by static analysis at the upper limit of fatigue loading. Furthermore, s_e/s_{max} on the envelope curve at the first cycle can be obtained.

2. The value of k_i at any arbitrary number of cycles can be determined from Eq. (3.22) using the value of k_1.

3. According to Eq. (3.21), s_e/s_{max} on the envelope at any arbitrary number of cycles can be obtained via k_i. Additionally, τ_e/τ_{max} can be calculated from the envelope curve based on the Popovics model.
4. Using the values of k_i, s_e, and τ_e, the straight line presenting the local bond stress-slip relation under fatigue loading is fixed according to Eq. (3.23).

$$\tau_i = \tau_e - k_i \cdot \frac{\tau_{\max}}{s_{\max}} \cdot (s_e - s_i) \tag{3.23}$$

Fig. 3.39 presents a comparison of the proposed local bond stress-slip models and the experimental results for the C21HS-F series. The proposed models display good agreement with the experimental results, except for those at the 100-150-mm interval, due to the limited amount of effective test data.

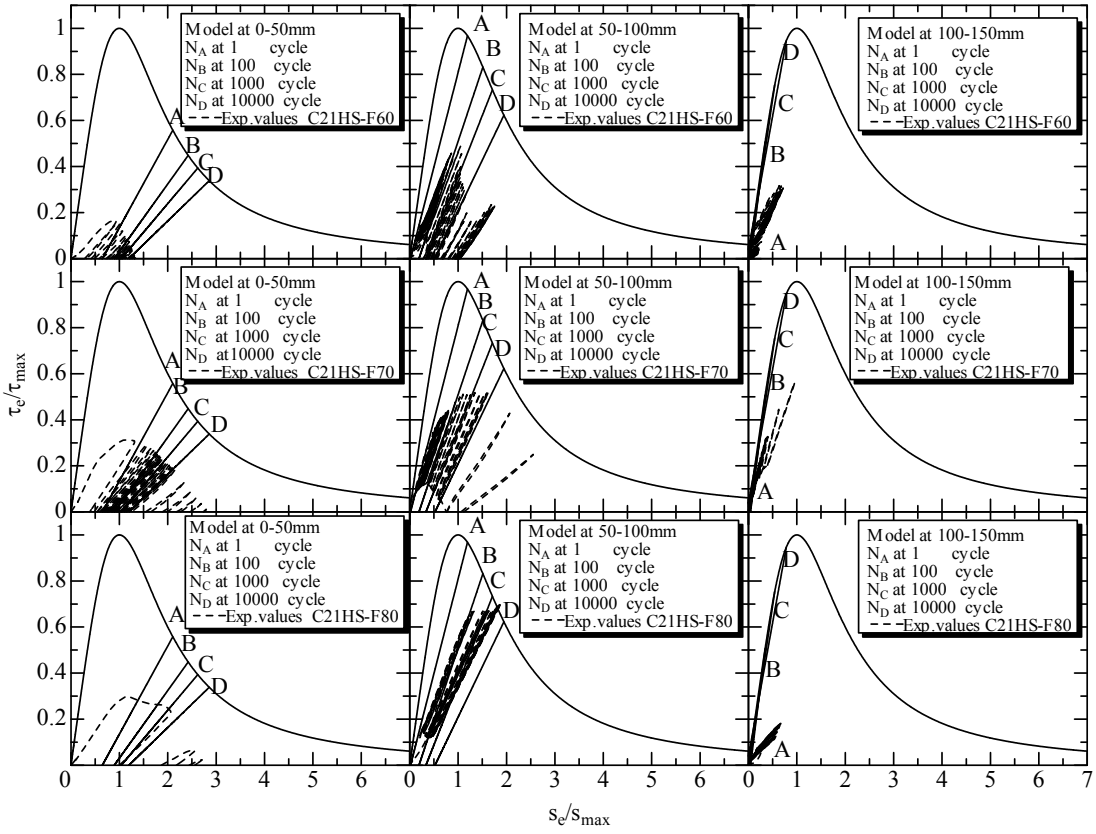

Fig. 3.39 Comparison of the local bond stress-slip relationships

Next, the following infinitesimal element analysis was conducted for an arbitrary number of cycles.

Assuming that the internal bond stress of the element is constant, the slip is obtained from the difference in elongation between the CFRP plate and the equivalent concrete part (concrete, adhesive, and steel). The bond stress is estimated from the proposed

bond stress-slip model for fatigue loading:

A. The slip at the load end s_1 is determined.
B. The bond stress of infinitesimal element i (τ_i) is calculated using Eq. (3.23).
C. The increment of force is $\Delta P_{f,i}$; the elongation of the CFRP plate is $\delta_{f,i}$, and the elongation of the equivalent concrete part is $\delta_{m,i}$. The infinitesimal element i is calculated using the following formulas:

$$\Delta P_{f,i} = \tau_i \cdot b_f \cdot \Delta x \tag{3.24}$$

$$\delta_{f,i} = \frac{\Delta x}{t_f \cdot b_f \cdot E_f}\left(\sum_{k=1}^{i-1} \Delta P_{f,k} + \frac{\Delta P_{f,i}}{2}\right) \tag{3.25}$$

$$\delta_{m,i} = \frac{\Delta x}{A_m \cdot E_f}\left(\sum_{k=i+1}^{n} \Delta P_{m,k} + \frac{\Delta P_{f,i}}{2}\right) \tag{3.26}$$

D. The slip s_i, tensile load $P_{f,i}$, and CFRP plate strain $\varepsilon_{f,i}$ are calculated using the following formulas:

$$s_i = s_{i-1} + (\delta_{f,i} - \delta_{m,i}) \tag{3.27}$$

$$P_{f,i} = P_{f,i} + \Delta P_{f,i} \tag{3.28}$$

$$\varepsilon_{f,i} = \frac{P_{f,i}}{t_f \cdot b_f \cdot E_f} \tag{3.29}$$

If the value of s_i exceeds the value of s_e, it is assumed that the bond stress-slip relation moves to the envelope curve, as shown in Fig. 3.40.

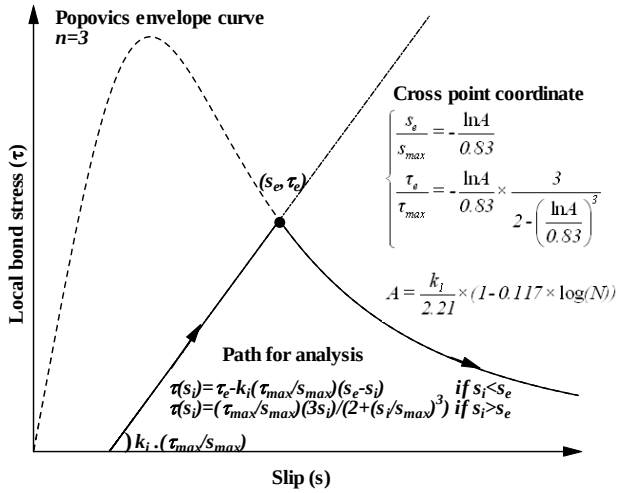

Fig. 3.40 Local bond stress-slip path for analysis

3.3.5.3.2 Comparison of the Analytical and Experimental Results

Fig. 3.41 compares the analytical and experimental results for the strain distributions of the CFRP plate for specimen C21HS-F70 after 100, 1,000, and 10,000 loading cycles. The results from the strain distribution analyses based on the proposed model correspond well to the test results, although the unloading-reloading straight-line paths obtained from the numerical analysis do not correspond well with the experimental results for the 100-150-mm interval (Fig. 3.39).

In the present research, linear regression analysis of the fatigue test results was conducted to develop the relationship for the ratio of the unloading branch stiffness (k_i) with the unloading stiffness at the first cycle as a function of the number of fatigue cycles (N). The strain distributions in the CFRP plate could be numerically calculated from the bond-slip model. The comparison of strain distributions between tests and predictions for specimen C21HS-F70 is shown in Fig. 3.41. Comparisons are undertaken for the given cycle for the same effective stress transfer length during the stage of debonding propagation. It was found that the proposed model was in close agreement with the test results. In other words, strain distributions could be evaluated by the proposed model.

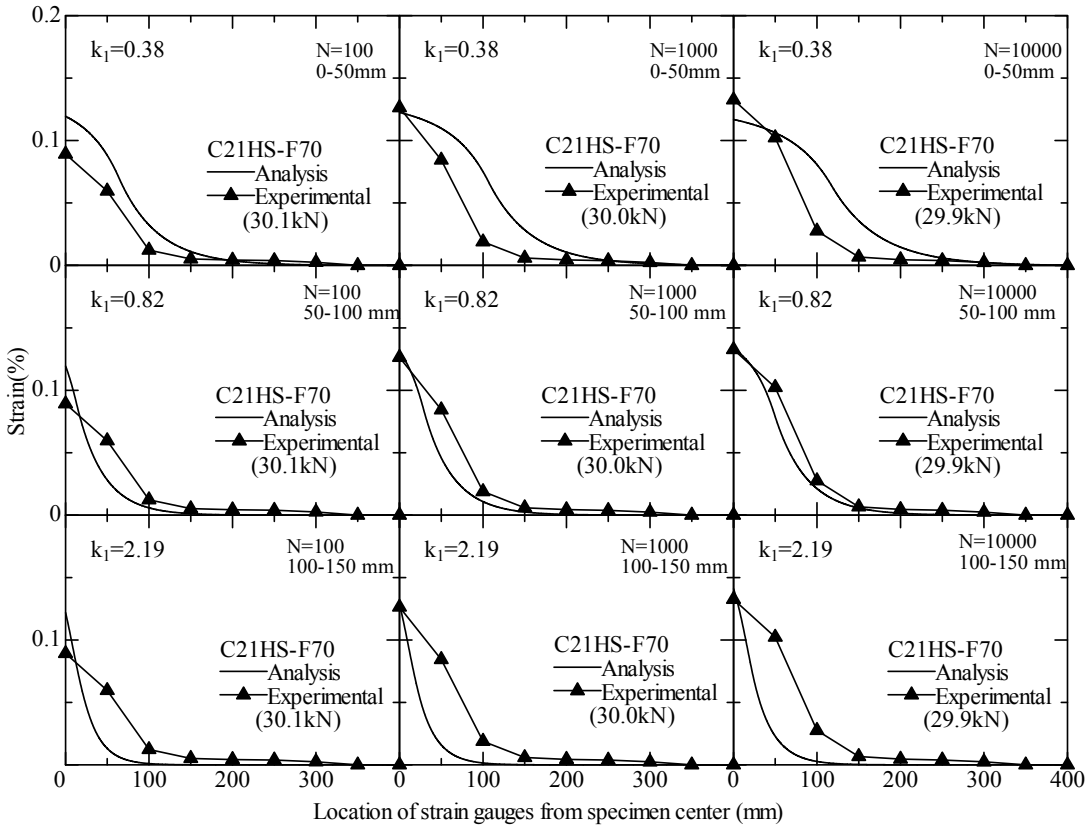

Fig. 3.41 Strain distributions compared with the C21HS-F70 results

3.3.6 Peeling Debonding Behavior under Fatigue Loading

The transverse displacements of the CFRP plate and concrete surface were measured for specimens C21HS-M1, C21HS-M2, C21HS-F70-T, C21HS-F75-T, C21HS-F80-T, and C21HS-F85-T to study the debonding phenomenon. The measurement details of the transverse displacement are shown in Fig. 3.42, and the test setup is shown in Fig. 3.43.

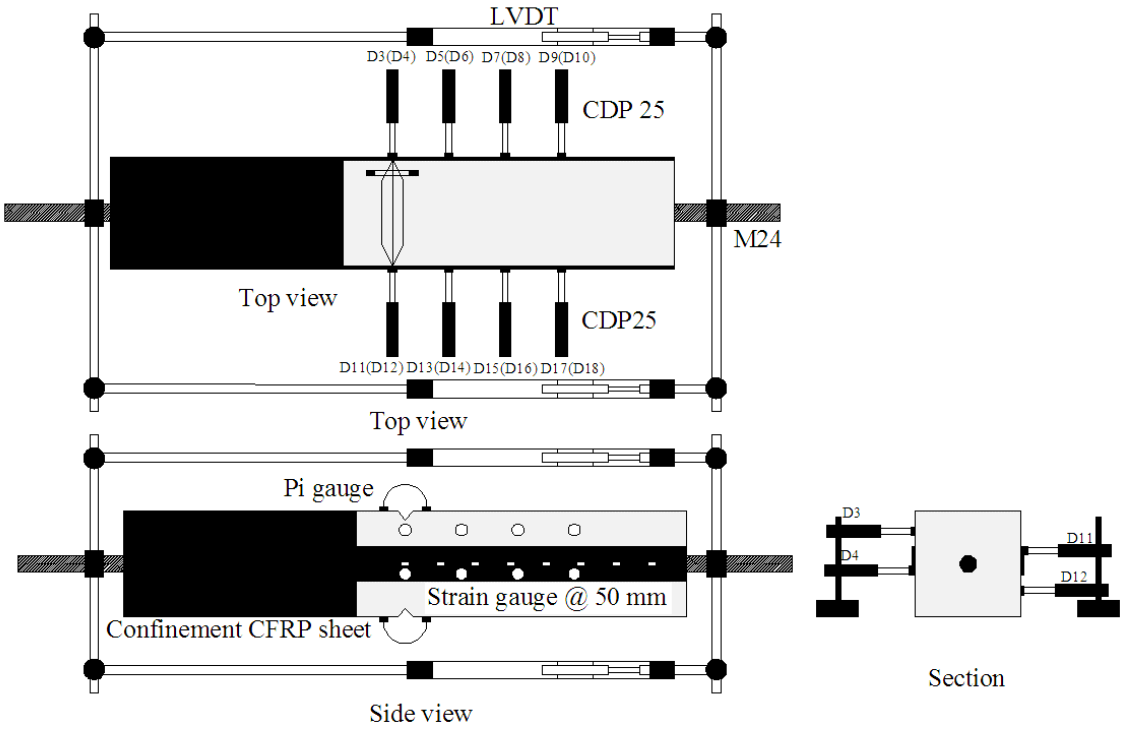

Fig. 3.42 Sketch of the transverse displacement measurement

Fig. 3.43 Test setup

3.3.6.1 Transverse Displacement Relationships

Fig. 3.44 to Fig. 3.48 present the distributions of the transverse displacement differences between the concrete substrate and the CFRP plate at the same sectional position. This difference in the transverse displacement is considered to correspond to "floating" of CFRP plate with respect to the concrete substrate. The transverse displacement difference exhibits some sudden increases representing peeling off of the CFRP plate. Some results clearly illustrate that the location of peeling off of the CFRP plate moved from the specimen center to the load end as the number of fatigue cycles increases.

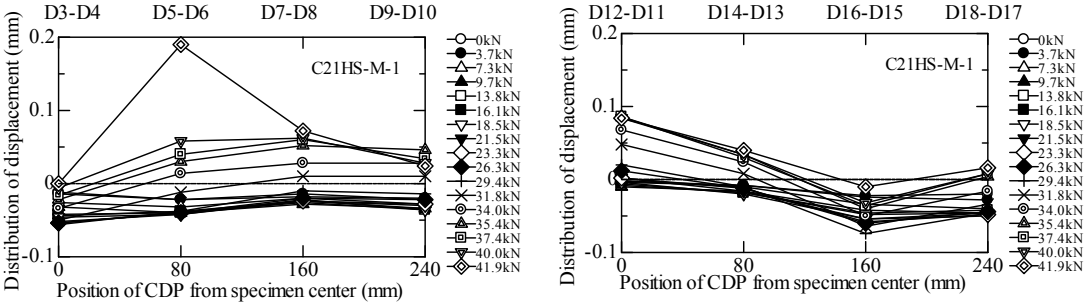

(a) Specimen C21HS-M-1

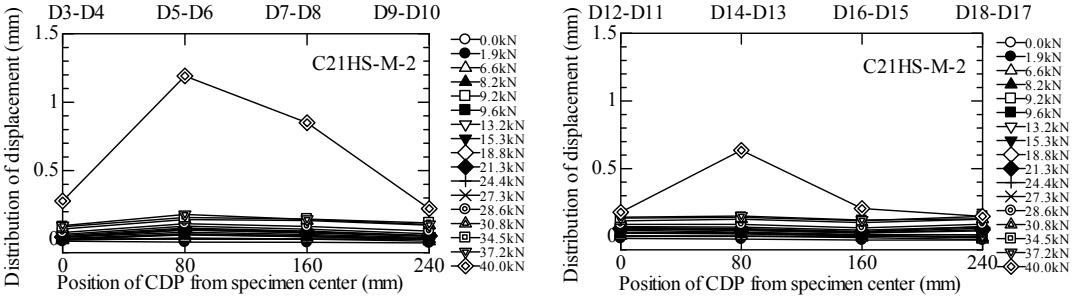

(b) Specimen C21HS-M-2

Fig. 3.44 Distribution of transverse displacement differences

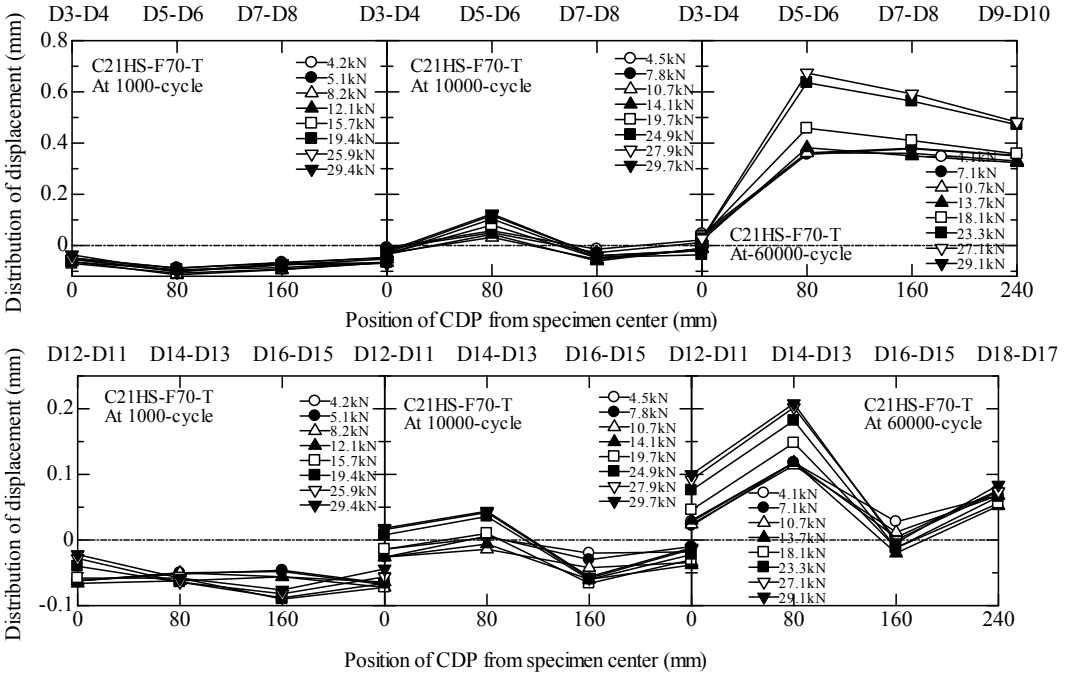

Fig. 3.45 Distribution of transverse displacement differences for specimen C21HS-F70-T

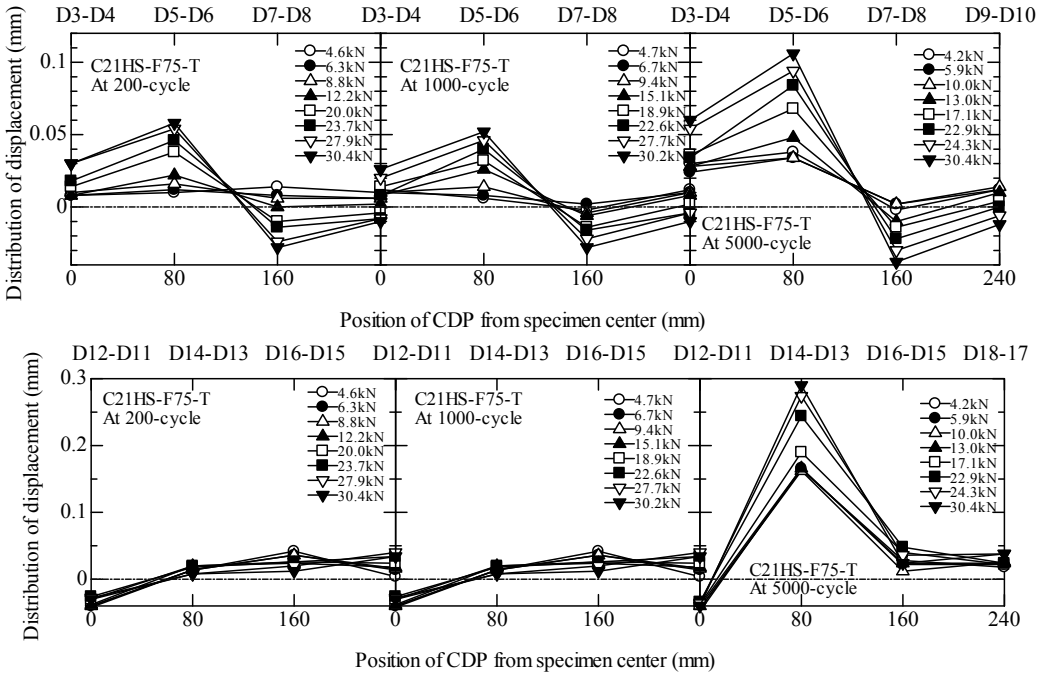

Fig. 3.46 Distribution of transverse displacement differences for specimen C21HS-F75-T

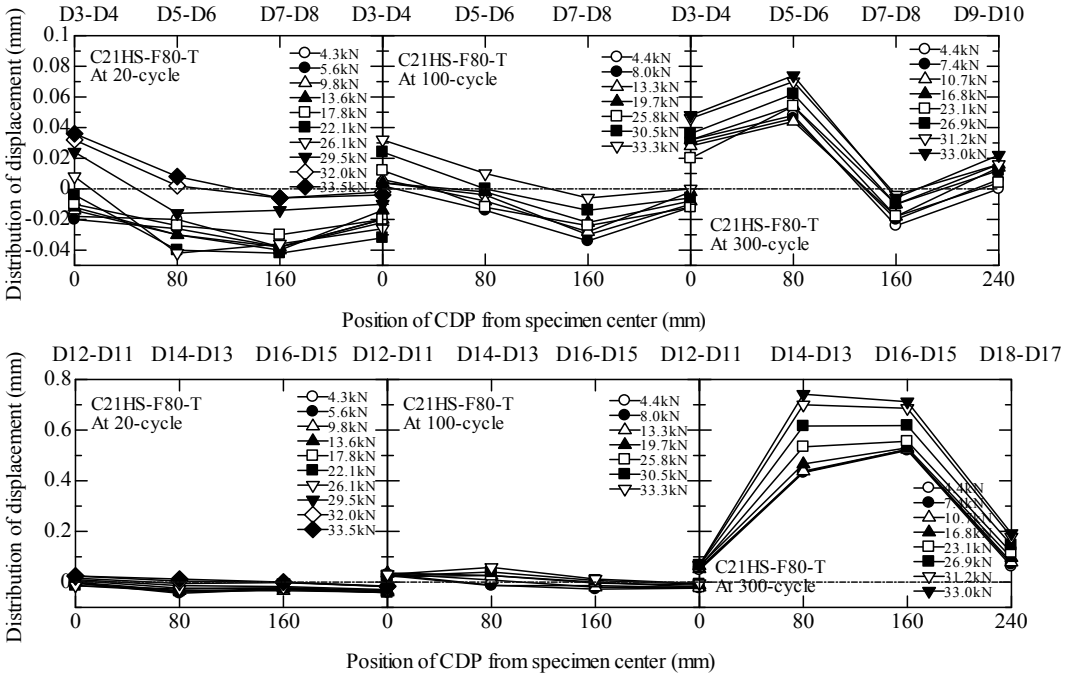

Fig. 3.47 Distribution of transverse displacement differences for specimen C21HS-F80-T

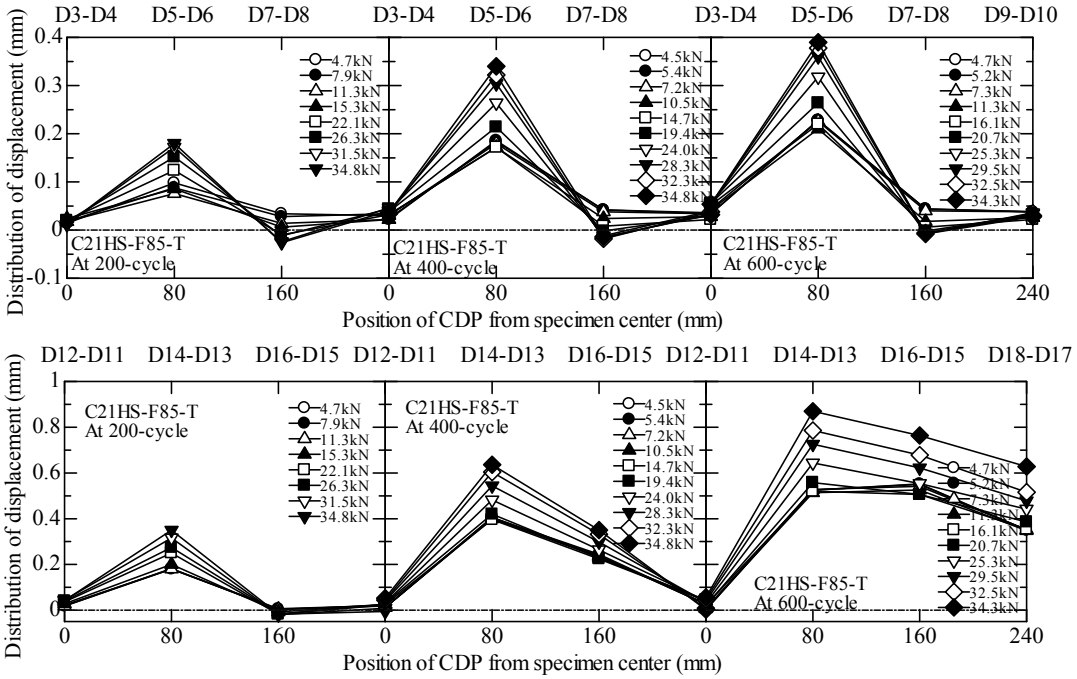

Fig. 3.48 Distribution of transverse displacement differences for specimen C21HS-F85-T

Around the “floating” position of the CFRP plate, the CFRP plate is pulled from the substrate at a certain angle (the “peeling angle”) due to the peeling force, as shown in Fig. 3.49. The interface is subjected to shear and tensile stresses; hence, debonding occurs due to mixed-mode fracture. The reason for the decrease in stiffness and the debonding of the plate under fatigue loading is considered to be an influence of the peeling.

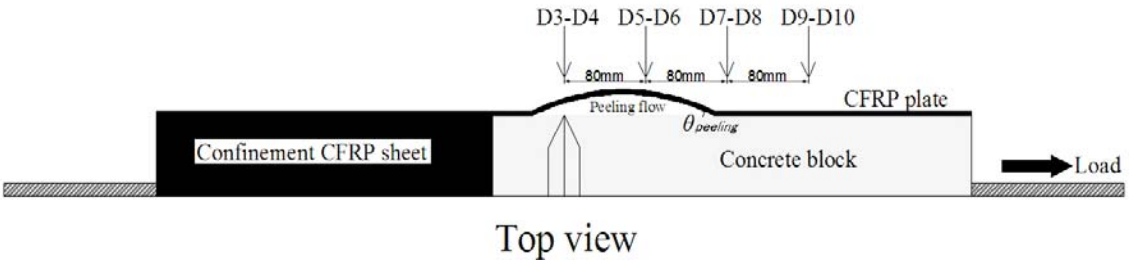

Fig. 3.49 Mechanism of peeling off of the CFRP plate

3.4 Conclusions

The main purpose of this chapter was to investigate the fatigue behavior of the bond behavior between the CFRP plate and concrete.

The double-faced bond specimens were divided into two groups according to the loading method (static or fatigue loading). The following conclusions can be drawn.

Nine specimens were tested under static loading. The type of debonding failure observed was similar to that observed in previous research. The failure face was nearly debonded from the concrete surface. The bond strength increased with increasing stiffness of the CFRP plate and increasing concrete strength. The experimental bond strength values agree well with the calculated values proposed previously. Furthermore, the peeling phenomenon in the CFRP plate was observed in the transverse displacement measurements.

Fifteen specimens were tested under fatigue loading. The primary fatigue failure modes were identified in these studies and are described as follows:

1. Fatigue failure occurs at the initiation of debonding from the notch position.

2. Fatigue debonding of the faces consists of two components. The first component is debonding from the concrete face near the notch, and the second component is debonding from the adhesive face to the load end.

3. *S-N* curves for the fatigue failure of the bond were proposed. The fatigue-limit bond stress after one million cycles was considered for specimens with concrete strengths of 13, 21, and 36 MPa.

4. The monotonic post-fatigue tests indicate that the peak load is not influenced by the fatigue cycles.

5. The stiffness of the local bond stress-slip curve decreases as the number of fatigue loading cycles increases. The reduction coefficient for stiffness is determined from the number of cycles.

6. A local bond stress-slip model was proposed based on the experimental results, and a numerical analysis was performed to confirm the proposed model. The local bond stress-slip model for fatigue loading is based on an evaluation of the stiffness and envelope curves produced by the Popovics model.

In addition, the transverse displacements of the CFRP plates and concrete substrate were measured. The variation in transverse displacement exhibited an obvious discernible peeling phenomenon with debonding propagation. The experiment results indicate that the CFRP plate, upon peeling off, moves from the specimen center toward the load end as the number of fatigue cycles increases. The peeling off of the CFRP plate is an important failure mode affecting the progression of debonding in the fatigue test.

CHAPTER 4

Mixed-Mode Debonding Behavior of CFRP Plates and Concrete

4.1. Introduction

For FRP plate-strengthened concrete members, failure often occurs by FRP plate debonding from the concrete substrate, which can be initiated from either the end of the FRP plate or the mouth of a flexural or shear-flexural crack. Premature failure initiated from the plate end is attributed to the presence of high shear and normal stress concentrations, which have been widely studied (Roberts, 1989[4.1], Malek et al, 1998[4.2], Rabinovich et al, 2000[4.3], EI-Mihilmy et al, 2001[4.4]).

Another possible location for interfacial cracks is the mouth of a flexural-shear crack in a concrete beam. When debonding of an FRP plate occurs as a result of a major flexural crack, there is no relative vertical displacement between the two sides of the crack. In this situation, the debonding of the FRP plate from the substrate of the concrete beam can be considered interfacial debonding in mode II. However, when the debonding failure of the FRP plate is initiated by a major flexural-shear crack, both vertical and horizontal displacements between the two sides of the flexural-shear cracks can be observed. Both shear and peeling in the vicinity of the crack are shown in Fig. 4.1. This debonding failure can be regarded as FRP plate debonding as a result of both interfacial shear and peeling effects (a combination of modes I and II), called mixed-mode failure. In this case, a reduction in the bond strength occurs, which increases the probability of premature local collapse. Hence, the bond performance of this type of structure, strengthened by an FRP plate, depends not only on the shear bond strength of the interface but also on the combined effect of shear bond and peeling. In evaluating the performance of the externally bonded FRP plate strengthening technique, the interfacial bond strength between the FRP plate and concrete for different failure modes is the crucial importance.

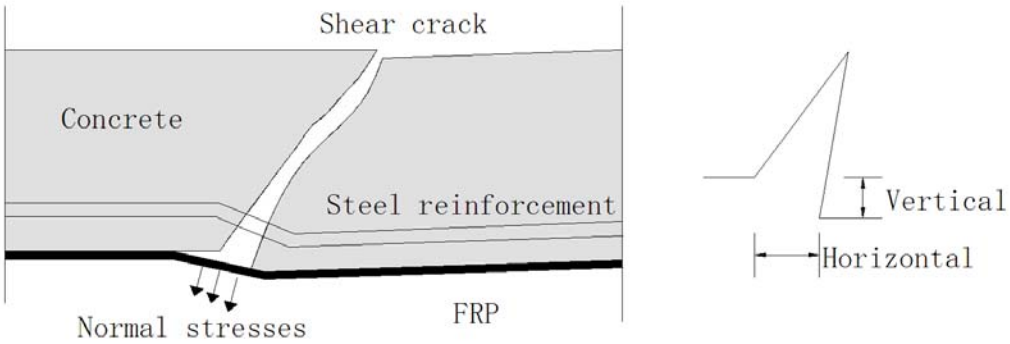

Fig. 4.1 Debonding failure induced by a flexure-shear crack in the concrete beam

As discussed in the previous chapter, the double-faced shear fatigue test experiment results indicate that the CFRP plate, upon peeling off, moves from the specimen center toward the load end as the number of fatigue cycles increases. The peeling off of the CFRP plate is an important failure mode affecting the progression of debonding in the fatigue test. Indeed, the peeling angle is the most important factor to respond to the peeling progress. Therefore, the mixed-mode debonding behavior is investigated by focusing on the peeling angle.

The main objective of this chapter is to investigate the effect of the mixed-mode debonding behavior between the CFRP plate and the concrete. To achieve this objective, special double-faced bond specimens, in which the plates are attached at specific initial angles, were employed to introduce combined shear and peeling effects on bonded CFRP plates. The strain distributions along the CFRP plates during the loading process for cases with different initial angles demonstrate the peeling behavior of the CFRP plates. The failure process was characterized according to the strain distribution at different stages. The effects of the concrete strength and the initial angle on the ultimate responses were studied based on the experimental results. Finally, a method for predicting the mixed-mode fracture bond strength is proposed.

4.2. Experimental Program

4.2.1. Specimens

Uniaxial tensile loading tests were carried out on specimens with CFRP plates bonded on two sides. A total of 12 specimens were prepared, with curved surfaces to connect two different cross sections for each specimen, to allow for the attachment of an initial angle. The specimen details are shown in Fig. 4.2. The level difference between two different cross sections of a specimen is called the step height. The M24 steel bars had no connection at the middle of the specimen, and a pre-crack was introduced before loading, meaning that the two concrete blocks were only connected with CFRP plates. Cylinders were tested at the same time as the specimens to determine the material properties.

The specimen list is shown in Table 4.1. All of the specimens were designed with a “pre-unbond” region setting near the center to clarify the combination of components of the fracture failure at the bonding part. Small initial angles of 2° and 4° and large initial angles of 10° and 20° and target concrete compressive strengths of 13.5 and 21 MPa were considered. The concrete properties are also listed in Table 4.1. High-strength CFRP plate of 1 mm in thickness (GM510) were utilized.

Other important evaluated FRP-concrete interface characteristic parameters include the properties of the adhesive layers. It has been found that adhesive layers with lower elastic moduli but good ductility can have higher interface bond strengths. The mechanical properties of adhesive layers can be adjusted by changing the elastic

modulus of either the resin or putty. However, the effective bond length increases when the elastic modulus of the adhesive layers decreases. In other words, it is possible to obtain different experimental results when different adhesives are used.

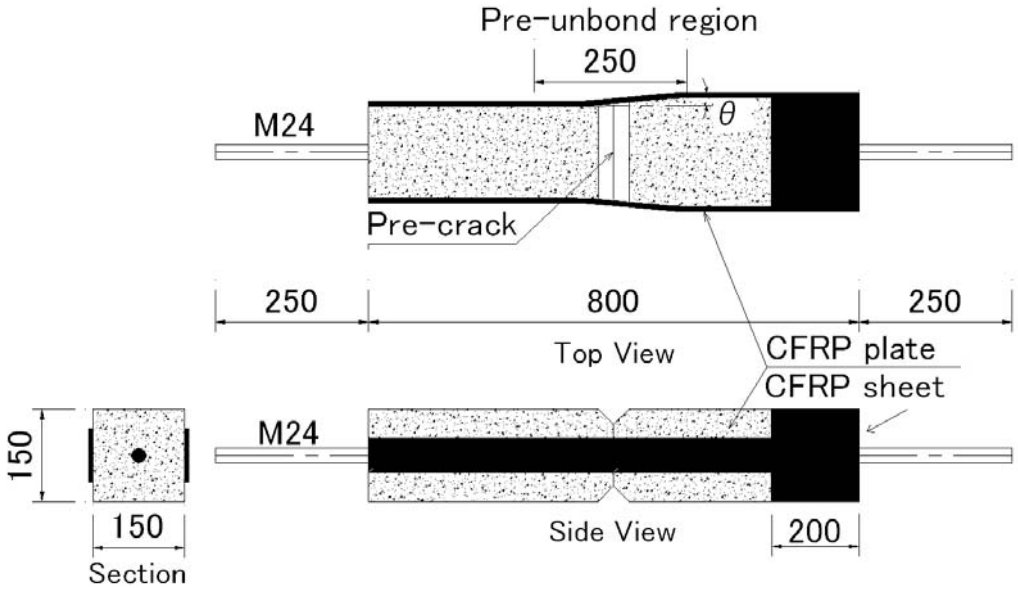

Fig. 4.2 Specimen details

Table 4.1 Specimen list

Specimen	Concrete compressive strength	Concrete splitting strength	Concrete 1/3 secant strength	Designed initial angle θ	Pre-unbond length	Step height	CFRP plate
	MPa	MPa	GPa	degree	mm	mm	
S13-2-1	18.4	1.97	20.3	2	250	8.8	High strength with 1 mm thickness
S13-2-2							
S13-4-1				4		17.5	
S13-4-2							
S13-10	16.9	1.89	19.6	10	200	35.0	
S13-20				20		72.5	
S21-2-1	31.0	2.87	25.4	2	250	8.8	
S21-2-2							
S21-4-1				4		17.5	
S21-4-2							
S21-10	30.8	2.46	23.0	10	200	35.0	
S21-20				20		72.5	

4.2.2. Loading and Measurement

All specimens were subjected to tensile force to cause shear and peeling debonding at the interface of the specimen. Fig. 4.3 presents the test setup for loading with an actuator for the large-initial-angle specimens and loading with a universal testing machine for the small-initial-angle specimens. For each combination of test variables, one specimen was instrumented with eight strain gauges on the CFRP plate surface on one side. These gauges were spaced at intervals of 50 mm from the center of the CFRP plate to the load end. On the opposite side, one gauge was used at the center of the plate. In addition, the total displacements and crack widths at the specimen center were measured using LVDTs and Pi gauges, respectively.

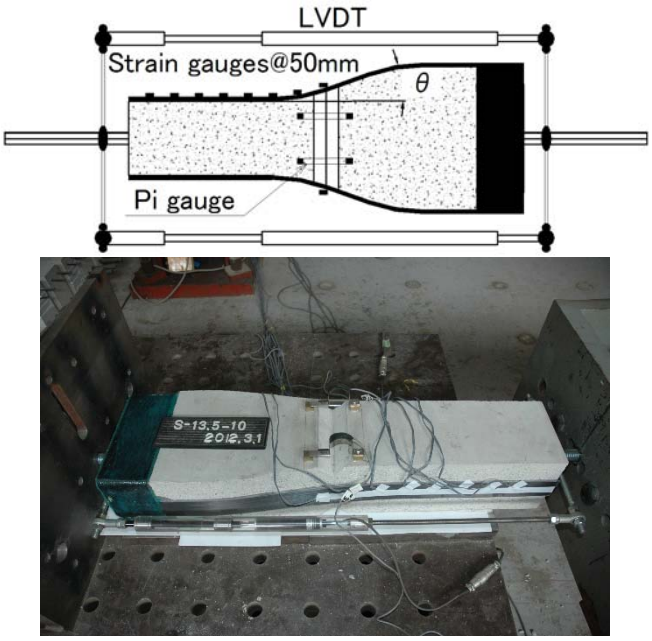

(a) For specimens with large initial angles

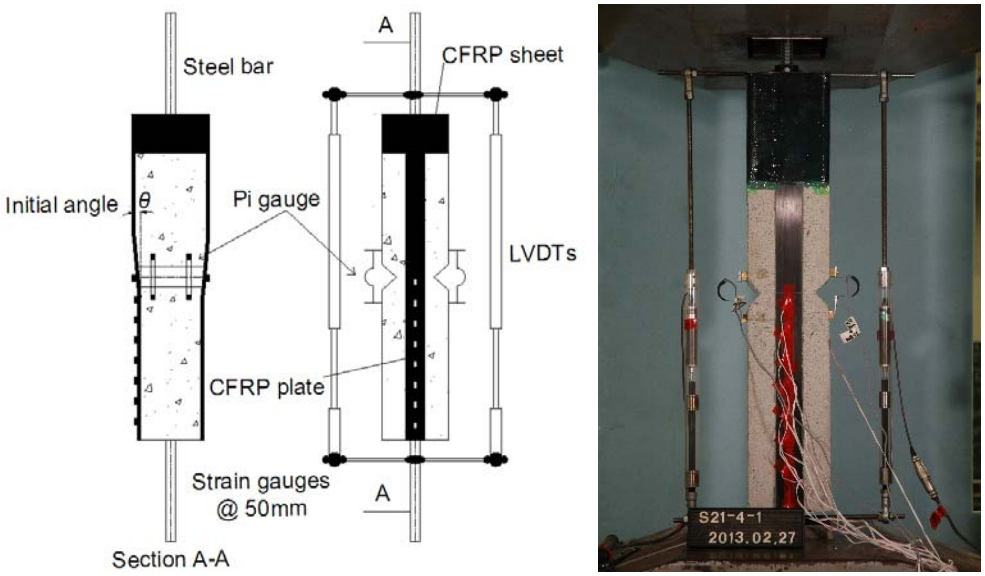

(b) For specimens with small initial angles

Fig. 4.3 Test setup

4.3 Experimental Results

4.3.1 Failure Progress

The experimental results are provided in Table 4.2. The calculated bond strength was determined using the previously proposed calculation method (Matsunaga et al. 2008[4.5]) for the shear bond strength of the CFRP plate. All specimens were subjected to tensile force until debonding failure occurred on either side. Typical failure surfaces from the experimental results are shown in Fig. 4.4. The post-failure photographs indicate that the failure surfaces of the specimens with initial angles of 10° and 20° were between the CFRP plate and the adhesive, whereas the specimens with initial angles of 2° and 4° were debonded at the concrete surface. The specimens with large initial angles exhibited clear peeling of the plate, whereas the debonding progress in the specimens with small initial angles was largely controlled by shear debonding. Nevertheless, all debonding was considered to be due to the combination of two fracture modes (peeling and shear).

Table 4.2 Experimental results

Specimen	Maximum load P	Calculated bond strength P_{cal}	P/P_{cal}	Failure face
	kN	kN		
S13-2-1	20.8	38.7	0.54	Concrete layer
S13-2-2	20.3		0.53	
S13-4-1	15.5		0.40	
S13-4-2	16.0		0.41	
S13-10	5.1		0.13	Adhesive layer
S13-20	5.5		0.14	
S21-2-1	23.4	41.4	0.61	Concrete layer
S21-2-2	24.3		0.63	
S21-4-1	20.8		0.54	
S21-4-2	17.0		0.44	
S21-10	7.3		0.19	Adhesive layer
S21-20	6.1		0.16	

Fig. 4.4 (a) Typical failure faces of the specimens with small initial angles

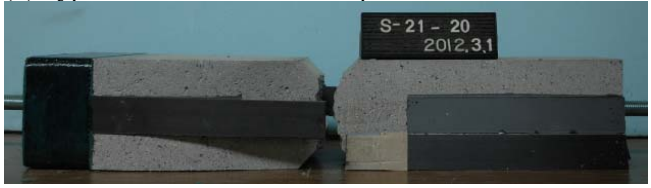

Fig. 4.4 (b) Typical failure faces of the specimens with large initial angles

4.3.2. Load-versus-Displacement Relation and Strain Distribution

The load-crack width curves are presented in Fig. 4.5. In the small-initial-angle specimens, the CFRP plate peeled off toward the load end of the specimen as the tensile load increased. However, in the large-initial-angle specimens, the 10° and 20° specimens exhibited different behaviors as the CFRP plate delaminated. In one specimen, there was an abrupt decrease up to the maximum tensile load and a gradual increase to failure. In the other specimens, the maximum tensile load up to the peak load was reached and then gradually decreased until failure. The sudden decreases in load evident in the curves represent the propagation of the CFRP plate delamination.

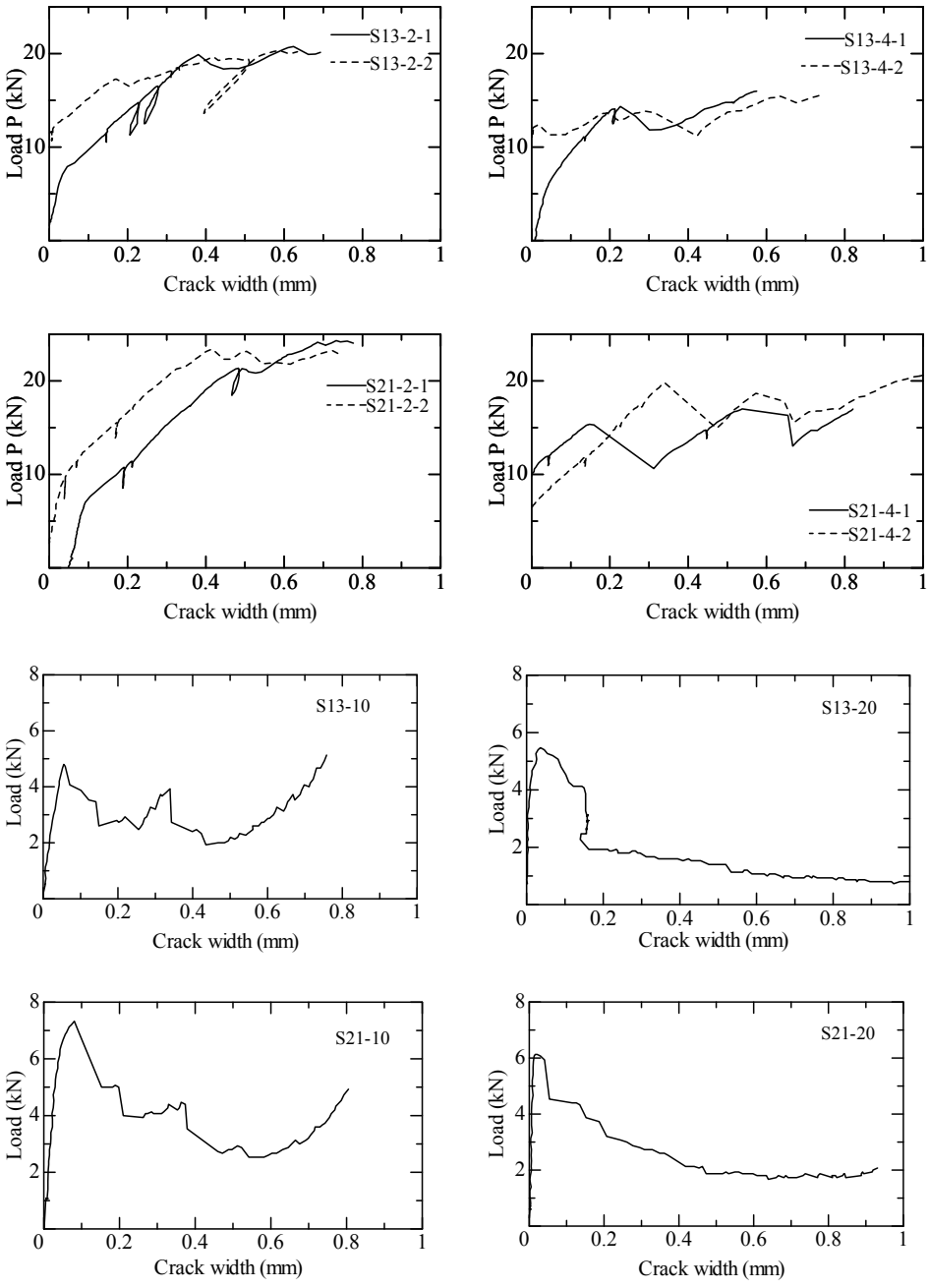

Fig. 4.5 Load-versus-crack width relationship

Fig. 4.6 presents the strain distributions observed, with tensile load-versus-crack width diagrams for some selected specimens. The strain distributions correspond to the marked plots on the tensile load-versus-crack width diagrams. As expected, some negative strains were observed due to bending of the CFRP plate during progressive debonding in the large-initial-angle specimens, as in the case of the FRP sheet (Alam et al. 2012[4.6]). As the debonding progressed, the negative strain moved toward the load end. In contrast, there was no negative strain in the debonding progress of the small-initial-angle specimens. The curve trends for the small-initial-angle specimens are similar to those for the shear bond behavior, which is consistent with the differences in the debonding failure faces discussed in the previous photographs.

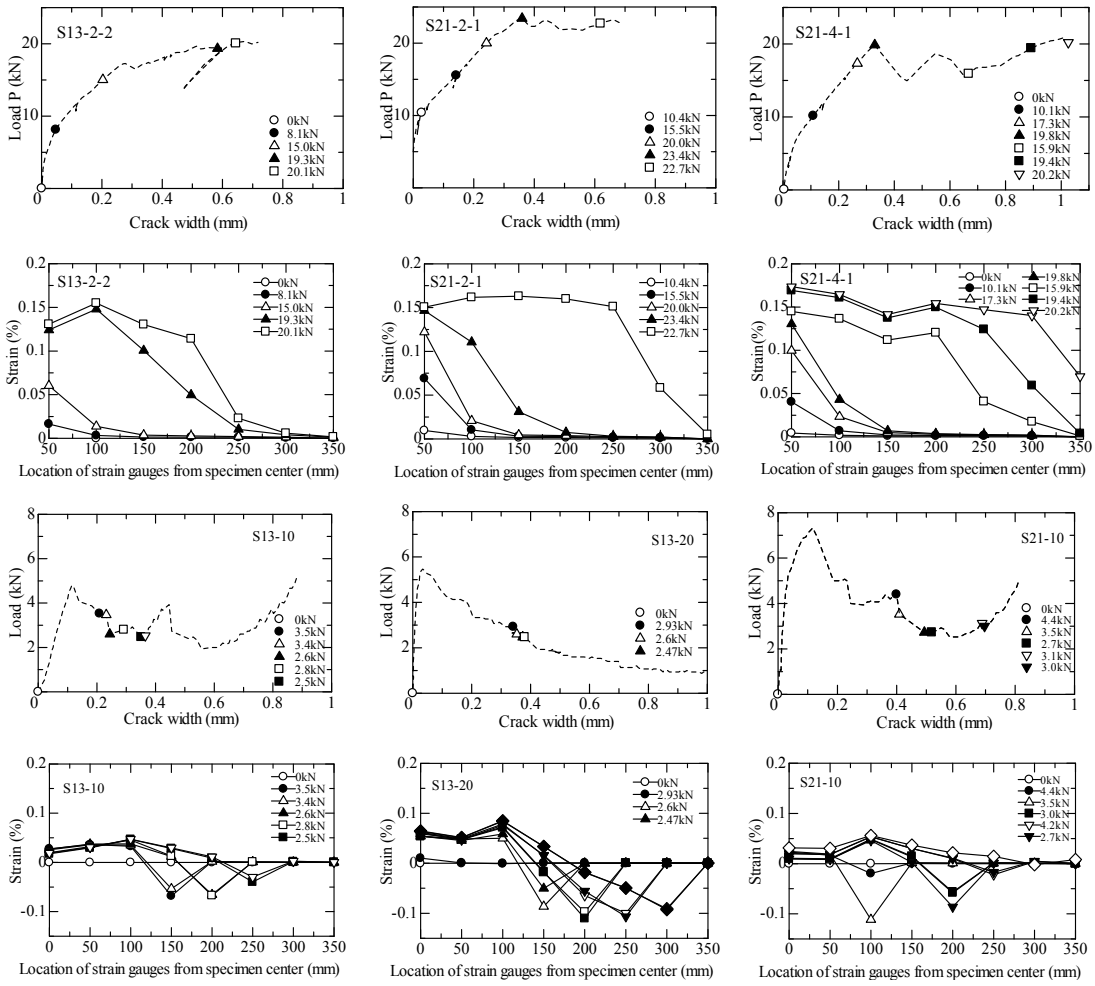

Fig. 4.6 Strain distributions corresponding to marked plots of the load-crack width relationship

4.4. Evaluation of the Bond Strength

The effect of the combination of fracture modes on the bond strength was evaluated using the same method as that for the FRP sheet (Alam et al. 2012[4.6]); thus, the relationship between the tensile load ratio (P/P_{cal}) and the peeling angle ($\tan \theta_p$) was used to evaluate the combination of fracture bond strengths. A detailed delamination

process is illustrated in Fig. 4.7. As the load increased, the plate delaminated due to the peeling effect, and the bond length and peeling angle (tan θ_p) between the CFRP plate and the concrete face decreased. The delaminated region is defined as the distance from where the pre-unbond region starts on the test part of the specimen to the strain gauges, where the minimum (negative) strain was observed in the cases of the large-initial-angle specimens. The residual of the CFRP plate bonded length is the effective bonded region, which gradually decreases until failure. The peeling angle was obtained as the angle between the axial direction and a tangential line from the specimen surface to the position of minimum strain appearing in the CFRP plate. The load P corresponding to this minimum strain was recorded from the data to fit the relation of the tensile load ratio and peeling angles. In the case of the small-initial-angle specimens, the values after the sudden decrease of the tensile load were selected because no negative strains were recorded. For example, in specimen S13-2-2, the values which for load P at the first sudden drop occurred until before the next sudden drop load value occurred, which was selected according to the debonding region of the starting point of step height to the strain gauge at 100 mm from the specimen center. Subsequently, the values continued to be selected step by step, corresponding to the debonding region and extending to the strain gauge at 150 mm. The same method for selecting values was applied to the debonding region extending to the strain gauge at 200 mm, 250 mm, 300 mm, and 350 mm from the specimen center.

The ratio of the tensile load P to the calculated bond strength P_{cal}, according to Eqs. (4.1) to (4.5) (Matsunaga et al. 2008[4.5]) was plotted against the peeling angle (tan θ_p), as shown in Fig. 4.8. The tensile load decreases as the peeling angle increases. The relationship between the tensile load ratio and peeling angle can be obtained as shown in the figure.

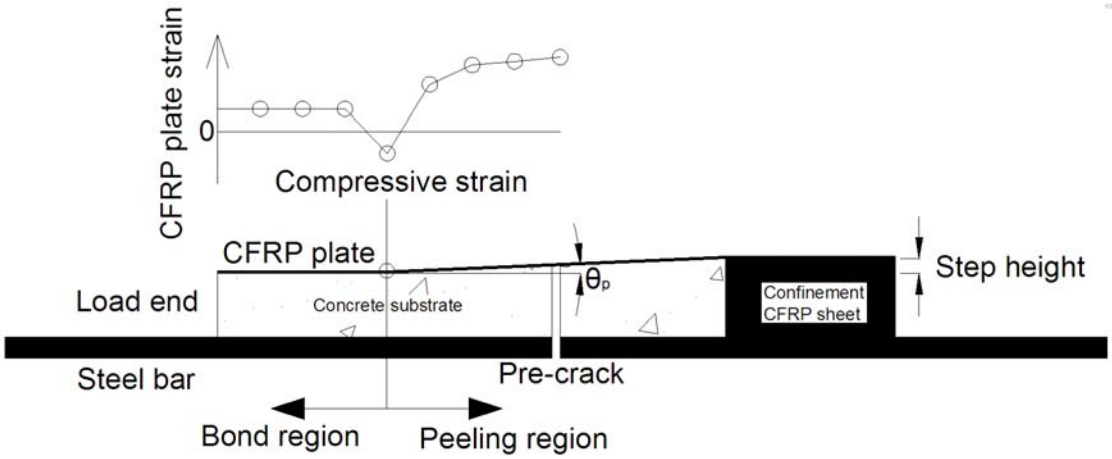

Fig. 4.7 Details of the delamination process

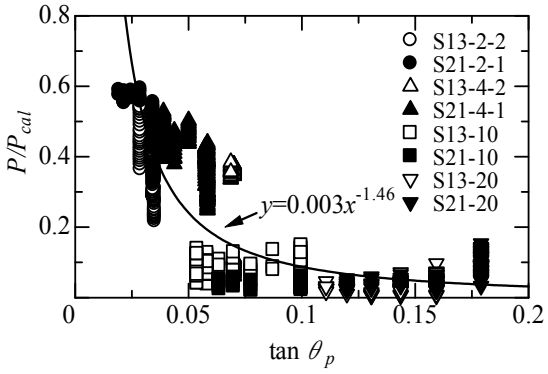

Fig. 4.8 Effect of the peeling angle on the bond strength

$$\tau_{b,\max} = 2.5 \times \sigma_B^{0.23} \tag{4.1}$$

$$l_e = \sqrt{\frac{2 \times t_f \times E_f \times s_e}{k_e \times \tau_{b,\max}}} \tag{4.2}$$

$$P_b = k_e \times \tau_{b,\max} \times b_f \times l_e (l_b > l_e) \tag{4.3}$$

$$P_b = k \times \tau_{b,\max} \times b_f \times l_b (l_b < l_e) \tag{4.4}$$

$$k = \frac{1-k_e}{2} \times \cos(\frac{l_b}{l_e}\pi) + \frac{1+k_e}{2} \tag{4.5}$$

where the maximum local bond stress is $\tau_{b,max}$, the concrete compressive strength in MPa is σ_B, the effective bond length is l_e, the width of the CFRP plate is b_f, the thickness is t_f, the elastic modulus is E_f, the local slip of the effective bond area is s_e (0.234 mm); the stress coefficient of the EBSB in the case of effective bond length is k_e (0.428); the bond length is l_b; the bond strength is P_b; and the stress coefficient of the EBSB is k (Kanakubo et al. 2003) [4.7].

Plots of the calculated shear bond strength with respect to the peeling angle and the evaluated tensile load ratio are shown in Fig. 4.9. The bond strength calculated using Eqs. (4.1) to (4.5) was obtained as the difference between the bond length (l_b) and the effective bond length (l_e). In this experiment, the tensile load was considered to have reached the shear bond strength when the entire plate was delaminated. In other words, the bond length decreased as the plate delaminated. Thus, the bond length is shorter than the effective bond length. The trends in the shear bond strength curves calculated according to the method described above are shown in the figure. The intersection points represent the bond strength for the combined fracture mode. Therefore, the corresponding values of P/P_{cal} can be calculated using the values of tan θ_p at these intersections. The values of P/P_{cal}, tan θ_p, and the calculated bond length for each specimen are provided in Table 4.3. The predictions agree well with the test results.

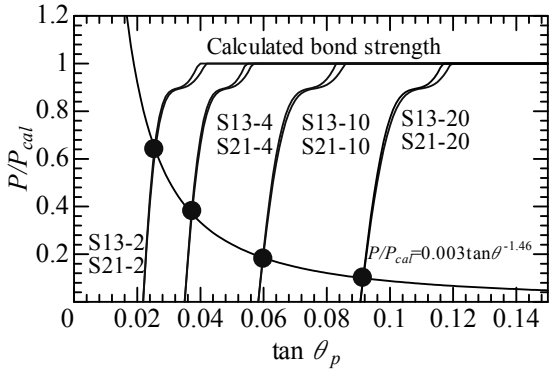

Fig. 4.9 Evaluation of the combined fracture bond strength

Table 4.3 Comparison of the test results

Specimen	Calculated bond length (mm)	Experimental values P/P_{cal}	Tan θ_p (cross point)	Calculated values P/P_{cal}	Experimental / calculated values
S13-2-1	61.5	0.54	0.026	0.62	0.87
S13-2-2		0.53	0.026	0.62	0.86
S13-4-1	39.5	0.40	0.038	0.36	1.13
S13-4-2		0.41	0.038	0.36	1.15
S13-10	13.9	0.13	0.060	0.18	0.71
S13-20	7.9	0.14	0.092	0.10	1.43
S21-2-1	61.5	0.61	0.026	0.62	0.99
S21-2-2		0.63	0.026	0.62	1.02
S21-4-1	39.5	0.54	0.038	0.36	1.52
S21-4-2		0.44	0.038	0.36	1.24
S21-10	13.9	0.19	0.060	0.18	1.04
S21-20	7.9	0.16	0.092	0.10	1.64

4.5. Conclusions

The bond behavior under the combined fracture mode was observed using special specimens that had a step height at the surface. The results confirm that the tensile load decreases as the peeling angle increases. The failure surfaces of the specimens with large initial angles were between the CFRP plate and the adhesive, whereas the specimens with small initial angles were debonded at the concrete surface. The peeling angle affected the failure surface and caused the transition of the failure mode, i.e., from Mode II to Mode I, in which the bond strength was less than the shear bond strength. The relationship between the peeling angle and the tensile load was determined to evaluate the bond strength under the combined fracture mode. A calculation method for the combined fracture mode was proposed based on the test results. The proposed method accurately predicts the bond strength between the CFRP plate and concrete under combined shear and peeling fracture conditions.

CHAPTER 5

Conclusions

In this thesis, several problems related to bond and peeling debonding failure in CFRP plate-strengthened concrete under fatigue loading were investigated. The main conclusions of this research are summarized below.

When debonding of the CFRP plate is induced by a shear crack in the strengthened beam, both horizontal and vertical displacements occur between the two sides of the crack. A series of static and fatigue loading tests was carried out to investigate the effect of the vertical displacement on the CFRP debonding behavior under fatigue loading. For specimens with bonded CFRP plates, final failure was associated with the debonding of the CFRP plate from the substrate of the concrete block, from the shear crack to the supporting point. In the vertical displacement measurements in the fatigue test, clear differences were observed in the deflection-versus-fatigue cycle relationship near the position of the shear crack. The peeling effect caused by the vertical displacement at a shear crack, due to crack propagation with fatigue cycles, was recognized.

The effect of parameter configuration on the fatigue failure mode was investigated through double-faced shear fatigue tests. The following were identified in these tests:

1. Fatigue failures occur at the initiation of debonding from the notch position.

2. The fatigue debonding at the faces consists of two components. The first component is debonding from the concrete face near the notch, and the second component is debonding from the resin face to the load end.

3. *S*-*N* curves for the fatigue failure of the bond were proposed. The fatigue-limit bond stress up to one million cycles was considered for specimens with concrete strengths of 13, 21, and 36 MPa.

4. The results of monotonic post-fatigue tests indicated that the peak load is not influenced by fatigue cycles.

5. The stiffness of the local bond stress-slip curves decreases as the number of fatigue loading cycles increases. The stiffness reduction coefficient was determined from the number of cycles.

6. A local bond stress-slip model was proposed based on the experimental results, and a numerical analysis was performed to validate the proposed model. (1) The tensile load-versus-deformation (crack width) curves exhibited nearly linear behavior with respect to the number of fatigue loading cycles, and the stiffnesses of the curves

gradually decreased as the number of loading cycles increased. (2) The local bond stress-slip relationship under fatigue loading exhibited nearly elastic behavior. The stiffnesses of the curves decreased as the number of loading cycles increased. (3) A local bond stress-slip model for fatigue loading was developed by evaluating the stiffness and envelope curves given by the Popovics model. (4) The proposed local bond stress-slip model and strain distribution obtained from the numerical analysis using the proposed model agreed well with the experimental results.

In addition, the transverse displacements measurements in double-faced shear tests indicate a clear peeling phenomenon as the debonding progressed. The experiment results indicate that when peeling off, the CFRP plate moved from the specimen center toward the load end as the number of loading cycles increased. These results show that the peeling off of the CFRP plate is an important failure mode that affects the progress of debonding in fatigue testing.

Furthermore, the bond behavior under the combined fracture mode was examined using special specimens that had a surface step height. The tensile load was found to decrease as the peeling angle increased. The relationship between the peeling angle and the tensile load was determined to evaluate the bond strength under the combined fracture mode. A calculation method for the combined fracture mode was proposed based on the test results. The proposed method accurately predicts the bond strength between the CFRP plate and concrete under combined shear and peeling fracture conditions.

The purposes of the present research were to investigate the characteristics of debonding in FRP-strengthened concrete in mixed-mode failure under fatigue loading and to develop and experimentally validate a calculation method for predicting the bond strength between a CFRP plate and concrete under combined shear-peeling failure conditions.

Fatigue loading resulting in shear-peeling fracture of the CFRP plate at the major shear crack in CFRP-plated RC beams in chapter 2 was confirmed. To understand in greater depth the fatigue bond behavior between concrete and CFRP plates, double-face shear bond tests were performed in chapter 3. The results indicated that local delamination due to shear-peeling in CFRP plates subjected to fatigue loading was the most important factor affecting the debonding progress of FRP-strengthened concrete structures. Therefore, to evaluate the bond strength of combinations, fracture mode was considered. In chapter 4, a simple calculation method for the bond strength of combination fracture mode, based on peeling angle derived from the shear-peeling phenomenon, was devised.

Based on the current research, some recommendations for design procedure can be made.

In CFRP-plated beams with relatively long shear spans or in which the end peel mode has been effectively mitigated, debonding initiates at flexural/shear cracks near the region of maximum moment. Under loading, these cracks open and induce high interfacial shear stress, causing delamination, which propagates across the shear span in the direction of decreasing moment. This mode of debonding is properly termed "intermediate flexural-shear crack-induced debonding." Available guidance for the design of external FRP plate-bonding systems should take the approach of limiting the stress (or strain) in the FRP plate to mitigate debonding. Indeed, the fatigue bond behavior of FRP plate-bonding systems is expected to limit the stress (or strain) that is recommended to mitigate bond failure associated with deterioration due to fatigue loading.

Moreover, fatigue-induced local delamination due to shear-peeling in FRP plates is an important factor that affects the service life of FRP-strengthened concrete structures. Hence, the bond strength with mixed-mode fractures should be considered in the initial design.

Furthermore, although mixed-mode failure could be quantified in the present research in terms of the loss of strength of the interface due to peeling angle variation, other parameters, such as type of adhesive and temperature, could possibly have affected the experimental results. Additionally, the rate of progression of interfacial degradation under fatigue loading is not currently predictable; hence, the following recommendations for future research are made to address limitations in the current knowledge.

1. Progressive damage propagation at the interface between concrete and CFRP plates should be further investigated. The failure sequence or governing factors must be investigated based on changing parameters. Detailed debonding/delamination failure mechanisms should be fully disclosed.
2. Detailed design guidelines should be developed for the fatigue limit state of RC beams externally strengthened with FRPs, particularly for the relationship of mixed-mode bond strength and fatigue life. Design guidelines should be improved to include detailed information, such as the level of environmental conditions, applied loading ranges, and expected fatigue lives.
3. Further experimental investigations over a variety of load ranges and frequencies, including more realistic peak overload and variable amplitude load, should be conducted.

REFERENCES

CHAPTER 1

1.1. Swamy, R. N., Jones, R., and Charif, A. “Shear adhesion properties of epoxy resin adhesives’’, Adhesion between polymers and concrete, H. R. Sasse, ed., RILEM, Paris, 1986. pp.741-755.

1.2. Van Gemert, D.A. “Repairing of concrete structures by externally bonded steel plates’’, Int. J. of Adhesion, 2, 1980. pp.67-72.

1.3. Kobatake, Y., Kimura, K., and Katsumata, H. “A retrofitting method for reinforced concrete structures using carbon fiber’’, Fiber reinforced plastic (FRP) reinforcement for concrete structures: Properties and applications, A. Nanni, ed., Elsevier Science, Oxford, U.K., 1993. pp.435-450.

1.4. L. Bizindavyi and K. W. Neale., “Transfer lengths and bond strengths for composites bonded to concrete”, Journal of Composite Materials for Construction, Nov., 1999. pp.153-160.

1.5. Chajes, M. J., Finch, W. W. Jr., Januszka, T. F., and Thomson, T. A. Jr. “Bond and force transfer of composite material plates bondedto concrete’’, ACI Struct. J., 93(2), 1996. pp.295-303.

1.6. Chajes, M. J., Januszka, T. F., Mertz, D. R., Thomson, T. A. Jr., and Finch, W. W. “Shear strengthening of reinforced concrete beams using externally applied composite fabrics’’, ACI Struct. J., 92(3), 1995. pp.295-303.

1.7. Neubauer, U., and Rostasy, F. S. “Design aspects of concrete structures strengthened with externally bonded CFRP plates’’, Proc., 7th Int. Conf. on Struct. Faults and Repair, ECS Publications, Edinburgh, U.K., 2, 1997. pp.109-118.

1.8. Xu Y. W., Qiao P. Z., and Davalos J. F. “Exploratory Evaluation of Mode-I Fracture Toughness of Concrete-Composite Bonded Interfaces”, 15th ASCE Engineering Mechanics Conference, New York, 2002.

1.9. Mitsui M., Fukuzawa K., and Numao T. “Influence of temperature on cleavage bonding properties between CFRP sheets and concrete”, ICCI-02, June, in CD-ROM, 2002.

1.10. Dai J. G., Sato. Y., Ueda T., and Muttaqin H. “Mode I Fracture Behaviors of FRP-Concrete Interfaces”, Proceedings of the Japan Concrete Institute, Vol. 25, 2003. pp.1577-1582.

1.11. Boyajian D., Davalos J. F., Ray I., and Qiao P. Z. “Evaluation of interface fracture of concrete externally reinforced with FRP”, 2nd International Conference of Durability of FRP Composites for Constructions, Montreal, Canada, 2002.

1.12. Karbhari V. M., and Engineer M. “Investigation of Bond between Concrete and Composites: Use of a Peeling Test”, Journal of Reinforced Plastics and Composites, Vol.15, 1996. pp.208-227.

1.13. Wu Z. S., Asakura T., Yoshizawa H., Yuan H., Kobayashi A., and Takahashi T “Experimental and analytical studies on peeling behaviors and spalling resistance effect of externally bonded continuous fiber sheets”, Proceedings of Japan Society of Civil Engineering, Vol. 49, No. 662, 2000. pp.45-58.

1.14. Kojima Y., Yoshizawa K., Muguruma T., Kobayashi A., Wakana K., Asakura T., and Wu Z. S., “A Design Method of Fiber Reinforced Plastic Methods as a Countermeasure for Concrete Spalling from Tunnel Lining”, Proceeding of JSCE, No. 746/VI-62, 2004. pp.101-116.
1.15. Dai J. G., Ueda T., Sato Y., and Jaqin H. “Dowel resistances of bond interfaces between FRP sheets and concrete”, CICE 2004, Australia
1.16. Md. Shah Alam, Toshiyuki Kanakubo, Akira Yasojima. “Shear-Peeling Bond Strength between Continuous Fiber Sheet and Concrete”, ACI Structural Journal, Vol. 109, No. 1, January-February 2012. pp. 75-82.
1.17. Priestley, M.; Seible, F., and Calvi, G. “Seismic Design and Retrofit of Bridges”, John Wiley and Sons, New York, NY, 1996.
1.18. Saadatmanesh H., and Ehsani M.R. “RC beams strengthened with GFRP plates. I: experimental study”, Journal of Structural Engineering, vol. 117, No. 11, 1991. pp.3417-343.
1.19. Ritchie P.A” Thomas D.A” Lu L.W., and Connelly G.M., “External strengthening of concrete beams using fibre reinforced plastic”, ACI Structural Journal, vol. 88, 1991. pp. 490-500.
1.20. Saadatmanesh H., and Malek A.M. “Design guidelines for strengthening of RC beam with FRP plates”, Journal of Composites for Construction, vol. 2, No. 4, 1998. pp. 158-164.
1.21. Meier U. “Strengthening of structures using carbon fibre/epoxy composites”, Constr Building Material; 1995, 9(6): pp.341-351.
1.22. Norris T., Saadatmanesh H., and Ehsani M.R. “Shear and flexural strengthening of R/C beams with carbon fiber sheets”, Journal of Structural Engineering,vol. 123, No. 7, 1997. pp. 903-911.
1.23. Swamy R.N., Jones R., and Charif A. “The effect of external plate reinforcement on the strengthening of structurally damaged RC beams”, The Structural Engineer, vol. 67, 1989. pp. 45-56.
1.24. Wei, A., Saadatmanesh, H. and Ehsani, M. R. “RC beams strengthened with FRP plates. II: Analysis and parametric study”, J. Struct Rngrg., ASCE, 117(11), 1991. pp. 3434-3435.
1.25. Triantafillou, T. C., and Plevris, N. “Strengthening of R/C beams with epoxy-bonded fiber-composite materials”, Mater. Struct. 25, 1992. pp. 201-211.
1.26. Sharif A., Alsulaimani G.J., and Ghaleb B.N., “Strengthening of initially loaded reinforced concrete beams using FRP plates”, ACI Structural Journal, vol. 91, No. 2, 1994. pp. 160-168.
1.27. Ziraba Y.N., Baluch M.H., Basunbul I.A., Azad A.K., and Al-Sulaimani G.J., and Sharif AM. “Combined experimental-numerical approach to characterization of steel-glue-concrete interface”, Materials and Structures, vol. 28, 1995. pp. 518-525.
1.28. Pham H., and Al-Mahaidi R., “Experimental investigation into flexural retrofitting of Reinforced Concrete Bridge beams using FRP composites” ,Composite Structures, vol. 66, 2004. pp. 617-625.
1.29. Brena S.F., and Macri B.M., “Effect of Carbon-Fiber-Reinforced Polymer

laminate configuration on the behavior of strengthened reinforced concrete beams", Journal of Composite for Construction, vol. 8, No. 3,2004.pp. 229-240.
1.30. Wight G. and Erki M.A., "Pre-stressed CFRP for strengthening concrete slabs in fatigue", International Conference on FRP Composites in Civil Engineering CICE 2001 Ed .J.G.Teng. Hong Kong, 2001. ISBN: 0-08-043945-4.
1.31. Heffernan, P. J., and Erki, M. A. "Fatigue behavior of reinforced concrete beams strengthened with carbon fiber reinforced plastic laminates" ,J. Compos. Constr., 82, 2001. pp.132-140.
1.32. Schlafli, M., and Bruhwiler, E. "Fatigue of existing reinforced concrete bridge deck slabs", Eng. Struct., 1998. pp.991-998.
1.33. Barnes, R. A., and Mays, G. C. "Fatigue performance of concrete beams strengthened with CFRP plates", J. Compos. Constr., 1999. pp.63-72.
1.34. Swamy R. N. "Debonding of Carbon Fiber Reinforced Polymer Plate from Concrete Beams", Proceeding. Ins. Civ. Engrs Structs & Bldgs, 134, 1999. pp.301-317.
1.35. Rahimi H., and Hutchinson A. "Concrete Beams Strengthened with Externally Bonded FRP Plates, Journal of Composites for Construction", ASCE, Vol. 5, No. 1, 2001. pp.44-56.
1.36. Bizindavyi, L., Neale, K. W., and Erki, M. A. "Experimental investigation of bonded fiber reinforced polymer-concrete joints under cyclic loading", J. Compos. Constr., 72, 2003. pp.127-134.
1.37. Dai, J.G., Sato, Y., Ueda, T. and Sato, Y. "Static and fatigue bond characteristics of interfaces between CFRP sheets and frost damage experienced concrete", Proceedings of 7th International Symposium on Fiber Reinforced Polymer Reinforcement for Reinforced Concrete Structures (FRPRCS-7), ACI, Farmington Hills, MI , 2005. pp.1515-1530.

CHAPTER 2

2.1. Ritchie P.A., Thomas D.A., Lu L.W., and Connelly G.M., "External strengthening of concrete beams using fiber reinforced plastic", ACI Structural Journal, vol. 88, 1991.pp. 490-500.
2.2. Saadatmanesh H., Ehsani M.R., "RC beams strengthened with GFRP plates I: experimental study", Journal of Structural Engineering, vol. 117, No. 11, 1991. pp.3417-343.
2.3. Wei, A., Saadatmanesh, H., and Ehsani, M. R. "RC beams strengthened with FRP plates. II: Analysis and parametric study", J. Struct Rngrg., ASCE, 117(11), 1991. pp.3434-3435.
2.4. Triantafillou,T. C.,and Plevris, N. "Strengthening of R/C beams with epoxy-bonded fiber-composite materials", Materials and Structures,2(5),1992. pp.201-211.
2.5. Karbhari, V. M.; Engineer, M.; and Eckel II, D. A., "On the Durability of Composite Rehabilitation Schemes for Concrete: Use of a Peel Test," Journal of Materials Science, V. 32, No. 1, 1997. pp. 147-156.
2.6. Triantafillou, T. C., and Plevris, N., "Strengthening of RC Beams with

Epoxy-Bonded Fiber-Composites Materials," Materials and Structures, V. 25, 1992. pp. 201-211.
2.7. Masoud, S., Soudki, K., and Topper, T. "CFRP-strengthened and corroded RC beams under monotonic and fatigue loads." J. Compos. Constr., 5(4), 2001. pp.228-236.
2.8. Masoud, S., Soudki, K., and Topper, T. "Post repair fatigue performance of FRP-repaired corroded RC beams: Experimental and analytical investigation." J. Compos. Constr., 9(5), 2005. pp.441-449.
2.9. Heffernan, P. J., and Erki, M. A. "Fatigue behavior of reinforced concrete beams strengthened with carbon fiber reinforced plastic laminates." J. Compos. Constr., 8(2), 2004. pp.132-140.
2.10. Toutanji, H., Zhao, L., Deng, Y., Zhang, Y., and Balaguru, P. "Cyclic behavior of RC beams strengthened with carbon fiber sheets bonded by inorganic matrix." J. Mater. Civ. Eng., 1(81), 2006. pp.28-35.
2.11. Papakonstantinou, C. G., Petrou, M. F., and Harries, K. A. "Fatigue behavior of RC beams strengthened with GFRP sheets." J. Compos. Constr., 5(4), 2001. pp.246-253.
2.12. El-Hacha, R., Wight, R. G., Heffernan, P. J., and Erki, M. A. "Prestressed CFRP sheets for strengthening reinforced concrete structures in fatigue." Proc., 6th Int. Symp. on Fiber-Reinforced Polymer (FRP) Reinforcement for Concrete Structures (FRPRCS-6), Vol. 1, Singapore, 2003. pp.895-904.
2.13. Brena, S. F., Benouaich, M. A., Kreger, M. E., and Wood, S. "Fatigue tests of reinforced concrete beams strengthened using carbon fiber-reinforced polymer composites." ACI Struct. J., 102(2), 2005. pp.305-313.
2.14. Architectural Institute of Japan. "Design Guideline for Earthquake Resistant Reinforced Concrete Buildings Based on Ultimate Strength Concept", 1988.
2.15. Japan Society of Civil Engineers. "Standard Specifications for Concrete structure-2002", Structural Performance Verification, March, 2002.
2.16. ACI-ASCE Committee 426. "The Shear Strength of Reinforced Concrete Members", ASCE St.Div.vol.99, ST6, June 1973.

CHAPTER 3

3.1. Maeda, Toshiya, Asano, Yasuyuki, Sato, Yasuhiko, Ueda, Tamon and Kakuta, Yoshio. "A Study on Bond Mechanism of Carbon Fiber Sheet", Proceedings of the Third International Symposium on Non-Metallic (FRP) Reinforcement for Concrete Structures, Vol. 1, Japan Concrete Institute, Japan, 1997. pp. 279-286.
3.2. Tanaka, T. "Shear Resisting Mechanism of Reinforced Concrete Beams with CFS as Shear Reinforcement. Graduation Thesis", 1996. Hokkaido University.
3.3. Yuan, H. Wu, Z.S. and Yoshizawa, H. "Theoretical solutions on interfacial stress transfer of externally bonded steel/composite laminates", Journal of Structural Mechanics and Earthquake Engineering, JSCE, No. 675/1-55, 2001. pp.27-39.
3.4. Kanakubo T., Furuta T., and Fukuyama H., "Bond Strength between Fiber-Reinforced Polymer Laminates and Concrete", Proceedings of 6th International Symposium on Fiber-Reinforced Polymer (FRP) Reinforcement

for Concrete Structures, Vol.1, 2003. pp.133-142.
3.5. Matsunaga K., Kanakubo T., et al., “Study on Bond between CFRP Plate and Concrete”, Summaries of Technical Papers of Annual Meeting of Architectural Institute of Japan, C-2, 2008. pp.307-310. (In Japanese).
3.6. Nakaba K., Kanakubo T., Furuba T., and Yoshizawa H., “Bond Behavior between Fiber-Reinforced Polymer Laminates and Concrete”, ACI Structure J., 98(3), 2001. pp.359-367.
3.7. Chajes M.J., Finch W.W. jr, Januska T.F. and Thomson T.A. jr. “Bond and force transfer of composite material plates bonded to concrete”, ACI Structural J. Vol. 93, 1996. pp.208-217.
3.8. Yuan, H. Wu, Z.S. and Yoshizawa, H. “Theoretical solutions on interfacial stress transfer of externally bonded steel/composite laminates”, Journal of Structural Mechanics and Earthquake Engineering, JSCE, No. 675/1-55, 2001. pp.27-39.
3.9. Wu, Z., Yuan, H. and Niu, H. “Stress transfer and fracture propagation in different kinds of adhesive joints”, ASCE Journal of Engineering Mechanics, Vol. 128, No. 5, 2002, pp.562-573.

CHAPTER 4
4.1. Roberts T.M., “Approximate analysis of shear and normal stress concentrations in the adhesive layer of plated RC beams”, The Structural Engineer, vol. 67, No. 12, 1989. pp. 229-23.
4.2. Malek, A. M., Saadatmanesh, H., and Ehsani, M. R. “Prediction of failure load of R/C beams strengthened with FRP plate due to stress concentration at the plate”, ACI Struct. J, 95(2), 1998. pp.142-152.
4.3. Rabinovitch H., and Frostig Y., “Closed-form high order analysis of RC beams strengthened with FRP strips”, Journal of Composites for Construction, vol. 4, No. 2, 2000. pp. 65-74.
4.4. El-Mihilmy M.T., and Tedesco J.W., “Prediction of anchorage failure for reinforced concrete beams strengthened with fiber-reinforced polymer plates”, ACI Structural Journal, vol. 98, No. 3, 2001. pp. 301-314.
4.5. Matsunaga K., Kanakubo T., et al., “Study on Bond between CFRP Plate and Concrete”, Summaries of Technical papers of Annual Meeting of Architectural Institute of Japan, C-2, 2008. pp.307-310. (in Japanese).
4.6. Alam M.S., Kanakubo T., and Yasojima A., “Shear-Peeling Bond Strength between Continuous Fiber Sheet and Concrete”, ACI Structure Journal, V.109. No.1, 2012. pp.75-80.
4.7. Kanakubo.T., Furuta.T., and Fukuyama.H. “Bond Strength between Fiber-Reinforced Polymer Laminates and Concrete”, Proceedings of 6th International Symposium on Fiber-Reinforced Polymer (FRP) Reinforcement for Concrete Structures, Vol.1, 2003. pp.133-142.

ACKNOWLEDGEMENTS

I would like to express my deepest appreciation to my thesis supervisor, Associate Professor Toshiyuki Kanakubo, for his valuable guidance and constructive supervision, invaluable feedback, and friendly communication during this research project over the years. Without his support and encouragement, this thesis could not have been completed. His broad research experience and keen insight have impressed me deeply throughout this research program and will certainly encourage me for the rest of my life.

I would also like to thank my thesis committee members, Prof. Yuki Sakai, Prof. Yasuo Yamada, Associate Prof. Gaku Shoji, and Assistant Prof. Akira Yasojima, for their valuable suggestions and constructive comments on my research.

I would like to acknowledge a technical staff member, Mr. Kojima, from the Kanakubo Laboratory for his extremely important assistance in the experimental work.

I also thank all of my friends for their help in the research, especially Mr. Kohei ASANO, Mr. Jianhua YU, Mr. Taichi KIMURA, Mr. Takayuki SANO, Mr. Kenji SUZUKI, Mr. Xiangwei GUAN, Mr. Daiki IGARASHI, Mr. Shimei MAN, and Mr. Ryoichi TSUKIZAKI.

Special thanks are also expressed to my family for their endless love and continuous support throughout this research study.

PUBLICATIONS ARISING FROM THE THESIS

1. Wei Zhang, Toshiyuki Kanakubo:
"Bond Behavior between Concrete and CFRP Plate under Fatigue Loading", Proceedings of the 4th Asian Concrete Federation International Conference, Tue-S4.3-01, 2010.11.

2. Wei Zhang, Toshiyuki Kanakubo:
"Experimental Study on Bond Behavior between CFRP Plate and Concrete under Combination of Fracture Mode (Ⅰ)", the 14th JSCE International Summer Symposium in 2012,Section V-197, 2012.9.

3. Wei Guanxiang, Wei Zhang, Toshiyuki Kanakubo:
"Experimental Study on Bond Behavior between CFRP Plate and Concrete under Combination of Fracture Mode (Ⅱ)", JSCE Annual Meeting in 2013, Section V-023, 2013.9. (In Japanese)

4. Wei Zhang, Toshiyuki Kanakubo:
"Local Bond Stress-Slip Relationship between CFRP Plate and Concrete under Fatigue Loading", Accepted for publishing in ACI Structural Journal, 2013.

5. Wei Zhang, Toshiyuki Kanakubo:
"Experimental Study on Bond Behavior between CFRP Plates and Concrete under Combination of Fracture Mode (Ⅱ)", Proceedings of the 4th Asia Pacific Conference on FRP Composites in Structures, Section B-4, 2013.12.